The crustal structure of the east Africa through earthquake seismology

P. K. H. Maguire

THE CRUSTAL STRUCTURE OF EAST AFRICA THROUGH EARTHQUAKE SEISMOLOGY

by

P.K.H. MAGUIRE

A thesis submitted for the degree of

DOCTOR OF PHILOSOPHY

at

THE UNIVERSITY OF DURHAM

GRADUATE SOCIETY.

ABSTRACT

First arrivals of local and regional earthquakes, recorded at the Kaptagat array station on the western flank of the Gregory Rift Valley in Kenya, have been analysed to determine the crustal structure westward from the Rift axis. Apparent velocities have been interpreted in terms of crustal velocities. Azimuth and epicentral distance of event has provided lateral and vertical control on crustal boundaries.

Normal shield crust, underlain by normal Moho is concluded to exist on the western flank of the Rift Valley. From the satisfactory propagation of S_n from events originating around the western Rift, normal Moho is considered to exist across the East African Plateau. A massive mantle derived intrusion is concluded to have penetrated the crust to within approximately 8 km of the Rift floor. This intrusion reaches to within about 7 km of the Elgeyo escarpment, the major Rift Valley boundary fault immediately to the east of Kaptagat.

In order to aid second arrival analysis, a synthetic seismogram programme based on short wavelength asymptotic theory for reflected and refracted waves has been written. A qualitative analysis of real and synthetic seismograms of events originating to the west of Kaptagat, suggests that the crustal structure is more complex than the simple two-layered model initially produced.

It is considered that the structure beneath the Gregory Rift is more equivalent to that beneath ocean Rift Systems than that beneath continental Rifts. However, rather than being a direct extension of the World Rift System, the Eastern Rift and associated Kenya dome should be considered as a single physical unit.

ACKNOWLEDGEMENTS

I should like to thank Professor M.H.P. Bott for allowing me to work in the Department of Geological Sciences at the University of Durham.

My thanks also go to Dr. R.E. Long, my supervisor, whose help, advice and encouragement was invaluable in the completion of this thesis.

Of my fellow research students, whose many stimulating discussions aided my own understanding of the science, geophysics, I must single out two names, Dr. Richard Backhouse, and Mr. Les Arnold. My thanks go to them for patiently answering my questions and queries and also for providing me with various computer programmes.

I am indebted, in truth, to all the staff and students of the department with whom I came in contact during my three years in Durham for making life not only enjoyable but also rewarding, both in thought and action.

I should like to thank Mrs Mary Cutting of the University of Leicester for typing the manuscript, and Mr. Derek Hudspeth of the University of Durham for printing the diagrams.

My research could not have been undertaken without the financial support of NERC, to whom I am indeed indebted.

Peter Maguire

CONTENTS

ERRATA

Page 3	Line 1	'Easterm' to read 'Eastern'
Page 7	Line 15	'GIBBON' to read 'GIBSON'
Page 13	Line 24	'curved' to read 'curves'
Page 19	Line 6	'Rhinegoeben' to read 'Rhinegraben'
Page 51	Line 1	'Theroetical' to read 'Theoretical'
	Line 28	'gently' to read 'gentle'
Page 107	Line 17	'siesmic' to read 'seismic'
Page 116	Line 18	'sutdies' to read 'studies'

CHAPTER 1.
INTRODUCTION

1.1. THE EAST AFRICAN RIFT SYSTEM

The East African Rift System extends some 2300 miles, from the Limpopo River in the south, across the Zambezi valley to the region of Lake Malawi; where upon it splits into the Western and Eastern Rifts, bifurcating around the Tanganyika Craton. North from Lake Rudolf, the System follows the Ethiopian Rift to Afar, a triple junction with the Red Sea and Gulf of Aden (Fig. 1).

Despite considerable variation in the pattern, the typical Rifts are grabens, about 50-80 km in width, of Tertiary and later age. However a similar pattern of faulting can be dated Jurassic or Late Karroo in some regions. Although there is strong correlation between Precambrian structural trends and Rift faulting (DIXEY 1956), it is unlikely that the fundamental cause of both features was a stress system operating from Precambrian times in eastern Africa. This is because the older trends followed by the Rift faults belong to Precambrian orogenic belts of different ages and structures. Rather, the ancient structural trends 'directed' the later course of rifting (KING 1970).

Traced along their length, the Rift Valleys show considerable variation in altitude. It is noticeable that regions of uplift are strongly associated with volcanic activity; in particular, the Ethiopian and Kenya 'domes', regions around Lakes Edward and Kivu in the Western Rift, and a region north of Lake Malawi.

Faulting is predominantly normal, with dips varying between 55 to 70 degrees; the boundary faults to the grabens being arranged en echelon, rather than composed of single large faults. In many places, the displacement from floor to Rift shoulder has been obscured by volcanic and sedimentary infill, but throws of up to 3 km have occurred

Fig. 1. Map of East Africa outlining Rift System, and incorporating KAPTAGAT, KARIBA and WWSSN Stations.

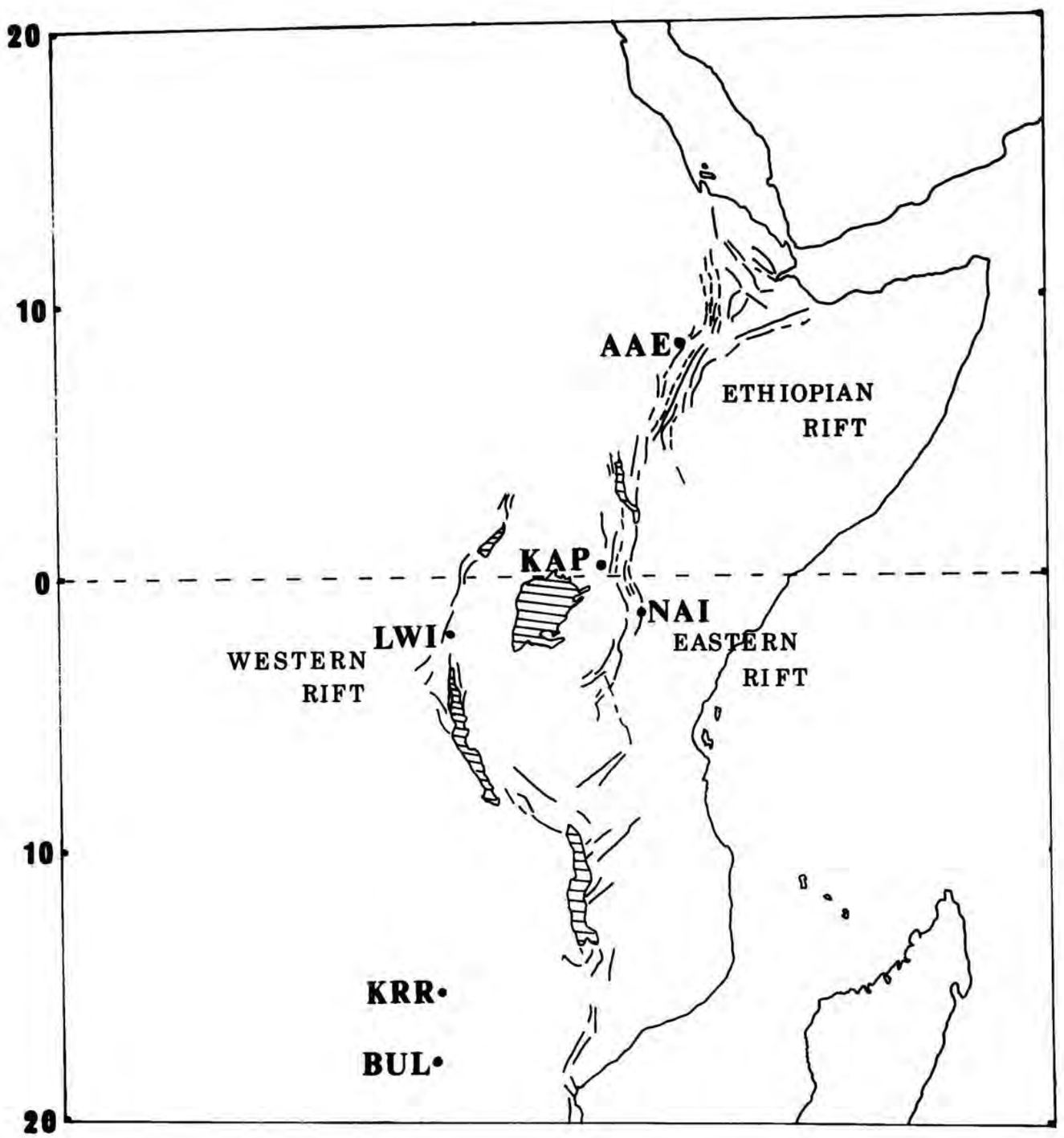
20
10
0
10
20
AAE
ETHIOPIAN
RIFT
KAP
NAI
LWI
WESTERN
RIFT
EASTERN
RIFT
KRR
BUL

in the basement rocks. Within the grabens, latest movements have commonly taken place along numerous closely spaced grid faults of small displacement. These features suggest a sequence of secondary adjustments to strains after the initial Tertiary Rifting.

1.2. THE EASTERN RIFT

The Easterm Rift (Fig. 2) is a north-south feature bisecting the Kenya dome. The latter is a broad ellipsoidal uplift, some 300 km across its minor axis, rising to nearly 3 km above sea level at its central point, between Naivasha and Nakuru. Here, the Rift is of classic graben structure, 60-70 km wide, with throws on the main faults of some 2000m. In this region, there are no parallel faults outside the Rift. Within it, dense subparallel faulting developed inwards from the Rift shoulders, which have been uplifted in conjunction with subsidence of the floor. Slightly to the north, on the western flank, lies the Kavirondo Rift. This is an ENE-WSW striking graben, with maximum throws on the boundary faults of the order of 1000m. Further to the north, i.e. immediately to the south of Lake Rudolf, the main Rift splays out into a faulted region some 350 km wide. A narrow, relatively shallow trough is the only connection with the main Ethiopian Rift. To the south, in northern Tanzania, the main Rift again splays out into a broad, block faulted and tilted, zone.

The oldest recognizeable Rift structure is the dissected monoclinal flexure, now represented by the Uganda escarpment and Turkwel fault (BAKER and WOHLENBERG 1971). These are of mid-Tertiary age, immediately predating the subsidence of the Turkana depression and the uplift of the Kenya-Uganda border, in the Lower to Middle Miocene. These movements were accompanied by massive basaltic and trachytic volcanism in Turkana (LOGATCHEV et al 1972), and the formation of the alkaline-carbonatite volcanoes of Eastern Uganda and the Kavirondo Rift. In the Upper Miocene, the volcanism migrated to the slight domal uplift of the central Rift, severing the connection with the Ethiopian volcanic area. The uplift was accompanied by immense fissure eruptions of phonolites and phonolitic trachytes. In the Lower to Middle Pliocene, the first extensive faults appeared along the whole of the western side of the Rift Valley, from the Kamasia range in the north, to the Crater

Fig. 2. The Eastern Rift Valley System including known faults and major lakes.

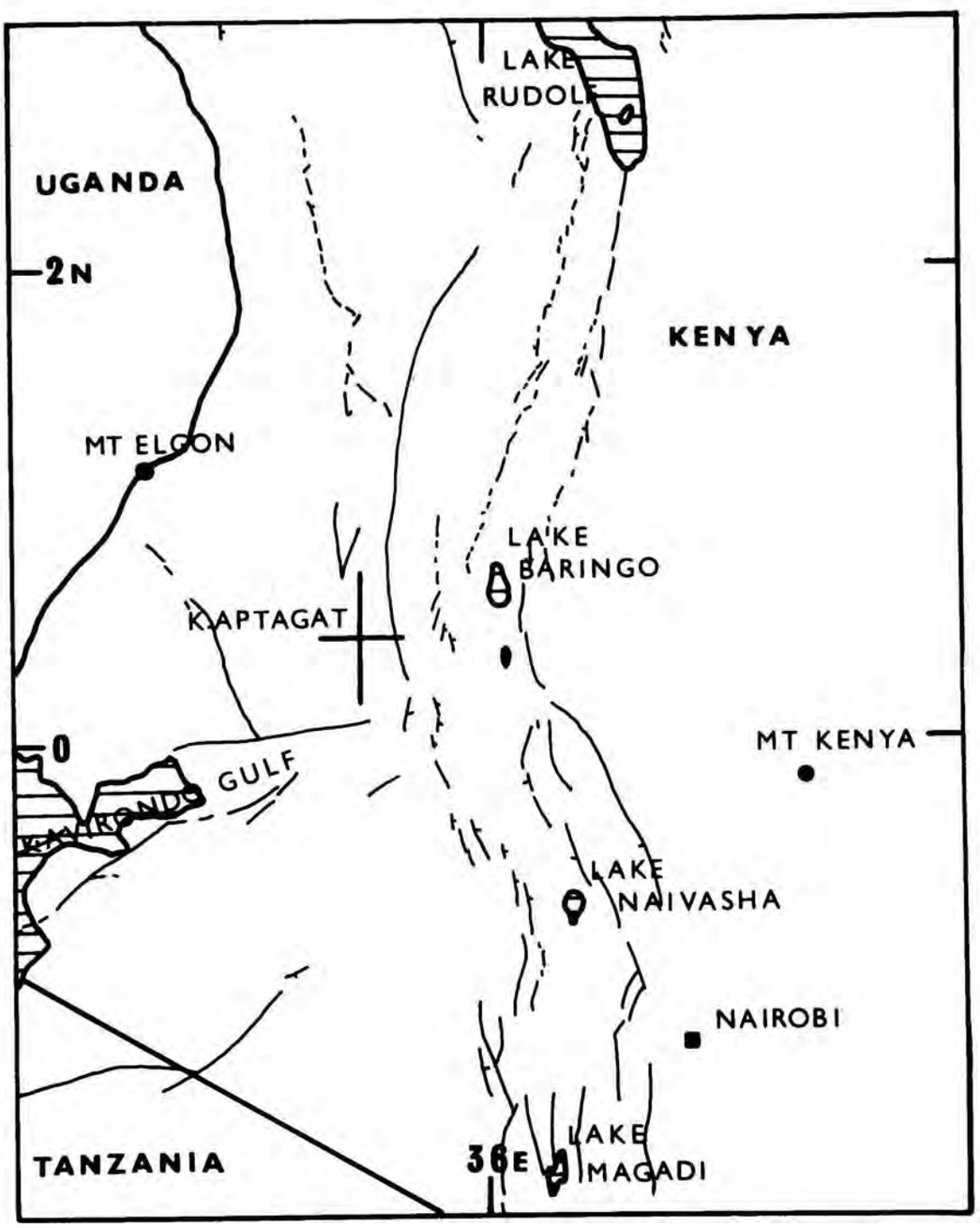
LAKE
RUDOLF
UGANDA
2N
KENYA
MT ELGON
LAKE
BARINGO
KAPTAGAT
0
GULF
MT KENYA
LAKE
NAIVASHA
NAIROBI
TANZANIA
36E
LAKE
MAGADI

Highlands in the South. The volcanic activity to the west stopped completely, and since that time has been localized to the centre and east of the Rift, revealing the underlying asymmetry of the magma generating process. In the late Pliocene, Rift-trough formation, with associated uplift of the marginal plateaux, took place along the whole length of the Rift. Boundary faults of an earlier generation were renewed, while new faults developed within, and at the extremities of the Rift. These caused a deepening of the floor, and the appearance of step faults at the margins. Massive basalt eruptions began in the Upper to Lower Pleistocene along the whole of the trough floor. At the same time, autonomous melting centres appeared to the east, forming the gigantic volcanoes of Mount Kenya and Kilimanjaro. In the late Quaternary, trachyte, basalt-trachyte and phonolite caldera volcanoes (McCALL 1967) built up axially in the floor of the main graben. Well to the east, slightly differentiated associations, mainly of basaltic composition, were erupted in three main areas, forming multicentre volcanic chains (WILLIAMS 1969). Thus a picture of migration of magmatism from the North to the South and East is apparent over the whole region (LOGATCHEV et al 1972). It is seen that post-Miocene basalts and phonolites of the Rift floor are less undersaturated than corresponding flows, erupted outside the Rift. The same volcanics tend to be less undersaturated and less alkalic than Miocene flows. Miocene flows of phonolite exposed to the west of the Rift are more undersaturated and more alkalic than similar flows from the Eastern margin. (WILLIAMS 1972.)

1.3 THE TANGANYIKA SHIELD AND THE WESTERN RIFT.

The Eastern and Western Rifts bifurcate to the north of Lake Malawi, around the Tanganyika Shield. This consists of a gneissic complex and meta-sedimentary or metavolcanic systems, with prevalently east-west trends, acting as a stable block from 1850 $\pm$ 250 my ago (CLIFFORD 1970). It terminates to the west of the Eastern Rift at the margin of the Mozambique belt (HEPWORTH and KENNERLEY 1970). This is an assemblage of Upper Proterozoic folded rocks and tectonised basement extending from the Limpopo in the south, into Ethiopia to the north. It may be partly Archean, but has been reactivated at successive periods and so has acquired common structural and metamorphic characteristics (McCONNELL 1972).

Volcanism in the Rungwe region, at the intersection of the Western and Eastern Rifts, commenced in the Late Miocene to Early Pliocene, and has continued up to the present day. North of this region lies the rejuvanated post-Karroo Rukwa trough. Rifting from the Miocene to the Quaternary formed a belt which runs NNW through Lake Tanganyika to the lava fields south of Lake Kivu. Lake Tanganyika occupies a subparallel graben defined by various pairs of faults, which cover an area some 160 km wide at its southern end. Southern Kivu and Kamituga basalt-trachyte volcanicity began at least 6 to 8 million years ago and stopped in the mid-Pleistocene. From Lake Kivu, the Western Rift swings round NNE through the Birunga lava flows. The bulk of the lavas are ascribed to the later part of the Pleistocene, but originating in the Pliocene. North of Lakes Edward and George; two Lakes connected by a series of en echelon faults; the Rift is offset through Ruwenzori, a parallel horst block rising to 5000m above sea level. It continues along the Semliki River, through Lake Albert, terminating abruptly against the strong NW to SE trends of the Madi series of the Sudan border, and the parallel structures of the Aswa shear belt in Northern Uganda (KING 1970).

The volcanism of the Western Rift is arranged in a north to south sequence of increasing age and duration, less extensive and reverse to that in the Eastern Rift (LOGATCHEV et al 1972). Along its length, the Western Rift is characterized by the number of large lakes and the Tertiary to Pleistocene sedimentary infil. These sediments decrease in thickness southwards from some 2.5 km in Lake Albert to negligible infil in Lake Tanganyika. They accumulated up to the Pleistocene, due to a westward drainage system from the Eastern Rift Valley watershed. In that age, crustal movement reversed such drainage into the Lake Victoria downwarp.

1.4 THEORIES OF RIFT FORMATION.

Crustal doming (WILLIS 1936), and subsidence of the Rift Valley floor as a result of isostatic forces (GIRDLER 1964), have been two of the theories put forward to explain the formation of the Rift Valleys. However, the total extension of the crust within the Eastern Rift could range up to 10 km from structural analysis (BAKER and WOHLENBERG 1971) which is too great to be accounted for by doming alone. Also, the depth of the graben is too great for the isostatic model to be adequate. Both doming and faulting must be related to some subcrustal process.

Since the advent of the ocean-floor spreading hypothesis, the Rift System has been considered in relation to ocean-floor genesis. This is due to the apparently similar structure of oceanic and continental rifts, and also to the connection of the East African Rift System with the 'new' Red Sea and Gulf of Aden. The poles of opening of these three regions have been located (Le PICHON 1968; GASS and GIBBON 1969; ROBERTS 1969; BAKER 1969; McKENZIE et al 1970; FREUND 1970), and the consequent crustal extension along the East African Rift System inferred. However Al CHALABI (1971) has cast doubt on the reliability of deducing the East African Rift pole from those calculated for the opening of the Red Sea and the Gulf of Aden, while geologists have doubted the simple three plate system on structural, geomorphological and geological grounds (MOHR 1970; FREUND 1970; BAKER and WOHLENBERG 1971; Le BAS 1971; LOGATCHEV et al 1972). From a further comparison of oceanic and continental rifts, it is clear that the two are associated with different petrographic and structural styles (OSMASTON 1971; Le BAS 1971).

The volcanism associated with oceanic rifting is dominantly basaltic, occurring along an essentially linear system. It is characterized by transverse faulting, tensional phenomena and the abundance of dykes. In contrast, volcanism associated with continental

rift valleys is per-alkaline, with abundant alkaline basaltic rocks grouping together in regions of crustal swelling. Transverse faults are rare and despite the normal character of the rifts, none of them show signs of continued opening (Le BAS 1971). Even though isotopic evidence suggests that the Red Sea and Eastern Rift Valley formed at about the same time (FAIRHEAD et al 1972), temporal correlation does not imply similarity in mechanism of neo-oceanic and continental rifts. The East African Rifts should therefore be thought of as physical units rather than as a direct continuation of the World Rift System (BAKER and WOHLENBERG 1971).

A number of petrogenic theories have been put forward to explain the crustal doming and volcanism associated with the East African Rifts.

The enormous volumes of alkaline magmas of salic differentiate character, often with associated carbonatites, in East Africa, can be more easily explained by partial melting of the crystalline source rocks than by fractional crystallization. The latter process would require a vastly greater volume of parent magma.

Before it was generally considered that the Rift Valleys were extensional features, BAILEY (1964) believed that lateral compression caused the crustal upwarping. Pressure would be relieved underneath the swell, allowing partial melting of differentiated constituents from the underlying mantle.

Le BAS (1971) invoked conversion of mantle peridotite from a density of 3.5 to 3.3 gm/cm^3 over a distance range of some 35 km, which results in uplift of about 3 km (MAGNITSKY and KALASHNIKOVA 1970), and degassing of the mantle (HARRIS 1970) to account for the observed structure and volcanism in East Africa.

GILL (1973) explained the difference in abundance of continental alkaline igneous provinces from their oceanic counterparts in terms of

the crust acting as a 'density filter'. Its efficiency is related to the degree of crustal separation operating locally. In Ethiopia, crustal extension is fairly large, with volcanism overwhelmingly basaltic; while in Kenya, extension is small and the volcanism is dominated by less dense phonolites and trachytes.

OSMASTON (1971) assumed that mantle material was intruded into a fracture at the base of a 200 km thick lithosphere. Initial separation would be very slow, since the intrusion would be hampered by loss of heat to the fracture walls. As it penetrated nearer to the crust, it would not possess sufficient buoyancy to hold the crust up, causing rifting. The doming would be caused by expansion, from thermal energy gained by the intrusive zone walls. As separation proceeded the walls of the mantle would become heated, and fresh diapiric mantle material would reach shallower levels. The volcanism and faulting would then migrate towards the median line of the system.

GASS (1972), in explaining the tripartite Rift zone of the Gulf of Aden, Red Sea and the Ethiopian Rift, assumes that the continental lithospheric plate will not rift unless it has been previously weakened in some way. From the fact that local thermal instabilities occur at the base of a cool lithospheric slab and progress upwards by 'penetrative convection' (ELDER 1970), he concludes that there is an upward perturbation of the lithosphere-asthenosphere boundary. This has two effects. Firstly, partial melting would take place in the upper mantle, thereby making a large volume of basaltic magma available for extrusion. Secondly, the thermal gradient would be steeper above such a region, causing a downward movement of the main mineral phase boundaries in the mantle. As the minerals change to their less dense polymorphs, the resulting volume increase would be relieved by vertical uplift. Fractures would occur in the overlying crust and mantle as it was updomed, to give ready access to ascending magma. The first melts would originate at depths of about 60 km, producing alkali basalt magma, corresponding

to the situation in much of East Africa. Continued magma injection through the already injected zone would raise the thermal gradient, with the region of partial melting rising nearer the surface. The extruded volcanics would then become less undersaturated in silica, being generated higher in the mantle than their predecessors. Finally, injection into previously injected basalts would lead to the formation of oversaturated tholeiitic basalts, generated from a parent magma at depths of some 10 km (GREEN and RINGWOOD 1967). This stage was reached in the Gulf of Aden 25 my ago, and in the Red Sea some 5 my ago. The presence of less alkaline rocks within the Ethiopian Rift (HARRIS 1969; MOHR 1970) could mark an intermediate stage in the process. This is suggested also, by the fact that basalts with tholeiitic affinities have been observed within the Rift in Northern Ethiopia, while alkali basalts are observed on the Rift flanks (MOHR 1971). This change in composition could relate to the lowering of the thermal gradient away from the Rift axis. However, this does not imply that all such lithothermal systems will develop into new sources of ocean floor. When such thermal perturbations occur well within a continental region, a 'topographic blister' is produced, as is observed in the Eastern and Western Rift Valleys.

Geophysical studies in East Africa have provided substantial evidence for the presence of 'anomolous' mantle material existing beneath the Rifts.

1.5. GEOPHYSICAL RESEARCH IN EAST AFRICA.

1.5.1. AFRICA.

Away from the Rift zones, Africa would appear to have a structure similar to that of stable shield regions. BLOCH et al (1969) produced a number of crustal shear-wave velocity models from an analysis of the dispersion of Love and Rayleigh waves, between Kariba and Pretoria, and between Pretoria and Bulawayo. (MODEL 1; SASD 2.) They found that phase and group velocities in Africa are similar to, but slightly less than those in other shield regions. GUMPER and POMEROY (1970) from interpretation of surface and body wave data, have produced a mean crustal and upper mantle model for Africa (MODEL 2), which is but a slight modification of BRUNE and DORMAN's (1963) model for the Canadian Shield.

Using local earthquake data, WILLMORE et al (1952) and GANE et al (1956) have deduced the crustal structure of the Western Transvaal as in MODEL 3 a, b. There is evidence for including an intermediate layer in a) which increases the depth to the Moho; 23 km of a 6.1 km/s P-wave velocity layer, overlying 16 km of 6.8 km/s material. The P_n and S_n velocities of 8.27 km/s and 4.83 km/s are higher than the 8.06 km/s and 4.55-4.72 km/s from GUMPER and POMEROY'S (1970) model. These in turn are higher than those found in the Eastern Transvaal (MODEL 4) (HALES and SACHS 1959). Slight regional variations in Pn and Sn velocities have also been observed in the North American continent, which may be related to differences in depth to the Moho (HERRIN 1969).

1.5.2. THE RIFT SYSTEM.

The East African Rift System is outlined by a zone of shallow seismicity, which continues through the Gulf of Aden to the Carlsberg Ridge. (ROTHE 1954). This observation led to the concept of the East

MODEL 1

BLOCH, HALES and LANDISMAN

H (km)	V_s (km/s)
3.9	3.45
3.9	3.55
7.8	3.63
3.9	3.68
7.8	3.83
3.9	3.88
3.9	4.04
9.1	4.21
24.7	4.62
	4.75

MODEL 2

AFRIC MODEL

GUMPER and POMEROY (1970)

H (km)	V_P (km/sec)	V_S (km/sec)	(gm/cc)
7.0	5.90	3.35	2.70
10.5	6.15	3.55	2.80
18.7	6.60	3.72	2.85
80.0	8.05	4.63	3.30
100.0	8.20	4.78	3.44
100.0	8.30	4.65	3.53
80.0	8.70	4.85	3.70
	9.20	5.25	3.76

MODEL 3

a) WILLMORE, HALES and GANE

H (km)	V_P (km/sec)	V_S (km/sec)
36	6.09	3.68
	8.27	4.83

b) GANE, ATKINS, SELLSCHOP and SELIGMAN

H (km)	V_P (km/sec)	V_S (km/sec)
35.1 (from P wave data)	6.18	3.66
	8.27	4.73

(including about 1.3 km of low velocity superficial material)

MODEL 4

HALES and SACHS

H (km)	V_P (km/sec)	V_S (km/sec)
28.2 (from P-wave data)	6.0	3.6
8.4	6.7 - 7.2	3.95 - 4.15
	7.96	

African Rifts being connected to the World Rift System (EWING and HEEZEN 1956). Along mid-ocean ridges, earthquakes are confined to the median rift and fracture zones offsetting the ridge (FRANCIS 1968). In East Africa, however, there is a much greater scatter of epicentres, possibly due to the long history and complex nature of the continental crust (FAIRHEAD and GIRDLER 1971). Along the Western Rift, earthquake activity is, in general, confined to the Rift itself (SUTTON and BERG 1958), except for a broad belt some 400 km long, stretching west from Lake Kivu (de BREMAECKER 1959). Teleseismic activity is closely associated with the Rift, with only small magnitude events occurring outside it, (SYKES and LANDISMAN 1964; FAIRHEAD 1968; FAIRHEAD and GIRDLER 1971), while focal depths are almost all less than 40 km (WOHLENBERG 1970).

In contrast to the above region, there appears to be less seismic (and little or no teleseismic) activity associated with the Eastern Rift (FAIRHEAD and GIRDLER 1971). In the northern region from 1^{o}S, 36^{o}E up to Lake Rudolf, no earthquakes with magnitudes $M \geq 4$ could be located by WOHLENBERG (1970) and MOLNAR and AGGARWAL (1971). Activity is largely confined to the Kavirondo and Speke Gulf Rifts and the faulting in northern Tanzania. Microseismic activity is also very low in the north of the Rift, but increases to the south, being confined to the Rift floor and bordering faults, with no detectable activity on the flanks (TOBIN et al 1969). Focal depths are small being in general probably less than 5 km from the surface (MOLNAR and AGGARWAL 1971). To the south in northern Tanzania, RYKOUNOV et al (1972) have shown that earthquakes with $1 \leqq M \leqq 3$ originate from foci distributed throughout the crust, and have a most probable focal depth of about 15 km.

Coincident with the regions of shallow seismicity associated with the Rift Valleys, is strong geothermal activity. THOMPSON and DODSON (1963), by analysis of the locations of numerous steam jets

and hot springs near the most recent volcanoes of the Eastern Rift (Menengai, Longonot and Suswa) concluded that there was high heat flow in this region. Geothermal activity and recent faulting tend to be coincident (WAYLAND 1935; WALKER 1969; DIXON and MORTON 1969; BUCHSTEIN and Le BAIL 1969; REEVES 1969), while there is a distinct lack of activity along the older faults in Eastern and Southern Tanzania (FAIRHEAD and GIRDLER 1971). All heat flow measurements since 1971 have been obtained from relatively deep Rift Valley Lakes by oceanographic techniques. VON HERZEN and VACQUIER (1967) showed that the values obtained from Lake Malawi were similar to those obtained from South African shield measurements; about 1.1 cal cm^{-2} sec^{-1}. Except for one high value, twelve readings from locations in Lake Tanganyika produced similar results ranging from 0.4 to 1.4 cal cm^{-2} sec^{-1}. Recently, high values have been obtained from Lake Kivu, consistent with the present volcanic activity.

The coincidence of volcanism, seismicity and geothermal activity with the Rift Valleys and associated domal uplifts, has been explained to some extent by research into the crust and upper mantle systems beneath these regions.

1.5.3 THE UPPER MANTLE

SUNDARALINGAM (1971) studied the dispersion of Love and Rayleigh waves along paths which cross the Rift System. From a comparison with the dispersion curves produced by the AFRIC model (MODEL 2) of GUMPER and POMEROY (1970) (FIG. 3), it was noticed that at short periods the two curves merged, implying a similar crustal structure throughout Africa. At longer periods lower phase and group velocities than those predicted by the AFRIC model, imply the presence of a low velocity upper mantle zone beneath the Rift System. From an examination of dispersion curves along paths AAE-NAI and AAE-LWI, an upper mantle anomaly under the Eastern Rift is concluded to be of

Fig. 3. Observed Rayleigh wave phase (dots) and group velocities (crosses) for the AAE-NAI path (SUNDARALINGAM 1971) with computed dispersion curves for AFRIC model of GUMPER and POMEROY (1970).

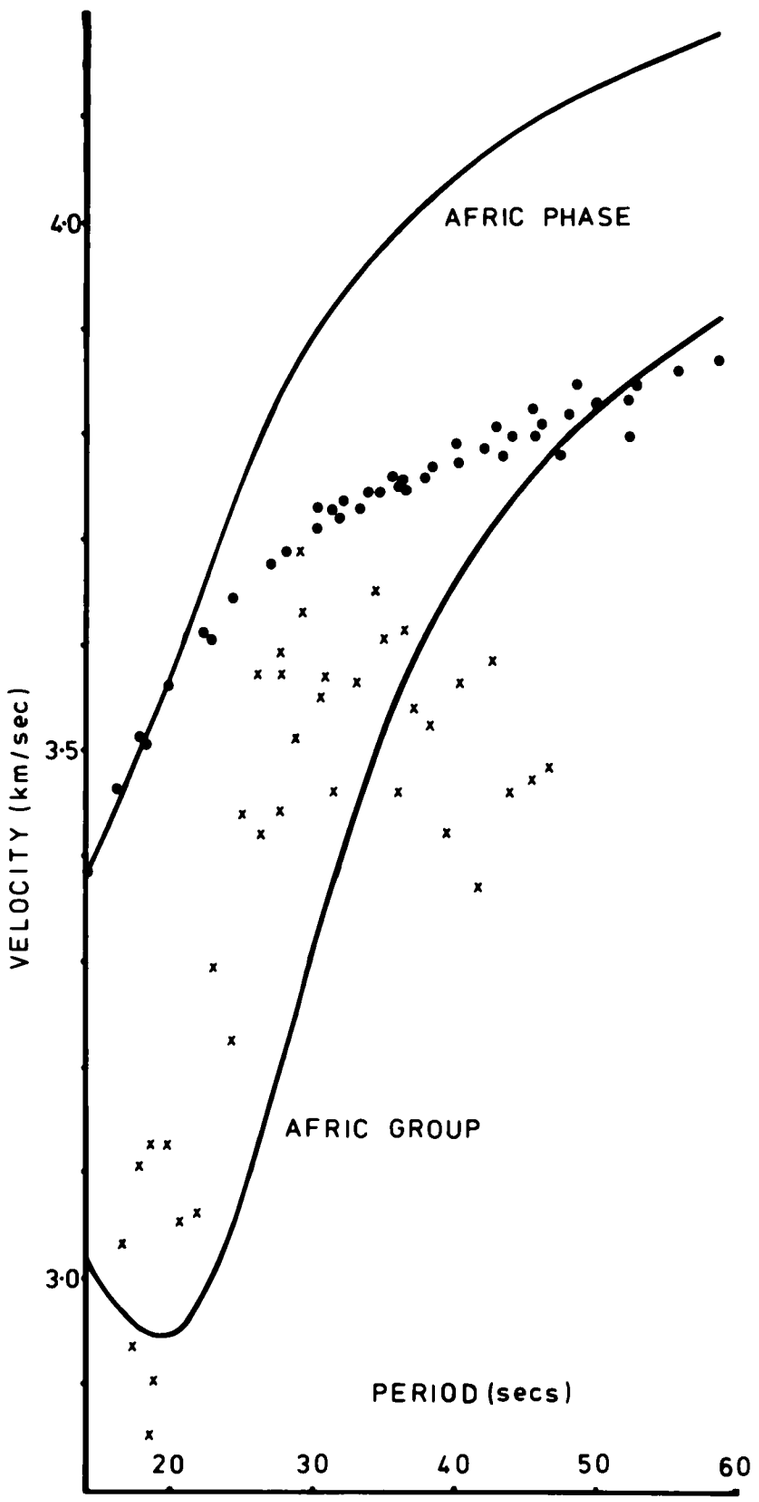
AFRIC PHASE
AFRIC GROUP
VELOCITY (km/sec)
4·0
3·5
3·0
PERIOD (secs)
20
30
40
50
60

greater extent than a similar region under the Western Rift. KNOPOFF and SCHLUE (1972) have interpreted the dispersion of Rayleigh wave phase velocities along the path AAE-NAI. Their results are consistent with a low S_n velocity mantle zone, about 120 to 200 km thick, existing beneath the Eastern Rift, with the possibility of a thin high velocity 'lid' at the top of the mantle. The Rayleigh wave phase velocities are low compared with most other shield regions, but similar to those obtained from the Basin and Range province of the Western United States, implying a similar gross mantle structure.

Body wave analysis appears to confirm the presence of an anomalous mantle zone beneath the Rift System. Station residuals, calculated from the analysis of teleseismic P wave travel times, show the stations at AAE and NAI to have large positive delays (HERRIN and TAGGART 1968; LILWALL and DOUGLAS 1970), while BUL has a small negative delay, typical of shield regions. SUNDARALINGAM (1971) has measured teleseismic P-wave delays at AAE, NAI and LWI relative to BUL, using events in the distance range $25^{\circ} \leqq \Delta \leqq 90^{\circ}$ (TABLE 1). Large positive delays at AAE and NAI, with a smaller positive delay at LWI, confirm the presence of a substantial low velocity zone in the upper mantle beneath the Eastern Rift, with a similar but less extensive zone beneath the Western Rift. BACKHOUSE (1972), has studied $\frac{dT}{d\Delta}$ and azimuth variations for events in the distance range $18^{\circ} \leqq \Delta \leqq 99^{\circ}$ from KAP. He deduced a model of a mantle low velocity zone, with sloping boundaries beneath the Gregory Rift. The zone attenuates rapidly to the west to sink beneath mantle material typical of the stable shield areas of Africa. From the absence of large azimuthal or distance variations in delay times measured at Kaptagat (limiting the angle of the 'wedge shaped zone' according to its velocity), he concluded that ultra low velocity material must exist within the anomalous zone, with relatively moderate dips on the zone boundaries.

TABLE 1

P-WAVE TELESEISMIC DELAY TIMES RELATIVE TO BULAWAYO (BUL) WITH 95% CONFIDENCE LIMITS

LOCALITY	DELAY
ADDIS ABABA (AAE)	2.7 ± 0.3 sec
NAIROBI (NAI)	2.3 ± 0.3 sec
LWIRO (LWI)	1.1 ± 0.3 sec
EASTERN RIFT STATION MEAN	2.5 ± 0.4 sec

This anomolous material is also evident from a study of the gravity data from East Africa. BULLARD (1936) showed that the broad negative anomaly over the whole of the East African Plateau, is consistent with that region being in approximate isostatic equilibrium, except over the Rift Valleys. In these areas, a long wavelength negative anomaly is superimposed on the broad regional low. Because the major anomalies have wavelengths of several hundreds of kilometres, they must be caused by mass distributions at depth, and not by near surface features. The broad negative anomaly coincident with the plateau, indicates that its mass effect must be compensated by a relative mass deficiency at depth (SOWERBUTTS 1969; GIRDLER et al 1969). Thus the cause of the anomalies has been related to low density material at the base of the lithosphere extending nearer the surface beneath the Rift Valleys. DARRACOTT et al (1972) from the results of gravity surveys in Southern Kenya and Northern Tanzania, consider that the lithospheric 'thinning' beneath the Eastern Rift dies out at about 4^{o}S.

1.5.4. CRUSTAL STRUCTURE.

The Rift Valleys have been shown to be bounded by normal faults, both from gravity (GIRDLER 1964) and geological data (DAVIES 1951). This is consistent with focal mechanism interpretations, which in general indicate normal or strike slip faulting in Eastern and Southern Africa (SYKES 1967; MAASHA and MOLNAR 1973). FAIRHEAD and GIRDLER (1971) conclude that the data is representative of a WNW-ESE tensional stress field. However, a compressive stress field has been observed in the Kafue Gorge on the Zambezi (HAST 1969), and one earthquake originating in Tanzania, has shown a component of thrust faulting (MAASHA and MOLNAR 1972). Thus it is possible, as de BREMAECKER (1959) concluded from the variation of fault directions, that no simple stress system operates throughout East Africa.

From the failure of S_n to propagate across the northern part of the Rift zone, GUMPER and POMEROY (1970) conclude that there is a 'gap in the lithosphere' in this region, indicative of anomolous Moho and upper mantle material beneath the Rift System. This is consistent with the results of MOLNAR and OLIVER (1969), who found that S_n does not propagate across the Eastern Rift to the north of Nairobi, yet does to the south. By mapping the region of Pn slowing down, and failure of Sn propagation, an inpressive correlation with the Rift System is observed. (FAIRHEAD and GIRDLER, 1971) (FIG 4). The anomalous Moho and upper mantle zone would appear to be closely related to the surface structure. RYKOUNOV et al (1972), from a local earthquake survey in the southern part of the Eastern Rift, concluded that crustal P-wave velocities in northern Tanzania (MODEL 5) are similar to those in stable shield areas. BONJER, FUCHS and WOHLENBERG (1970) predict the existence of normal shield crust beneath NAI, AAE and LWI. From the spectral analysis of long period body waves from two earthquakes in the Hindu Kush, they calculated depths to the Moho of 43, 39 and 35 km respectively

Fig. 4. Map of Africa, showing possible extent of the region of slow P propagation, (stippled) after FAIRHEAD and GIRDLER (1971).

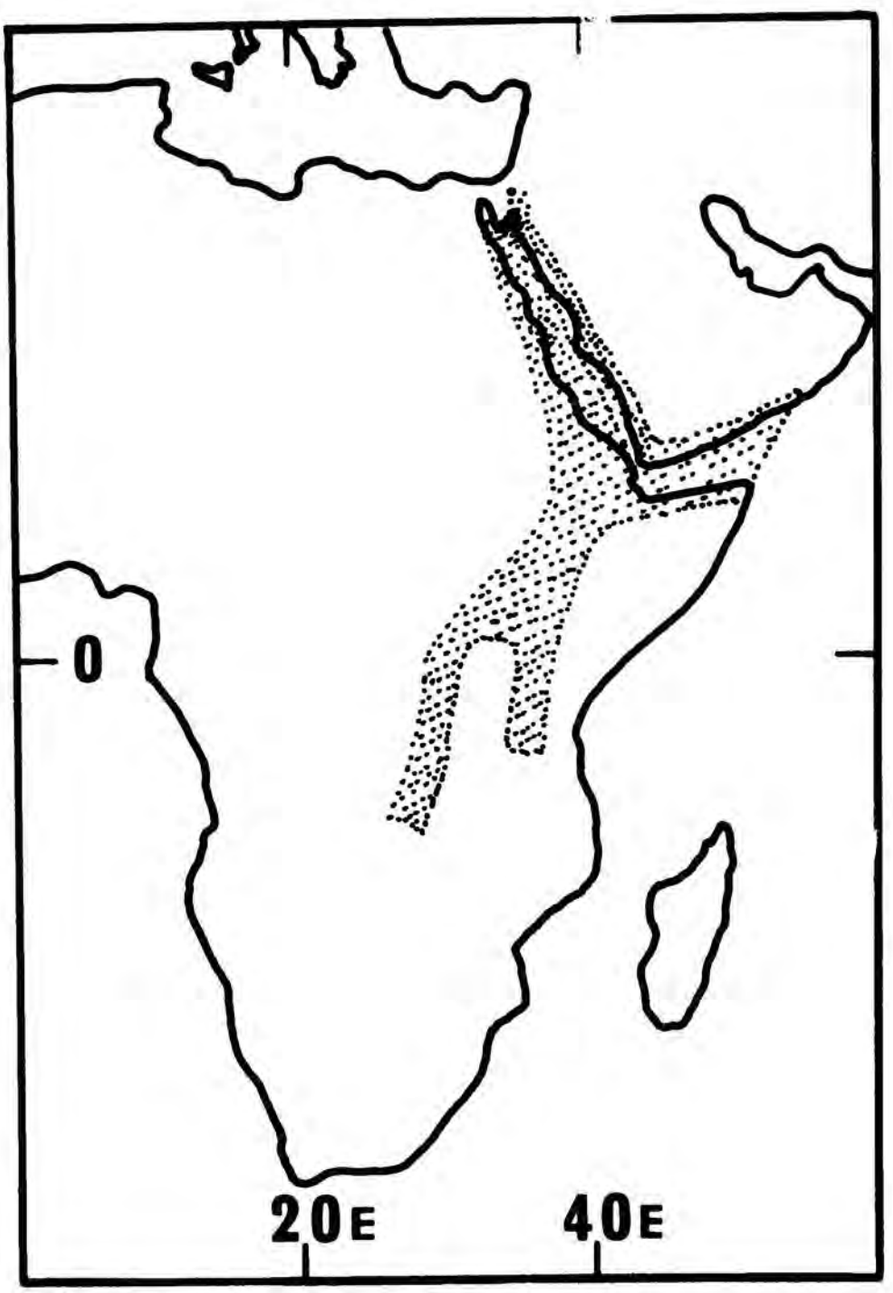
0
20E
40E

MODEL 5

RYKOUNOV, SEDOV, SAVRINA and BOURMIN

H (km)	V_P (km/sec)
18	5.8 ± 0.3
17 - 19	6.5 ± 0.3

MODEL 6

BONJER, FUCHS and WOHLENBERG

NAI		AAE		LWI	
H (km)	V_P (km/s)	H (km)	V_P (km/s)	H (km)	V_P (km/s)
16 (-17)	6.0	24	6.0	2	3.5
27 (-26)	6.7 (-7.1)	15	6.9	11	6.0
	8.2		8.2	22	6.7
					8.2

beneath these stations, with for NAI, an upper crustal layer of P-velocity 6.0 km/s (MODEL 6). From events recorded at NAI - AAE, LONG et al (1972) have shown that the surface wave data are consistent with near normal crust and topmost mantle existing to within some 50 km, east of the Eastern Rift axis. The fact that Sn is propagated between the Western and Eastern Rifts (MOLNAR and OLIVER 1969) suggests that normal Moho exists beneath the Lake Victoria downwarp. Thus the anomolous Moho and immediate upper mantle zone appears to be of limited lateral and longitudinal extent beneath the Eastern Rift.

A reversed seismic refraction line, shot from Lake Rudolf to Lake Hannington, has been interpreted in terms of an 18.5 km thick layer of P-wave velocity 6.4 km/s, overlying a layer of velocity 7.5 km/s (MODEL 7) (GRIFFITHS et al 1971). On reinterpretation, GRIFFITHS (1972) indicates the presence of an axial basic intrusion rising to within 10 km of the surface, and above which the crust is partially intruded. At a depth of about 20 km, there is a highly irregular contact with the 7.5 km/s material, presumed to be the upper surface of the low velocity, anomalous mantle zone.

The presence of the intrusion is confirmed by gravity studies over the Gregory Rift, which have shown the presence of a short wavelength positive anomaly over the axis of the Rift. This anomaly is 40 - 80 km wide, varying in amplitude from 30 - 60 mgals. SEARLE (1970) has interpreted a number of profiles across the Rift from latitude 0.25N to 1.25S in terms of a mantle-derived crustal intrusion of positive density contrast, reaching to within a few kilometres of the Rift walls in the vicinity of the equator.

The depth to its upper surface is about 8 km, except beneath the axis of the Rift, where it reaches to within 2 km of the Rift floor. BAKER and WOHLENBERG (1971) from gravity measurements ENE to WSW of Menengai explain the positive peak by a similar intracrustal

MODEL 7

GRIFFITHS, KING, KHAN and BLUNDELL

Dep (km)	V_P (km/s)	Depth (km)	V_S (km/s)
2.8 ± 0.5	3.0 ± 0.5 (assumed)	2.8 ± 0.5 (assumed)	1.8 ± 0.3
18.5 ± 4.5	6.38 ± 0.07	20.4 ± 6.2	3.53 ± 0.14
	7.48 ± 0.11		4.53 ± 0.21

body of positive density contrast, the top of which is 10 km wide, 1.5 km below sea level beneath the axis of the Rift (FIG. 5).

Using the seismic control of GRIFFITHS et al (1971), KHAN and MANSFIELD (1971) have interpreted the anomaly in terms of a simple intrusion of mantle material of single density contrast, penetrating the crust to a depth of 20 km beneath the Rift. This zone deepens to the Moho outside the flanks of the Rift.

The evidence for an axial basic, mantle-derived intrusion, reaching to within a few kilometres of the Rift floor, as postulated by GRIFFITHS (1972), SEARLE (1970) and BAKER and WOHLENBERG (1971), is supported by Quaternary grid faulting and the presence of numerous steam jets and fumaroles within the Rift Valley (SEARLE 1970). The positive anomaly follows the trend of the grid faults much more closely than that of the Tertiary faults bounding the Rift, and the grid faults and geothermal activity probably occur where the crust is thinnest. DARRACOTT et al (1972) consider that crustal penetration along the axis of the Gregory Rift ceases at about 2^{o}S. This is consistent with the results of MAASHA and MOLNAR (1972). If it is assumed that large stress drops reflect greater strength of material, then the scatter in earthquake locations and higher stress drops observed to the south of the Rift system, indicate that this region is a more stable area than that to the north.

An airmagnetic survey across the Eastern Rift in the Lakes Magadi and Hannington area revealed dominant NW - SE trending anomalies in each case. The half wavelength indicates their origin to be deep in the Earth's crust (WOHLENBERG and BHATT 1972).

In the Western Rift, DOPP (1964) has interpreted P-wave arrivals from local earthquakes in terms of an upper crustal layer of velocity 5.57 km/s overlying a layer of velocity 6.76 km/s. They are separated by a north - south striking boundary dipping 15 degrees to the west.

Fig. 5. Crustal structure computed from Bouguer gravity profile across the Gregory Rift just south of Menengai, after BAKER and WOHLENBERG (1971).

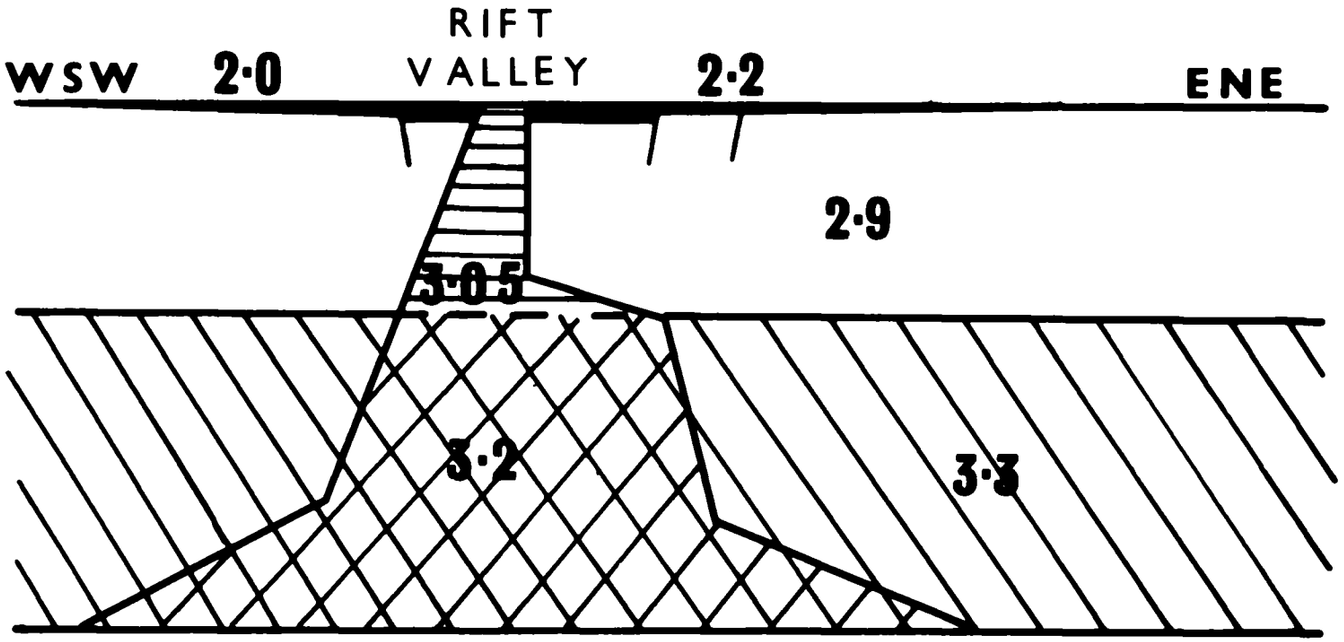
RIFT
VALLEY
WSW
2·0
2·2
ENE
2·9
3·05
3·2
3·3

These apparently normal crustal velocities and the lack of an axial positive Bouguer anomaly, as is evident over the Eastern Rift, would seem to indicate that there is little or no crustal penetration by anomalous mantle material beneath the Western Rift. However WOHLENBERG (1970) does provide evidence for a low velocity subcrustal layer, as postulated for the Rhinegoeben (LANDISMAN and MUELLER 1966; BERCKHEIMER and MEISSNER 1967) and the Basin and Range Province of the Western United States (COOK 1969).

CHAPTER 2

COLLECTION OF THE DATA

A small aperture array was set up at Kaptagat on the western flank of the Gregory Rift Valley in late 1968. Teleseismic arrivals recorded at the array have been used to study the deep structure beneath the Eastern Rift. Local and regional earthquakes originating from around the Eastern Rift, the Western Rift and the intervening East African Plateau have also been monitored and are being analysed to provide a detailed seismicity map of these areas. Selected local and regional events recorded at the array are used in this analysis to provide information about crustal structure, westward from the axis of the Gregory Rift in the vicinity of Kaptagat.

2.1. LOCAL GEOLOGY.

One of the requirements in siting an array is that it should lie on uniform geological structure, if possible. The Kaptagat array was situated on the Uasin Gishu lava flows, 2390m above sea level at latitude 35° 27'E, longitude 0° 27'N.

The lavas form part of the Kapsabet plateau, a structurally upstanding block bounded to the east, south and west by major faults. To the east lies the western boundary fault of the Gregory Rift, the Elgeyo escarpment. The major fracture to the west, running SSE from its emergence beneath the volcanic rocks of Mount Elgon is the Nandi fault. The Nyando fault, forming the northern escarpment of the Kavirondo Rift Valley lies on the southern boundary of the Kapsabet block. It runs ENE from the Kavirondo region, through a major fault zone to disappear beneath the uppermost flows of the Tinderet volcano. Between Tinderet and the Gregory Rift Valley, an east-west drainage pattern suggests control by movement on the Nyando fault.

The Uasin Gishu surface consists mainly of Tertiary lavas, overlying the Precambrian basement. These lavas, plateau phonolites, were erupted from Middle to Late Miocene, postdating the early periods of Tertiary uplift (SANDERS 1963; JENNINGS 1964; WILLIAMS 1970). Isotopic ages for the lavas lie between 12 to 13.5 my (KING and CHAPMAN 1972). They dip gently to the west and, it is thought, originated from fissures near the Rift shoulders. This is inferred from the gentle dips and the north-south trend of the lava contours. However, the fissures have not been identified despite deep erosion of the Rift shoulder volcanics. Two major phonolite flows are distinguished and the high ground near the Elgeyo escarpment may represent subsequent flows. The lower of the two phonolite flows is sparsely porphyritic, while the upper contains abundant large nephelines and glassy phenocrysts. A few isolated exposure of tuff confirm, that there was sufficient time lapse for the accumulation of a thin mantle of pyroclastic material

between the two phonolite flows. The lower flow forms the greater part of the plateau surface, while the later flow overlies it with a near continuous erosion scarp at the junction. The lavas immediately overlie the Precambrian basement complex. This consists of various gneiss forms, regionally striking NNW to SSE, with steep dips to the north east. In the north of the Kapsabet block, there is a predominance of biotite and hornblende-biotite migmatites, while to the south the basement is composed of biotite and granitoid gneisses (JENNINGS 1964).

The Kaptagat array is situated on the upper of the two phonolite flows, immediately to the east of the erosion scarp with the lower flow. The thickness of lava obtained from borehole measurements in the vicinity of the station can give an estimation of the depth to the basement beneath the array. From an examination of the height of the base of the lava flows, it is seen that there is an extremely gentle northward dip of the basement complex. The only borehole site at which the phonolite was pierced showed that it was 144m thick, under about 4m of soil. This site was situated on the lower phonolite flow about 15 km SW of Kaptagat. This suggests, together with minimum thicknesses from other boreholes and the near horizonal basement that about 170-200m of phonolite lie beneath the array. It may be considered, therefore, to lie on a thin, approximately horizontal, laterally uniform layer of volcanics over the basement.

2.2. THE ARRAY: SITING AND EQUIPMENT.

The array was in the form of an inverted L, each arm consisting of five vertical Willmore Mark II seismometers at approximately 1 km spacing (Fig. 6). The sites were surveyed to an accuracy of the order of $\pm$30m by compass and line method and differences in height were small, being less than 100m (TABLE 2). The pits were set in solid phonolite outcrops thus ensuring good ground motion coupling. The array was situated about 600 km from the East African coastline and microseism noise was low, about 7m The natural frequency of the seismometers was therefore set at about 0.05c/$_s$, due to this low noise level.

The equipment and system used was similar to that described by LONG (1968). The signals from the ten seismometers, together with that from a long-period seismometer were recorded onto 14 track magnetic tape, at a speed of 15/160 in/sec. Also recorded were a reference signal, a time code generated from a standard quartz crystal clock and a radio signal to check the clocktime against Greenwich Mean Time. Power was fed to the amplifier packages on the seismometers from a central recording station, along the same twin field telephone cable which carried the frequency modulated seismic signal. The whole system could be checked as well as calibrated by means of a calibration unit within the seismometer package. This was triggered by a pulse sent down the line from the central station. Playback facilities were available at Kaptagat, but the main data processing block is housed in Durham.

Fig. 6. Plan of Kaptagat Array with Red (R) and Yellow (Y) lines of seismometers.

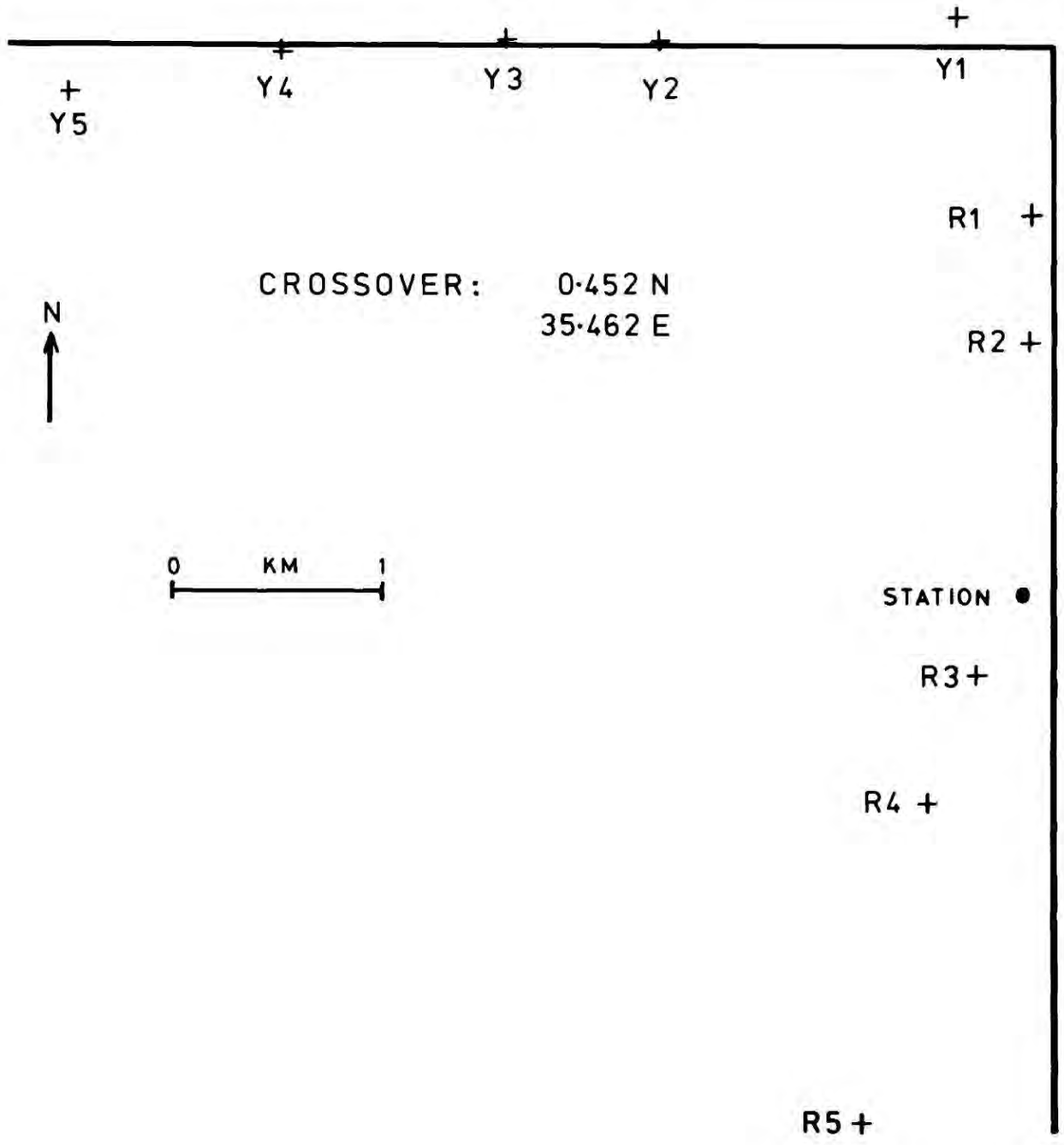
Y5
Y4
Y3
Y2
Y1
R1
CROSSOVER: 0·452 N
35·462 E
N
R2
0 KM 1
STATION
R3
R4
R5

TABLE 2

SEISMOMETER SITE CO-ORDINATES

AND ALTITUDES

(relative to cross over point)

PIT	X (km)	T (km)	ESTIMATED ERROR (km)	ALTITUDE (m)
R1	-0.098	-0.766	±0.010	+ 10
R2	-0.114	-1.425	±0.020	+ 20
R3	-0.365	-3.077	±0.010	+ 30
R4	-0.663	-3.736	±0.030	+ 10
R5	-0.925	-5.200	±0.010	+ 30
Y1	-0.446	0.166	±0.001	0
Y2	-1.888	0.003	±0.015	- 30
Y3	-2.645	0.025	±0.030	- 50
Y4	-3.720	-0.013	±0.010	- 50
Y5	-4.750	-0.250	±0.060	- 70

2.3. THE ARRAY: FUNCTION.

A two dimensional array of seismometers allows for the determination of both apparent ground velocity and azimuth of approach for earthquake waves. For velocity filtering, the simple configuration of two lines of seismometers at right angles will provide sharp velocity and azimuth responses dependent on

1) the azimuth of approach of the seismic signal

and 2) the dimensions of the array in relation to the wavelength of the signal.

The sharpest response is to be found when the array arms are comparable in length to the signal wavelength. (BIRTILL and WHITEWAY 1965). The frequency spectrum of an arrival varies with the nature of and distance to the source. Body waves originating less than 100 km from the array will contain significant energy up to about $20c/_s$. The energy content falls off rapidly with distance, such that teleseismic events contain most energy at a frequency of about $2c/_s$. The array with dimensions of the order of 5 km, will thus provide a sharp response for velocity filtering of local and regional events. High velocities from teleseismic events will not be determined accurately unless exact measuring techniques are applied.

CHAPTER 3
REDUCTION OF THE DATA

In this analysis, three parameters related to an earthquake signal are initially required

1) The apparent ground velocity of the first arrival across the the array.
2) The apparent azimuth of the first arrival at the array.

and 3) The epicentral distance from the earthquake source to the array.

Velocity filtering allows for the determination of parameters 1) and 2). The outputs from all the seismometers are recorded individually and delays are inserted in each record corresponding to an arrival of particular azimuth and velocity. These delays are altered until the maximum response of the summed records is reached for a particular velocity vector. This vector then indicates the true velocity and azimuth of the particular arrival.

A second method for determining parameters 1) and 2) above is onset time analysis.

By measuring the onset times of a seismic signal at each seismometer of the array, the two parameters may be determined by a least squares method from the equations relating onset times to the relative co-ordinates of the seismometers. The second method is likely to produce more accurate results (CORBISHLEY 1969) and has been used in this analysis.

3.1. ONSET TIME ANALYSIS.

Two methods for the reduction of onset times have been used

1) for a plane wavefront crossing the array for distant events

and 2) for a signal emanating from a point source crossing the array, for local events.

3.1.1. PLANE WAVEFRONT.

Assume a plane surface on which lie N seismometers at points (x_i, y_i) with respect to an arbitrary origin, in practice the cross-over point.

Let the signal traverse the array at constant velocity V from azimuth α. The i^{th} seismometer is represented by the radial distance R_i and azimuth Θ_i (Fig. 7).

The apparent velocity along R_i is

$$V/\cos(\theta_i - \alpha)$$

and the arrival time relative to that at the origin is given by

$$t_i = -R_i(\cos(\theta_i - \alpha))$$

$$= -\left\{\frac{x_i \sin\alpha}{V} + \frac{y_i \cos\alpha}{V}\right\}$$

If the arrival times for a given event are measured relative to some arbitrary zero time, preceding the i onsets, we may write

$$O_i = t_i + \tau$$

or

$$O_i = \tau - \frac{x_i \sin\alpha}{V} - \frac{y_i \cos\alpha}{V} + e_i \qquad (1)$$

where relative to the zero base line,

O_i is the observed arrival time

τ is the arrival time at the origin

and e_i is the error on O_i.

Fig. 7. Schematic diagram for plane wave crossing the array.

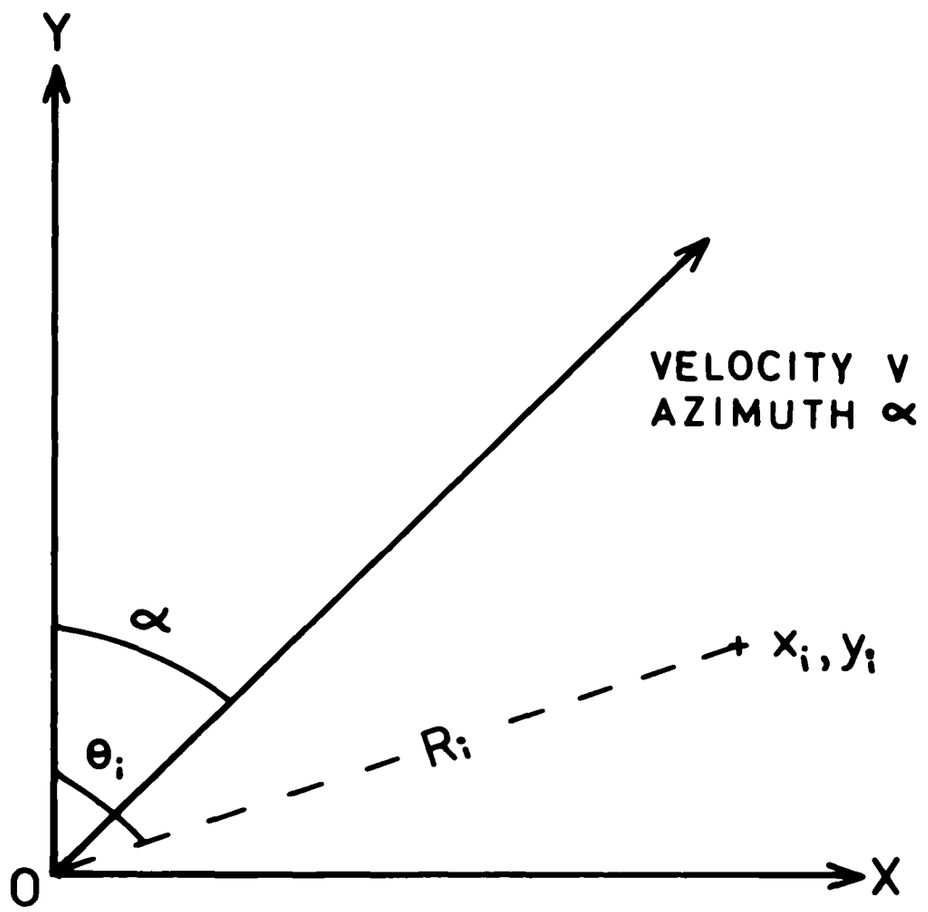
Y
VELOCITY V
AZIMUTH ∝
∝
x_i, y_i
θ_i
R_i
0
X

With N seismometers we have N equations with i : 1 → N. In each equation O_i is an observed quantity and x_i, y_i are the known co-ordinates of the seismometers.

With three unknowns incorporated in N equations, we may use the method of least squares to give $\frac{\sin\alpha}{V}$, $\frac{\cos\alpha}{V}$ and τ if the e_i are normally distributed.

3.1.2. METHOD OF LEAST SQUARES.

If e_i are the errors in n different equations of type:-

$$y_i = \sum_{j=1}^{m} a_j x_{ij}$$

the most probable values of a_j : j = 1, m can be found by making:-

$$\frac{\partial \sum_{i=1}^{n} e_i^2}{\partial a_k} = 0 \text{ for } k = 1, m.$$

The equations of condition are as:-

$$y_i = \sum_{j=1}^{m} a_j x_{ij} + e_i \qquad (2)$$

Now

$$\sum_{i=1}^{n} e_i^2 = \sum_{i=1}^{n} \left(y_i^2 - 2y_i \sum_{j=1}^{m} a_j x_{ij} + \left(\sum_{j=1}^{m} a_j x_{ij} \right)^2 \right)$$

and

$$\frac{\partial \sum_{i=1}^{n} e_i^2}{\partial a_k} = 2 \left(\sum_{i=1}^{n} \left(\left(\sum_{j=1}^{m} x_{ik} x_{ij} a_j \right) - x_{ik} y_i \right) \right)$$

For the best estimate of a_k

$$\sum_{j=1}^{m} \sum_{i=1}^{n} x_{ik} x_{ij} a_j = \sum_{i=1}^{n} x_{ik} y_i$$

producing m equations (k : 1 → m) with m unknowns, the normal equations. Writing in matrix form

$$XA = Y$$

the X matrix being symmetric.

The method of matrix inversion is used to solve these equations to obtain the values of the regression coefficients $a_j : j = 1, m$.

If the inverse of the matrix X is the matrix C then

$$CX = I$$

where I is the unitary matrix

thus

$$A = CY \qquad (3)$$

This is true as long as X is non-singular.

By this means, the most probable values of $\frac{\sin\alpha}{V}$, $\frac{\cos\alpha}{V}$ and τ may be determined, provided that the number of equations; that is the number of seismometers in operation is greater than three. α and V may thus be evaluated.

3.1.3. SIGNAL ORIGINATING FROM A POINT SOURCE.

As in the case of a plane wavefront, consider a plane surface on which lie N seismometers at points x_i, y_i with respect to an arbitrary origin (Fig. 8). The distance from the source to the i^{th} seismometer.

$$D = ((x_i + \Delta \sin\theta)^2 + (y_i + \Delta \cos\theta)^2)^{\frac{1}{2}}$$

The difference between this and the distance from the source to the origin is

$$D - \Delta$$

so for each seismometer the delay with respect to the time of arrival at the origin is

Fig. 8. Schematic diagram for curved wave-front crossing the array.

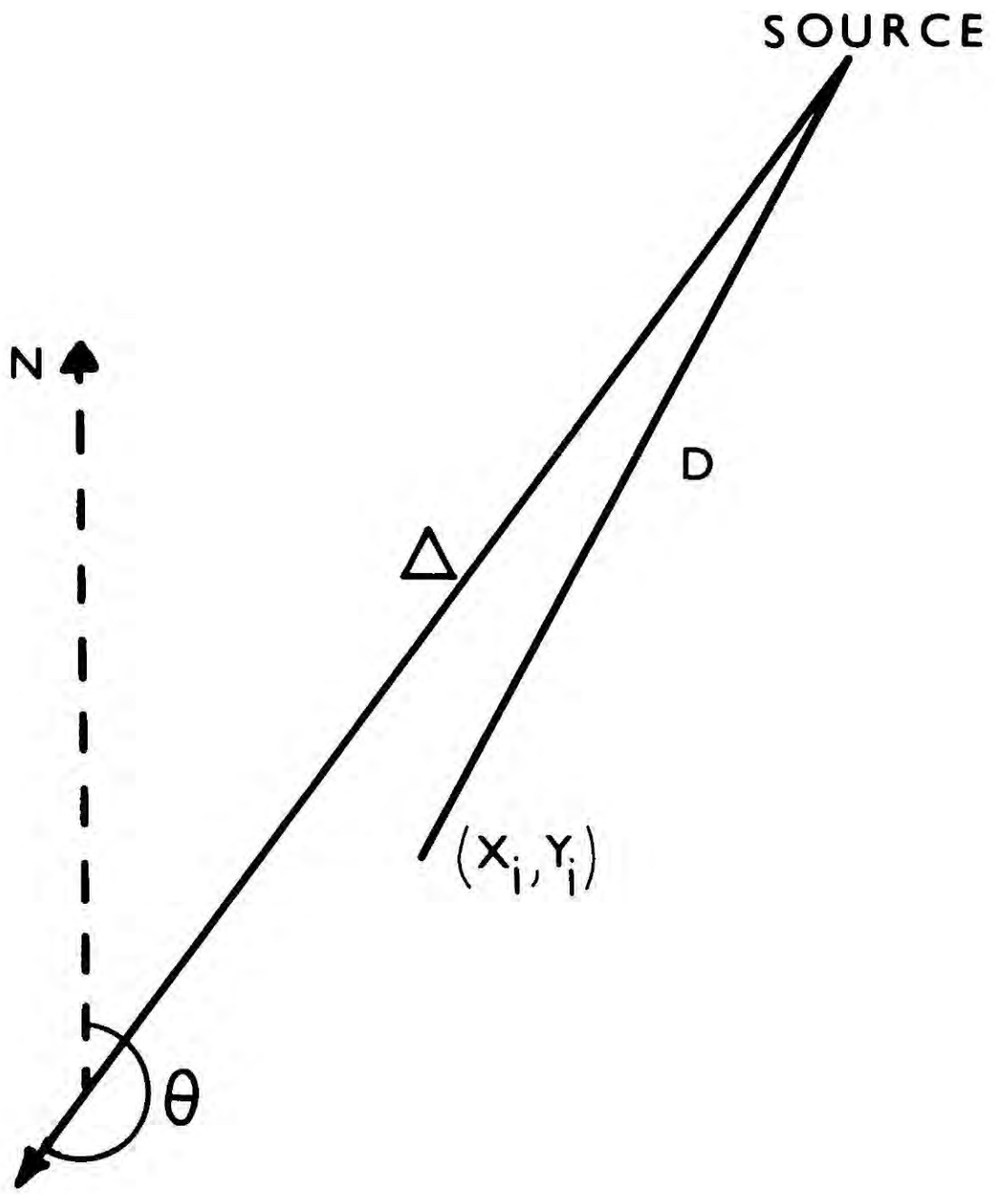
SOURCE
N
D
Δ
(X_i, Y_i)
θ

$$\delta t_i = \frac{D - \Delta}{V_A}$$

where V_A is the apparent velocity across the array.

If t_o is the arrival time at the origin, and t_i the arrival time at the i^{th} seismometer then

$$t_i = t_o - \delta t_i + e_i \qquad (4)$$

where e_i is the error on t_i.

With N seismometers there are N equations with four unknowns,

$$\Theta,\ V_a,\ \Delta \text{ and } t_o$$

The equations of condition (4) are non-linear in Θ and V_a, and therefore cannot be directly solved except by an iterative process. In order to reduce the number of unknowns in this analysis, the origin was taken at seismometer Y1. This eliminated the unknown t_o. Azimuth of event was therefore determined relative to Y1. By successively correcting V_a, Θ and Δ, the minimum value of $\sum_{i=1}^{n} e_i^2$ was obtained for the optimum values of V_a, Θ and Δ. It was found that Δ was not critical in determining the minimum value of $\sum_{i=1}^{n} e_i^2$ except for 16 events with $\sum_{i=1}^{n} e_i^2/n-1$ <0.003 seconds.

3.1.4. HEIGHT CORRECTION.

Differences in height of the seismometer sites will cause respective delays in the onset times of arrival at the ten sites.

The onset times must be corrected to

$$t_i^1 = t_i + (h_i - h_o)\left(\frac{1}{V_s^2} - \frac{1}{V_a^2}\right)^{\frac{1}{2}} \qquad (5)$$

where, h_i are the seismometer altitudes

ho, the height of the reference place (through the origin in 3.1.1. through seismometer Y1 in 3.1.3)

V_s, the signal velocity in the material beneath the sites.

V_a, the apparent velocity across the array.

The mean density of phonolite obtained from a number of samples from Kaptagat is 2.5gm/cc corresponding to a value of 4.5 km/s for V_s (BACKHOUSE 1972).

For the curved wavefront analysis the total delay in the arrival time t_i of a signal at the i^{th} seismometer with respect to Y1 is

$$\delta t_i = \frac{D - \Delta}{V_a} + \left(\frac{1}{V_s^2} - \frac{1}{V_a^2} \right)^{\frac{1}{2}} (h_i - h_o)$$

representing a conical wavefront crossing the array.

The plane wavefront analysis incorporates a linear least squares fit of a plane wavefront to the onset times at the array seismometers. However equation (5) is non linear. If t_i^1 is approximated to

$$t_i^{11} = t_i + (h_i - h_o)/V$$

i.e. a vertical signal path is assumed, then the matrix analysis of 3.1.2 may still be implemented.

The maximum value of $|h_i - h_o|$ is 0.07 km.

The error involved in assuming a vertical signal path is

$$E = |h_i - h_o| \left(\frac{1}{V_s} - \left(\frac{1}{V_a^2} - \frac{1}{V_a^2} \right)^{\frac{1}{2}} \right)$$

$$\simeq |h_i - h_o| \frac{V_s}{2V_a^2}$$

for $V_a = 6.0$ km/s

$E \simeq 4$ ms.

This is less than the reading accuracy of the onset times (see 3.4.2.), and hence may be neglected.

3.1.5. COMPARISON OF PLANE AND CURVED WAVEFRONT ANALYSES.

Using onset time analysis, it is possible to read the onset of a clear arrival to 0.01 seconds (see 3.2.). Thus an estimated error on the delay time of arrival between any seismometer site and the array origin will be 0.02 seconds.

If we consider a signal crossing the array parallel to one arm, then the delay time of arrival between the outermost seismometer of the other arm and the cross-over point will be

$$\delta t = \frac{1}{V_A} ((a^2 + \Delta^2)^{\frac{1}{2}} - \Delta)$$

where a is the arm length

and Δ the distance from the source to the array origin.

On expansion

$$\delta t = \frac{a^2}{2 \Delta V_a}$$

The maximum value of a is approximately 5 km, while for crustal velocities V_A is of the order of 5 to 8 km/s. The distinction between a curved and plane wavefront will become apparent when $\delta t > 0.02$ seconds.

that is when

$$\Delta < \sim 125 \text{ km.}$$

Errors in azimuth and velocity due to the assumption of a plane wavefront have been calculated for sources at 10, 30, 50 and 100 km for V_A equal to 6.4 km/s (Fig. 9). It is seen that the largest errors in velocity occur at true azimuths of 50 and 230 degrees.

Fig. 9. a) Error in velocity for curved wavefront analysed by plane wavefront formulation for a true ground velocity of 6.4 km/s.

b) Error in azimuth for curved wavefront analysed by plane wavefront formulation for a true ground velocity of 6.4 km/s.

Curves — — — correspond to 10 km
—·—·— epicentral 30 km
····· distances 50 km
——— 100 km

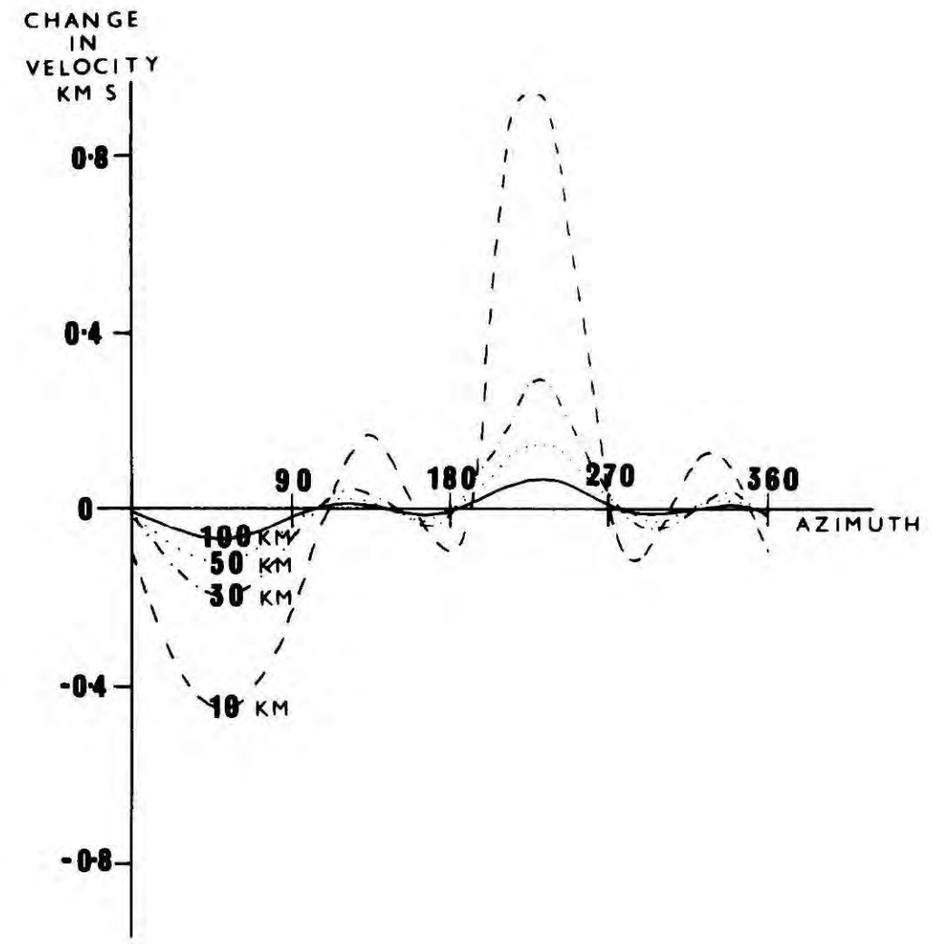
CHANGE
IN
VELOCITY
KM S
0·8
0·4
0
-0·4
-0·8
90
180
270
360
AZIMUTH
100 KM
50 KM
30 KM
10 KM

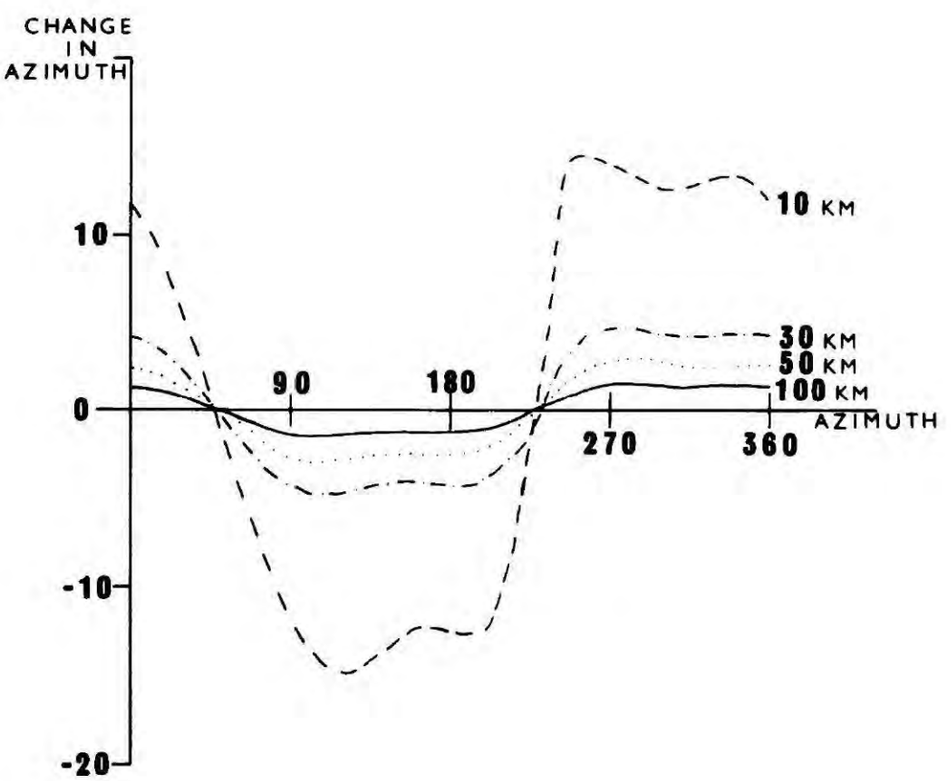
CHANGE
IN
AZIMUTH
10
0
-10
-20
90
180
270
360
AZIMUTH
10 KM
30 KM
50 KM
100 KM

3.1.6. ERRORS.

1. PIT LOCATION.

The estimated errors in the location of the pits are all less than or equal to $\pm$ 30 metres, excepting for Y5, which has an estimated error of $\pm$ 60 metres. This latter figure arose from the difficulty in surveying this site. By systematically moving the pits to the limits of their position accuracy, an estimate of the error in apparent velocity and azimuth of an event can be determined (Fig. 10). Such errors vary with true azimuth; the maximum error in azimuth being $\pm$ 1.05 degrees for any apparent velocity across the array, while the maximum error in velocity is no greater than $\pm$ 0.15 km/s for an apparent velocity of 8 km/s.

2. ERROR DUE TO THE PLANEWAVEFRONT ASSUMPTION FOR EARTHQUAKE ARRIVALS ORIGINATING FURTHER THAN 125 KM FROM THE ARRAY.

This error in azimuth and apparent velocity will vary with true azimuth, the amplitude of such variations decreasing with distance from the array. At 125 km for an 8.0 km/s arrival the maximum error in apparent velocity is $\pm$ 0.05 km/s, while the maximum error in azimuth is $\pm$ 1.0 degrees.

By changing the 'origin of the array from Y1 for the curved wavefront analysis to the crossover point for the planewavefront analysis, a slight variation in azimuth of event will be evident between the two analyses. The variation is a maximum of 4 minutes of arc for an arrival, originating 125 km from the array, and crossing the array normal to the line joining Y1 to the crossover point. This variation is negligible in comparison with the slight error introduced by the plane wavefront assumption.

Fig. 10. Estimate of error in apparent ground velocity due to inaccuracies in pit location for a true ground velocity of 8.0 km/s.

———————— line of pits moved systematically perpendicularly to N-S, E-W axis.

---------- individual pits moved on each line, varying angle between R and Y line from minimum to maximum.

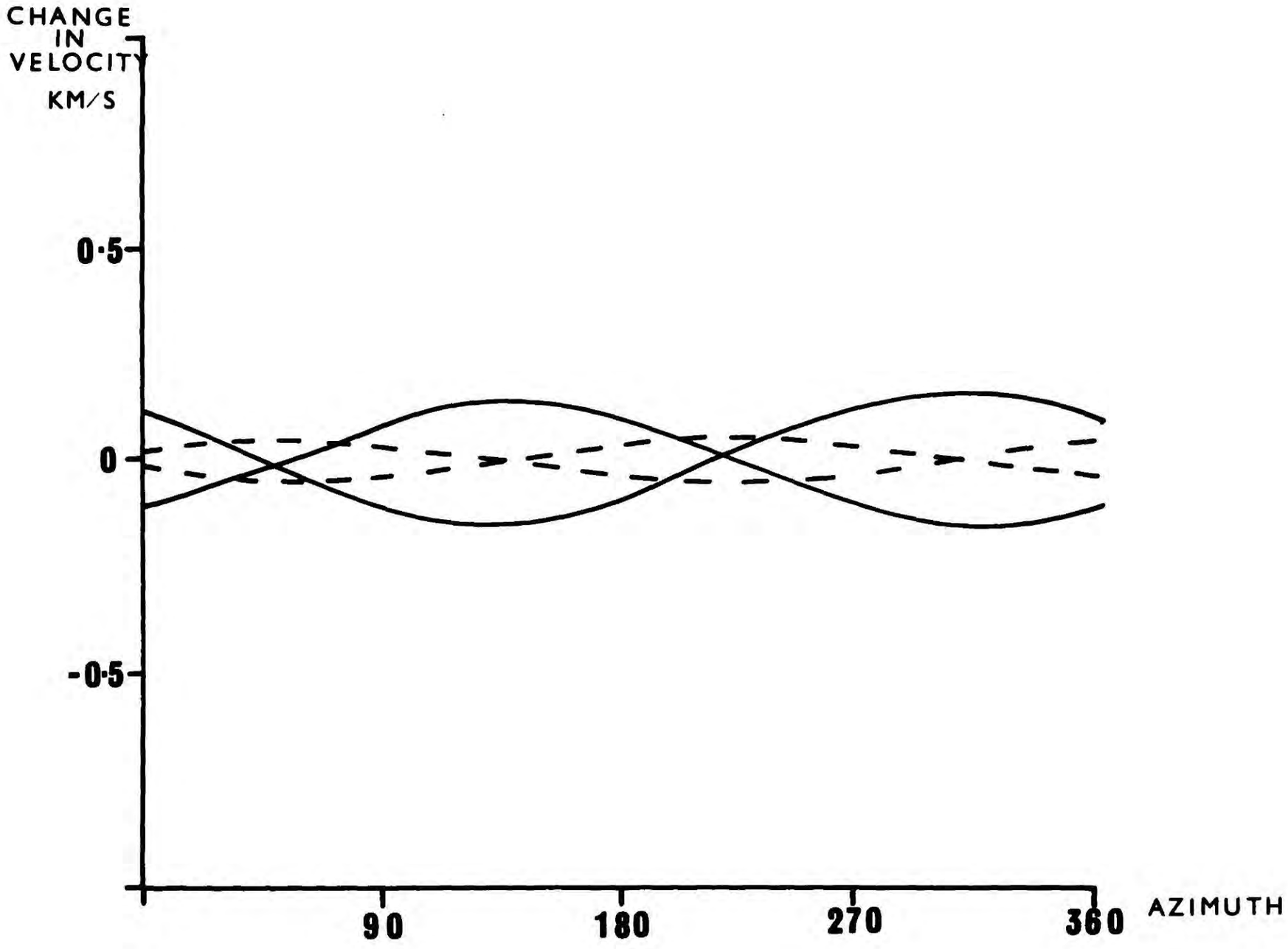
CHANGE IN VELOCITY KM/S
0·5
0
-0·5
90
180
270
360
AZIMUTH

3.1.7. PIT RESIDUALS.

The residuals ε_i are obtained from the observed minus calculated onset times of arrival of an event at each seismometer. Lateral inhomogeneities in structure, through which the rays travel from the source to each one of the ten seismometers will cause delays in the onset times dependent on that lateral variation. It is assumed that such variation occurs only in the immediate near surface structure, from the fact that the residuals do not appear to be dependent on the distance of the events.

Let the residual at the i^{th} seismometer for the k^{th} event

$$e_{ik} = \rho_i + e^1_{ik}$$

where ρ_i is the time error introduced by the near surface structure under the i^{th} seismometer.

For the plane wavefront formulation

$$y_{ik} = \sum_{i=1}^{m} a_{jk} x_{ij} + \rho_i + e^1_{ik} \qquad (6)$$

By solving these equations by least squares method in the presence of e^1_{ik}, it is possible to determine the most probable values of all the a_{jk}, together with the n values of ρ_i.

However a site correction ρ_i will consist of a constant term and an azimuthally varying term

$$A_i + B_i f(\Theta)$$

The term $f(\Theta)$, thus makes equation (6) non-linear.

A preliminary analysis was therefore carried out by analysing

$$e_{ik} = \rho^1_i + e^{11}_{ik}$$

determining

$$\rho^1_i = A^1_i + B^1_i f^1(\Theta)$$

without altering the values of a_{jk} by an amount dependent on ρ_i, to determine the true values of ρ_i

A_i^1 will provide information on lateral inhomogeneities beneath the sites, while if $f^1(\Theta)$ is assumed to be a first order sinusoidal function, $B_i^1 f^1(\Theta)$ can provide information about the structure in terms of a dipping layer beneath the array station (CORBISHLEY 1969). If $f^1(\Theta)$ is taken to be a higher order sinusoidal function, a closer fit to the residuals is more likely, but this would complicate any interpretation of the structure beneath the array.

By solving

$$e_{ik} = A_i^1 + B_i^1 \sin(\Theta_k^1 + \phi_i^1) + e_{ik}^{11}$$

by the method of least squares in the presence of e_{ik}''

where Θ_k^1 is the azimuth of the k^{th} event

and ϕ_i^1 the phase angle associated with the i^{th} seismometer

the most probable values of A_i, Bi and ϕ_i may be determined. The site correction ρ_i^1, will be a maximum when the azimuth Θ_k^1 is in the direction of dip, which is when

$$\Theta_k^1 = 90 - \phi_i^1$$

3.2. DETERMINATION OF ONSET TIMES.

The first arrival times of over a hundred local and regional events were picked, using a waveform matching process.

The records from Kaptagat are stored on 14 channel 1 inch magnetic tape. All ten seismometer channels were played out onto paper simultaneously, together with the binary time-coded clock channel. The playout speed of the 16 channel Jet-Pen Recorder was set such that one second corresponded to approximately 50 mm. Thus a reading accuracy of 0.5 mm corresponded to an onset time accuracy of 0.01 seconds.

In general, the signal to noise ratio for the local and regional events considered, was of the order of 2:1. For most of the arrivals, and especially those which were somewhat emergent, it was therefore difficult to recognize the first break on an unfiltered record. It was therefore concluded that a waveform matching process must be used, in order to determine the arrival stepout at each seismometer for a single event. In order to provide consistency throughout the results, this process was used for all the events considered. CORBISHLEY (1969) found that this method produced the lowest repeatable error in picking onset times as compared with measuring the arrival times of the first peak, or measuring the first cross-over point. MUIRHEAD (1968) in discussing variations in onset times, introduced by variations in seismometer characteristics, concluded that only high frequency events should be used, and that the onset time should be measured from the first convenient part of the waveform in order to minimize such variations. The first arrival of the events considered, in general appeared to have a frequency of about 2-3c/$_s$. In order to match the waveforms it was found necessary to filter the records. Three bandpass filters were available to filter the ten channels, and a band width of 0.3 - 5c/$_s$ was used. The events were thus played out three to four times depending on the number of operative seismometers,

with one filter kept on one channel, while the other two were stepped over the remaining recording channels. This was done in order to eliminate any relative delays, which the filters might impose on the records. The frequency range used in filtering the records provided a smooth waveform, suitable for matching across the records of the operative seismometers. In order to check the onset times calculated in this way, a number of events with very sharp onsets were also analysed by directly measuring the onset times of the first break on the unfiltered records. The resulting two evaluations of apparent velocity and azimuth of these events produced results lying within the confidence limits of the two parameters V and $\sim$ (see 3.5.1).

By tracing the output of one seismometer onto transparent paper and matching this waveform with the outputs from the other seismometers, the relative displacement of this curve can be measured in relation to a baseline, usually preceeding the onsets. Correlating the records by eye, in fact will give better results than velocity filtering methods since the latter is restricted to correlation over a fixed length of record for each trace, the window length being dependent on the storage size in the computer. Variations in tape speed and paper playout speed were taken into account by measuring the length of one second for each playout and correcting the onset times accordingly so that the time interval was consistent for all the seismometer channels for one event. Alignment of the Jetpens was also checked for each playout by triggering a calibration pulse on the Jetpen recorder. This alignment appeared to vary by a small amount for each playout and the onset times were corrected accordingly.

3.2.1. RANDOM READING ERRORS.

Variations in the measurement of onset times inherent in the analysis due to the subjectivity of the scientist, give reading errors which are assumed to be independent Gaussian variables with variance

σ^2. Thirty events were played out six times each, and an estimate of σ obtained from the relative values of the onset times for each playout of the thirty individual events. It was found that $\sigma \simeq 0.009$ seconds. Kelly (1964) has derived the root mean square error in slowness (the reciprocal of phase velocity) and azimuth due to random reading. From his derivations, the r.m.s. error in velocity has been calculated as

$$K \frac{\sigma V^2}{\sqrt{(mD)}} \left(\mathrm{VAR}[XX] \cos^2\beta - 2\,\mathrm{COVAR}[X, Y] \sin\beta \cos\beta + \mathrm{VAR}[YY] \sin^2\beta \right)^{\frac{1}{2}}$$

with the r.m.s. error in azimuth given by

$$\frac{\sigma V^2}{\sqrt{(mD)}} \left(\mathrm{VAR}[XX] \sin^2\beta + 2\,\mathrm{COVAR}[X, Y] \sin\beta \cos\beta + \mathrm{VAR}[YY] \cos^2\beta \right)^{\frac{1}{2}}$$

where m is the number of seismometers

V the phase velocity of an arrival

β the azimuth of the source from the array

XY the coordinates of the seismometers with respect to a N-S, E-W cartesian system

$$\mathrm{VAR}[XX] = \frac{1}{m} \sum_{i=1}^{m} (x_i - \bar{x})^2$$

$$\mathrm{COVAR}[XY] = \frac{1}{m} \sum_{i=1}^{m} (x_i - \bar{x})(y_i - \bar{y})$$

$$\text{and } D = \mathrm{VAR}[X]\,\mathrm{VAR}[Y] - \mathrm{COVAR}[XY]^2$$

The random reading errors should not be more than about 0.125 km/s and 0.5 degrees for velocity and azimuth respectively. This is for a phase velocity of 8 km/s, each error varying with the azimuth of the event from the array (Fig. 11).

Fig. 11. Random reading errors in velocity and azimuth at the Kaptagat array as a function of azimuth for an arrival with apparent velocity 8.0 km/s.

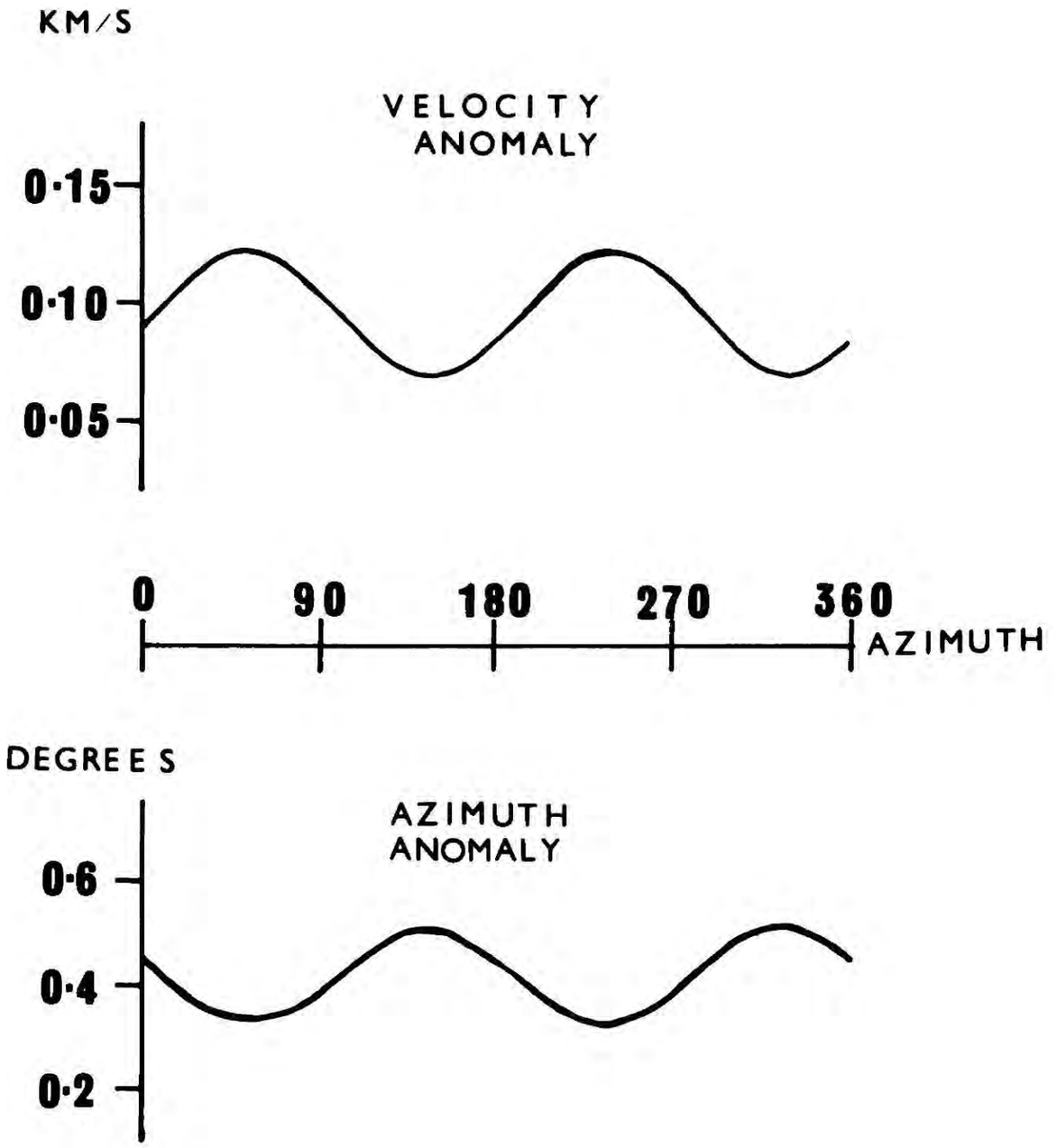
KM/S
VELOCITY
ANOMALY
0·15
0·10
0·05
0
90
180
270
360
AZIMUTH
DEGREES
AZIMUTH
ANOMALY
0·6
0·4
0·2

It is found that the combined error due to

1) pit location

2) plane-wavefront assumption for distant events

and 3) random reading

is approximately ± 0.2 km/s on the apparent velocity across the array and ± 2.5 degrees on the azimuth of approach of the seismic signal, for all azimuths of approach.

3.3. EPICENTRAL DISTANCE.

Two types of body wave emanate from a seismic source in a solid medium, a compressional P wave and a shear S wave. These two waves travel with different velocities in the same media. Thus by measuring the time interval between the first P onset and the first S onset of an event recorded at the array, an estimate of the epicentral distance may be determined.

3.3.1. INTERPRETATION OF P-S TIME AS DISTANCE.

Three unknowns relate the P-S time to epicentral distance

1) The ratio of the P velocity to S velocity along the ray path
2) The focal depth of the event
3) The structure through which the rays pass.

1) P VELOCITY TO S VELOCITY RATIO.

The ratio of P-velocity to S velocity can be related to Poisson's ratio as

$$R = \alpha/\beta = \left(\frac{2 - 2\sigma}{1 - 2\sigma}\right)^{\frac{1}{2}}$$

where α is the P wave velocity

β is the S wave velocity

and σ is Poisson's ratio.

For most rocks σ is approximately equal to 0.25. It is seen that a variation in σ of $\pm$ 0.03 about 0.25 causes a variation in R of $\pm$ 0.05 about 1.73 (Fig. 12). In this analysis a mean crustal value for σ of 0.254 is taken to correspond to

$$R = 1.74$$ (ANDERSON 1965).

For a horizontally homogeneous n-layered model, with an event focus in layer $j (1 \leq j < n)$

Fig. 12. Variation in P velocity to S velocity ratio, R with Poisson's ratio, σ.

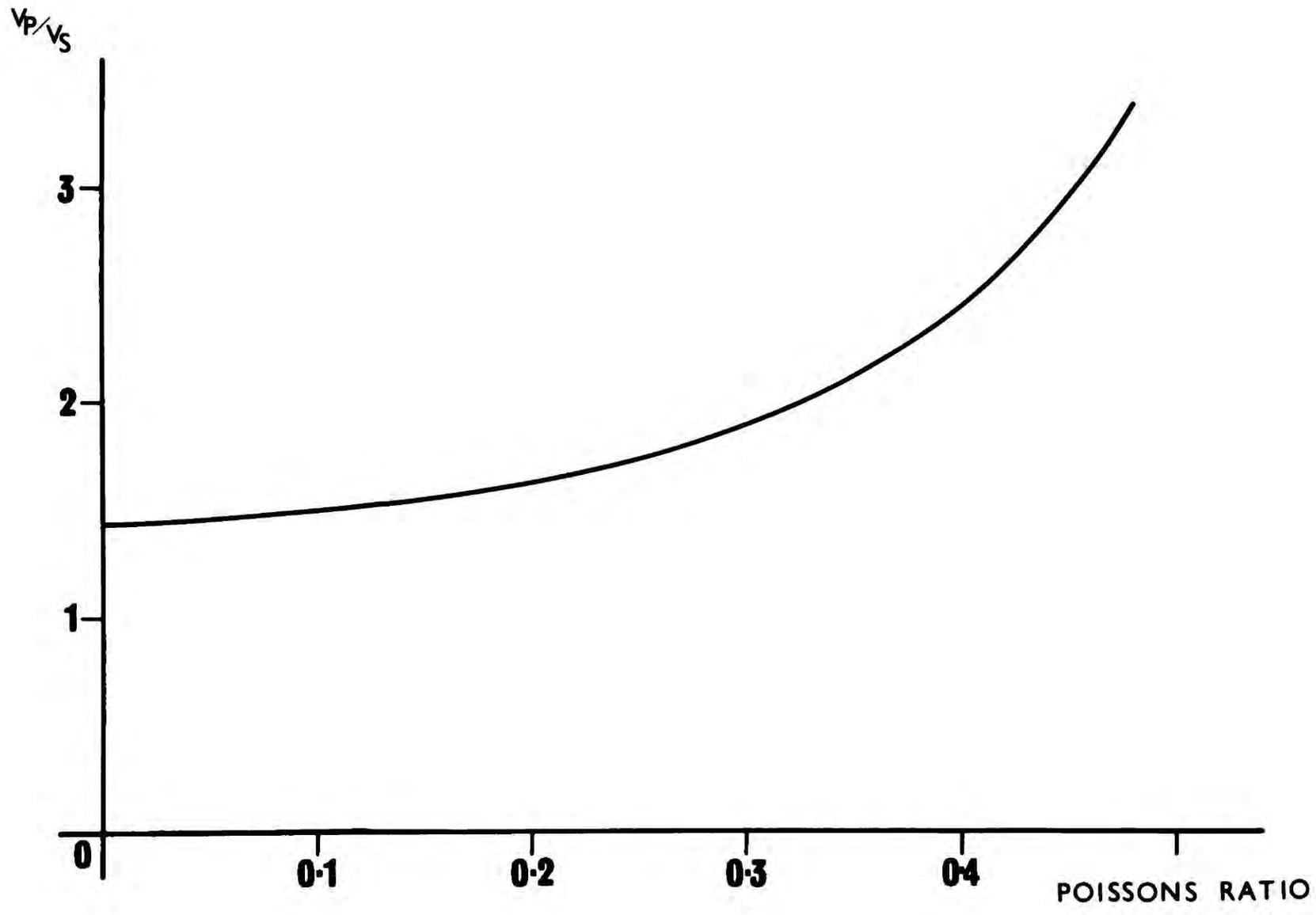
V_P/V_S
3
2
1
0
0·1
0·2
0·3
0·4
POISSONS RATIO

$$T_{ps} = x\left(\frac{1}{\beta_n} - \frac{1}{\alpha_n}\right) + \sum_{i=1}^{j} Z_i \left\{ \frac{(\beta_n^2 - \beta_i^2)^{\frac{1}{2}}}{\beta_i \beta_n} - \frac{(\alpha_n^2 - \alpha_i^2)^{\frac{1}{2}}}{\alpha_i \alpha_n} \right\}$$

$$+ \left(\left(\sum_{i=1}^{j} Z_i \right) - Z \right) \left\{ \frac{(\beta_n^2 - \beta_j^2)^{\frac{1}{2}}}{\beta_n \beta_j} - \frac{(\alpha_n^2 - \alpha_j^2)^{\frac{1}{2}}}{\alpha_n \alpha_j} \right\}$$

$$+ \sum_{i=j+1}^{n} 2 Z_i \left\{ \frac{(\beta_n^2 - \beta_i^2)^{\frac{1}{2}}}{\beta_n \beta_i} - \frac{(\alpha_n^2 - \alpha_i^2)^{\frac{1}{2}}}{\alpha_n \alpha_i} \right\} \qquad (8)$$

where T_{ps} is the P-S time of the event.

Z_i the thickness of the i^{th} layer.

Z the focal depth of event.

and α_i, β_i, the P and S velocity in layer i.

In order to determine the variation in epicentral distance with variation of R, assume R is constant along the ray path.

Then for a surface focus event

$$X = \frac{T_{ps}}{(R-1)} \alpha_n - \alpha_n \sum_{i=1}^{n} \frac{2 Z_i}{\alpha_n \alpha_i} (\alpha_n^2 - \alpha_i^2)^{\frac{1}{2}}$$

Hence for constant α_i, Z_i and T_{ps}

$$\Delta x = - \frac{T_{ps} \alpha_n}{(R-1)^2} \Delta R$$

Consider a crustal model with normal shield velocities with assumed values of

T_{ps} = 10 seconds

α_n = 6.0 km/s.

corresponding to a local event with a direct wave first arrival.

A change in R from 1.74 to 1.74 $\pm$ 0.05 produces a change in epicentral distance ■

$$x \simeq \pm 5 \text{ km.}$$

For T_{ps} = 100 seconds

α_n = 8.0 km/s

corresponding to a regional event with P_n as the first arrival, the same change produces a change in epicentral distance

$$\Delta x \sim 70 \text{ km}$$

Hence the error in epicentral distance due to an incorrect mean value of R increases quite substantially with increasing P-S time.

2. FOCAL DEPTH.

For constant α_i, R, Z_i and T_{ps}, and assuming the focal depth remains within layer j, from equation 8

$$\Delta x = - \frac{(\alpha_n^2 - \alpha_j^2)^{\frac{1}{2}}}{\alpha_j} \Delta Z$$

Consider a single layered crust overlying a normal Moho

Assume $\alpha_j = 6.4$ km/s

$\alpha_n = 8.0$ km/s

Then $\Delta x \simeq 0.75 \Delta Z$

Hence a variation in focal depth throughout the crust would cause a variation in epicentral distance comparable to the thickness of the crust.

3. STRUCTURE THROUGH WHICH RAYS PASS.

The ratio of P-S time to epicentral distance also depends on crustal structure. From a comparison of five reasonable models, four related to the African continent, and assuming horizontally layered structures and a constant focal depth, (Fig. 13) it is seen that the dependence is slight for P-S times of about 6 seconds, corresponding to an epicentral distance of about 50 km. The variation in epicentral distances increases with increasing P-S time to about $\pm$ 8 km at 15 seconds after which it is dependent only on the velocity of the Moho refractor.

Fig. 13. **P-S time (up to 14 secs) versus epicentral distance for 5 models and two focal depths 0 and 20 km.** Range of models included between limiting lines for each focal depth.

1) NAIROBI (BONJER, FUCHS and WOHLENBERG 1970)

2) AFRIC (GUMPER and POMEROY 1970)

3) RYKOUNOV et al (1972) (underlain by 8.1 km/s Moho).

4) GRIFFITHS et al (1971) (omitting surface volcanics).

5) $V = 5.65 + 0.0335z$.

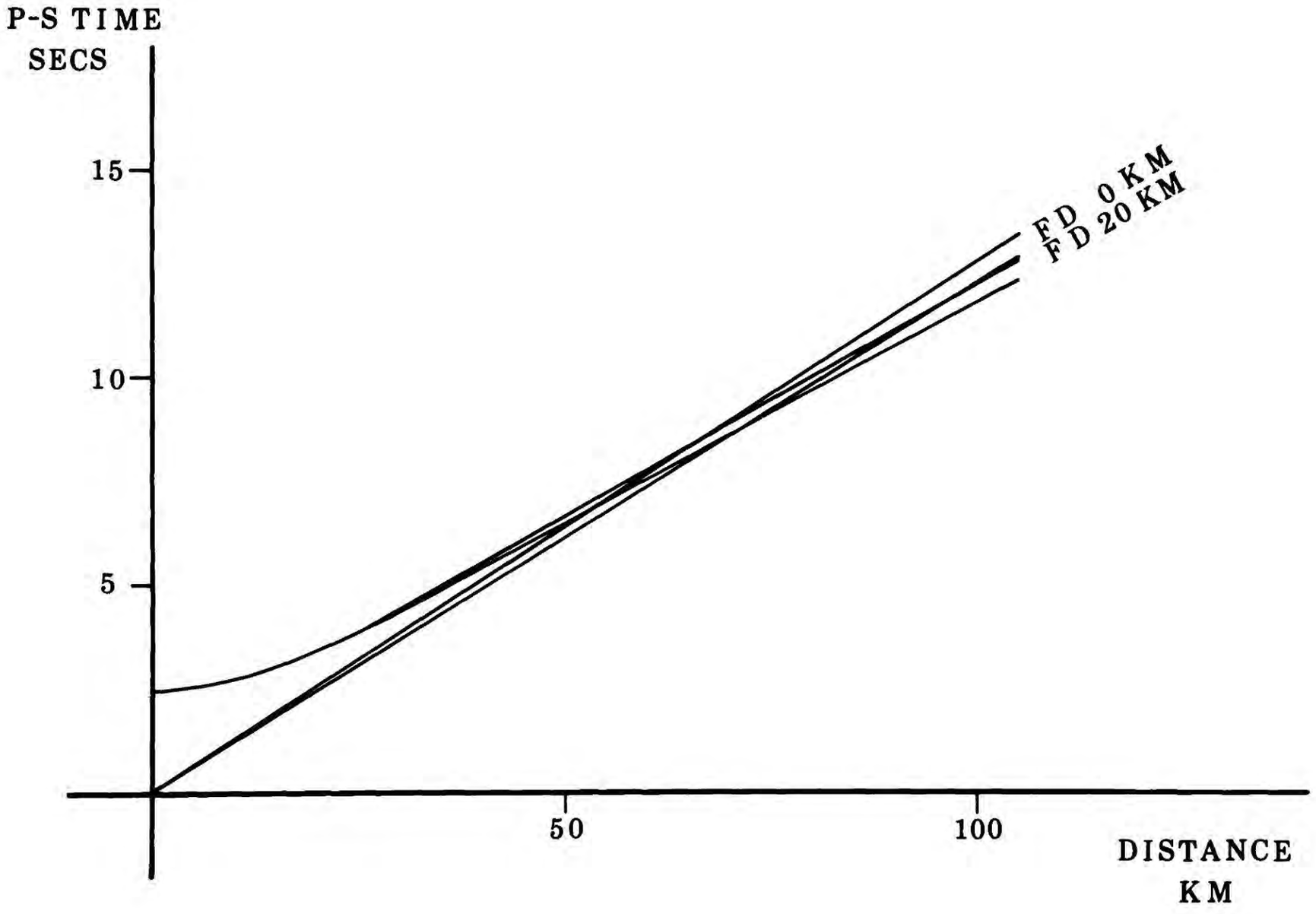
P-S TIME
SECS
15
10
5
50
100
DISTANCE
KM
FD 0 KM
FD 20 KM

Thus, in relating P-S time to epicentral distance, a substantial error increasing with epicentral distance is introduced before any measurement of onset times is carried out.

A variation in R of ± 0.05, a variation in focal depth of ± 10 km and a variation in the structure of normal shield crust corresponding to four models (1-4 in Fig. 13) would correspond to an estimated error of ± 10 km for local events, increasing to ± 90 km for regional events.

3.3.2. STRUCTURE OF RECORDS.

In order to relate epicentral distance to the P-S time of an event, it is necessary to distinguish between the various P and S phases on the record.

For earthquakes originating up to about 100 km from the array, local events, the records were characterized by a sharp P onset, followed by one or two seconds of large amplitude interfering arrivals. The P-wave train then remained at approximately constant amplitude until the beginning of the S group, characterized by an increase in amplitude and frequency (Fig. 14a). This second burst of energy was of longer duration than the initial P wave group, due to the superposition of S and surface wave arrivals.

For earthquakes originating up to about 200 km, the records retained the same structure as the local events outlined above but with P and S groups more complicated by crustal structure and increasing in amplitude from phase to phase (Fig. 14b). In this range S_n and S_g are almost indistinguishable, but both are separated from the surface wave group.

Beyond 200 km, corresponding to regional events, an increasing number of interfering arrivals caused the records to become extremely complicated but the pattern of P group, S group, surface wave group

Fig. 14. Examples of three events recorded at Kaptagat originating between azimuths 180 to 270 degrees.

1) epicentral distance <100 km.

2) epicentral distance <200 km.

3) epicentral distance >200 km.

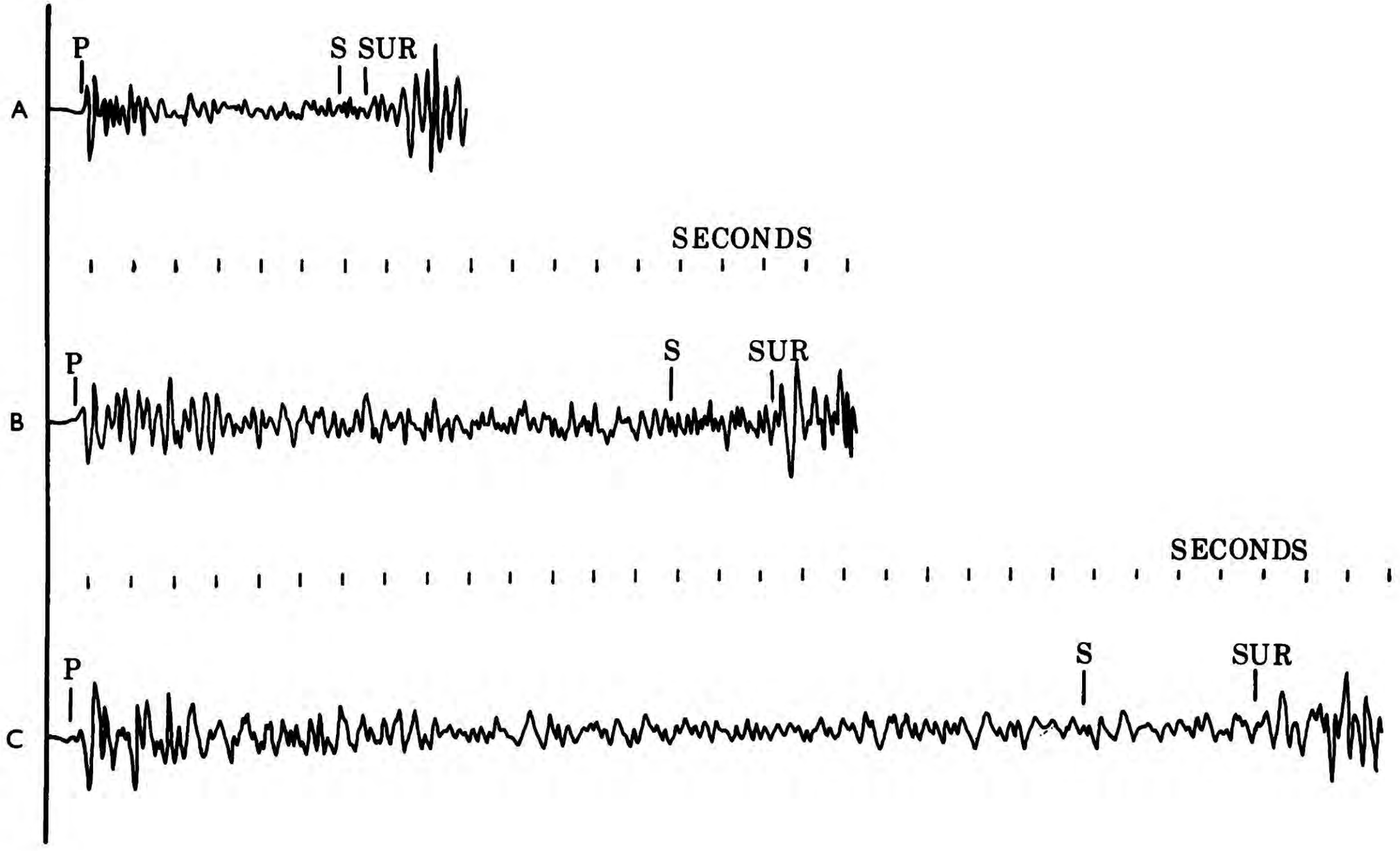
A
P
S
SUR
SECONDS
B
P
S
SUR
SECONDS
C
P
S
SUR

was distinguishable on most of the records (Fig. 14c). The S group was recorded as poor, fair or good dependent on the ease of identification.

3.4. P-S TIME MEASUREMENT.

The records from Kaptagat were all obtained from vertical component instruments, with resultant difficulty in identifying the S onsets, best recorded on horizontal seismometers. The first P onset was picked to an accuracy of 0.01 seconds on all the records, which theoretically ought to have been the same for the first S onset. However due to the difficulty mentioned above, this was not so. The initial S phase, following the same ray path as the initial P phase was picked, where possible, by noting an increase in frequency and amplitude of the earthquake wave train. For those events in which the S phase was lost in the end of the P wave train, the Surface wave onset was picked, which was of large amplitude on all the records. An empirical value for the P-S time was then determined from a relation between P-S time and P- Surface time calculated from those events with good S onsets (Fig. 15). Since this is an empirical method, the variation in group velocity of the surface wave train due to dispersion, although small, will be accounted for, assuming the dispersion is the same for all azimuths of approach.

The P-S times of 90% of the events were calculated from the records from seismometer Y1. When this was inoperative seismometer Y2 was used.

3.4.1. ERRORS.

1) INCORRECT READING OF THE INITIAL S OR SURFACE ONSET TIME.

On none of the records was the identification of the first S or Surface onset considered exact. For those events with good onsets, it was likely that the error was no more than one or two periods. However, for those events with poor onsets and large P-S times an error of up to ± 3 seconds was considered possible, corresponding to

Fig. 15. Empirical plot of P-S versus P-Sur times for events rccorded to south and west of Kaptagat.

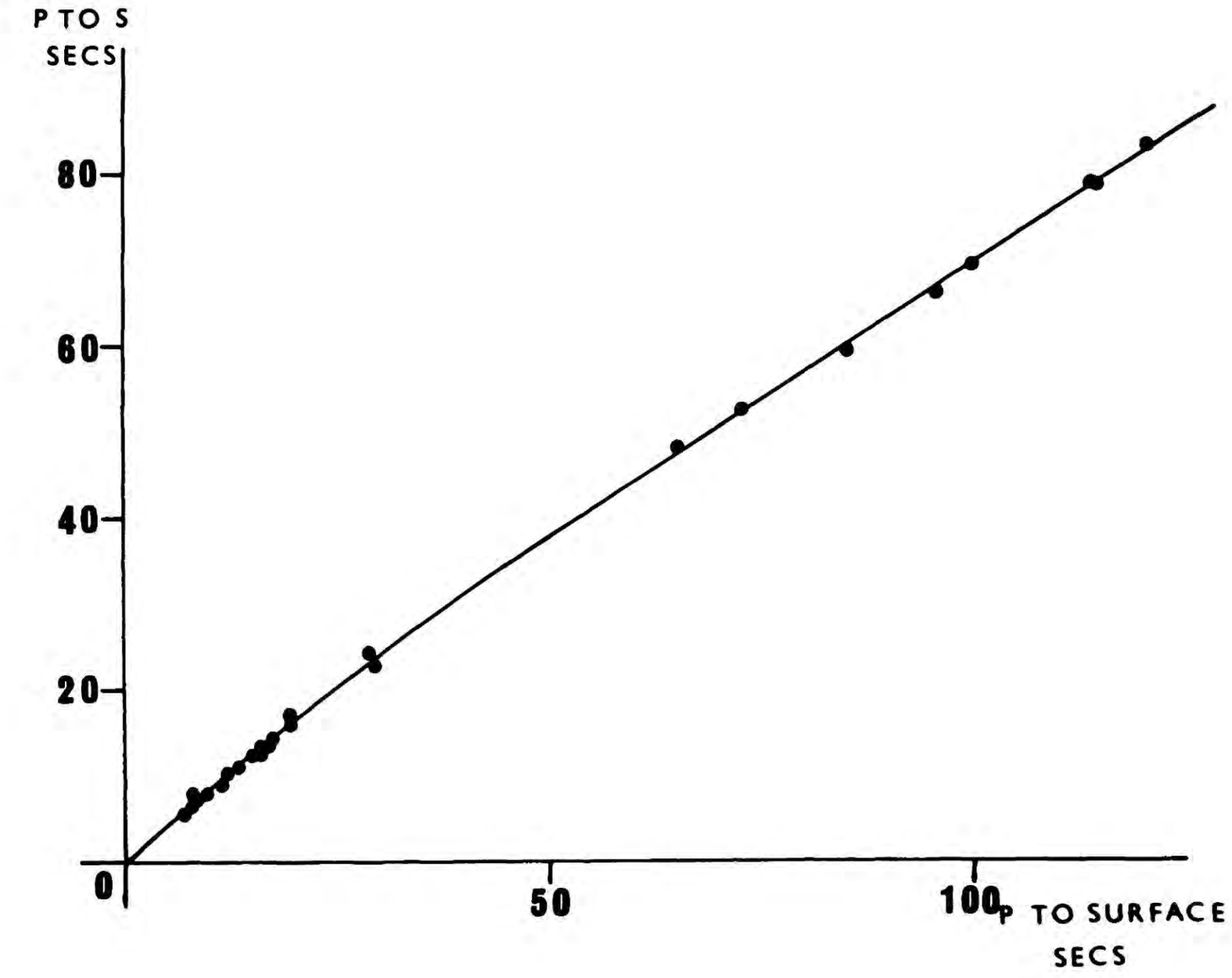
P TO S
SECS
80
60
40
20
0
50
100
P TO SURFACE
SECS

an error in epicentral distance of approximately $\pm$ 30 km.

Thus an error was estimated as increasing from 0 to $\pm$ 3 seconds for a P-S time increase of 0 to 30 seconds to include the worst possible case. For events with P-S times greater than 30 seconds, the error was assumed constant at $\pm$ 3 seconds.

2) Misidentification of S phase.

The epicentral distance was calculated on the assumption that the same P and S phase were being picked. However, refracted S arrivals were of low amplitude on all the records. For earthquakes originating within approximately 200 km of the array, it was impossible to distinguish between the direct and any refracted S arrival. Thus the error due to misidentification of the S-phase would be less than the error due to misidentification of the S onset, whether it be Sg, S* or S_n.

For events with P-S times of greater than 20 seconds, picking the P_n - Sg time, rather than the P_n - S_n time would cause the computed epicentral distance to be greater than the true value by an amount dependent on the epicentral distance.

Consider a simplified model of a 35 km thick crust with a P velocity of 6.4 km/s, S velocity 3.5 km/s, overlying a normal Moho with P velocity of 8.0 km/s, S velocity 4.6 km/s. The error in epicentral distance increases from 7 km at 200 km to 450 km at 800 km if P_n - Sg, rather than P_n - S_n is read.

However on one event S_n was clearly seen. This event was also recorded at five stations of the WWSS, one being at Nairobi. The WWSS report gave the epicentral distance as 710 km from Kaptagat, while from the Kaptagat record, the epicentral distance was computed as 706 km. The surface wave group was well recorded for all events with

P-S times of greater than 30 seconds. From comparison with the above event, it was considered that the same P and S phase were being identified for the calculation of P-S times for all the regional events.

3) Flat Earth Approximation.

In calculating epicentral distance the flat earth approximation has been used which introduces a very slight inaccuracy in the location of regional events. For an event originating 500 km from the array, the approximation will cause an error of 200 metres in epicentral distance, which is negligible compared with the errors outlined above.

4) Error due to reading records from seismometer Y2.

For those 12 events for which seismometer Y1 was inoperative, the maximum error in epicentral distance due to reading the P-S time from the Y2 record will be $\pm$ 1 km which is again negligible in comparison with the errors outlined above.

The error due to

1) Incorrect reading of the P-S time

and 2) variation in the model relating P-S time to epicentral distance.

increases from an order of $\pm$15 km for local events originating up to 100 km from the array, to $\pm$100 km for regional events with epicentral distances of 800 km.

However it should be emphasized that epicentral location is not critical in the following analysis.

3.5. THE DATA.

The first arrival onset times of 130 local and regional events have been picked and their azimuth and apparent velocity across the array determined. All the events were initially analysed assuming a plane wavefront crossing the array, after which 83 events with P-S times of less than 15 seconds (corresponding to epicentral distances of less than approximately 140 km) were analysed assuming a curved wavefront arrival. An estimate of the error in apparent velocity and azimuth of the individual events was calculated as follows.

3.5.1. 95% CONFIDENCE LIMITS.

From the plane wavefront analysis (3.1.1, 3.1.2) we have (equation 3)

$$A = CY$$

On expansion

$$\sum_{l=1}^{m} (a_l = \sum_{j=1}^{m} c_{lj} \sum_{i=1}^{n} x_{ij}\, y_i)$$

or

$$\sum_{l=1}^{m} (a_l = \sum_{i=1}^{n} y_i \sum_{j=1}^{m} c_{lj}\, x_{ij})$$

showing that a_l is a linear function of y_i. Now C is solely a function of X and thus $\sum_{j=1}^{m} c_{lj}\, x_{ij}$ is also solely a function of X and may be represented by a single k_{li}.

Hence

$$a_l = \sum_{i=1}^{n} y_i\, k_{li}$$

and it may be shown (DOUGLAS 1967) that:-

$$\text{VAR}\left[a_1\right] = \sum_{i=1}^{n} k_{1i}^2 \ \text{VAR}\left[y_i\right]$$

$$= \sigma^2 \sum_{i=1}^{n} k_{1i}^2$$

where $\text{VAR}[X]$ is the variance of X and $\sigma^2 = \text{VAR}[y_i]$ or the variance of the errors $e_i : i = 1, n$.

An estimate of σ^2 can be determined as

$$S^2 = \frac{\sum_{i=1}^{n} (e_i')^2}{n - m}$$

where n - m is the number of degrees of freedom and e_1' is determined by substituting the regression coefficients into the equations of condition.

It can be shown that $\sum_{i=1}^{n} k_{1i}^2$ is simply the 1^{th} diagonal element in the inverted matrix C. Now since a_1 is a linear function of y_i and y_i is normally distributed, a_1 will be normally distributed with a 95% confidence limit

$$\pm t \sqrt{S^2 \sum_{i=1}^{n} k_{1i}^2}$$

where t is Students t and depends on the number of degrees of freedom, n-m. In particular, with ten or less seismometers operating, n-m will be equal to or less than 7, and t will be greater than 2.306.

If $a_1 = \frac{\sin \alpha}{V}$ and $a_2 = \frac{\cos \alpha}{V}$

we may compute the 95% confidence limits on α and V by relating them to the standard errors of these two quantities, knowing that if

β_1 is the standard error on a_1

β_2 is the standard error on a_2

then as

$$V = f(a_1, a_2)$$

and $\alpha = g(a_1, a_2)$

$$\beta_v^2 = \left(\frac{\partial f}{\partial a_1}\right)^2 \beta_1^2 + \left(\frac{\partial f}{\partial a_2}\right)^2 \beta_2^2$$

and similarly for β_α^2

For the curved wavefront analysis (3.1.3), the equations (4) are non-linear, therefore the previous confidence limit analysis cannot be used.

However 95% confidence limits for the events with P-S times of less than 15 seconds were determined on the planewavefront analysis. These limits span the errors to the computed parameters Θ and Va on the curved wavefront analysis in all cases except one. This one exceptional event was that with the smallest P-S time. However $\sum_{i=1}^{n=1} e_i^2/_{n-1}$ from the curved wavefront formulation was less than $\sum_{i=1}^{n} e_1^2/_n$ from the plane wavefront for this event; (n, the number of operative seismometers).

This implies a more accurate location from the former analysis. Hence the 95% confidence limits calculated on the plane wavefront analysis were used to give an estimate of the error in velocity and azimuth computed from the curved wavefront analysis for all the events with P-S times of less than 15 seconds.

3.5.2. RESULTS.

98 of the events had a 95% confidence limit of less than or equal to $\pm$ 0.5 km/s on their first arrival velocity, while no event was considered with this error greater than $\pm$ 1.0 km/s. The large number of events analysed, whose 95% confidence limit on the first arrival velocity was greater than $\pm$ 1.0 km/s, included those arrivals recorded by only four or five operating seismometers, and also those emergent and low magnitude events whose first arrivals could not readily be distinguished from the background noise.

The confidence limits tend to increase with increasing velocity, which is to be expected for signals crossing a small uncalibrated array. The complete data set (TABLE 3) has been drawn up in two plots

1) Apparent velocity versus P-S time (Fig. 16)

and 2) Apparent velocity versus azimuth (Fig. 17).

The events were firstly located using a P-S time versus distance ratio obtained from the AFRIC model of GUMPER and POMEROY (1970) (MODEL 2).with a mean focal depth of 10 km. They were relocated using the crustal model derived from this analysis with

1) focal depths dependant on the apparent velocity across the array for local events

and 2) a mean focal depth of 16 km for regional events (Fig. 18).

3.5.3. EVALUATION OF SITE CORRECTIONS.

The values of e_{ik} (see 3.1.7) from the planewavefront analysis were determined from the best fit of a planewave through the onset times of an event at all the operating seismometers. The e_{ik} from the curved wavefront analysis were controlled by assuming that

$$\rho^{1}_{Y1} = 0 \qquad \text{(see 3.1.7).}$$

Let δ_{ik} be the residual at the i^{th} seismometer for the k^{th} event,

TABLE 3

THE DATA

EVENT	P TO S TIME (SECONDS)	VELOCITY (KM/S)	95%	AZIMUTH (DEGREES)	95%
1	2.7	9.6	0.2	99	4
2	3.0	7.6	0.2	328	3
3	4.0	6.6	0.4	205	8
4	4.2	6.5	0.2	185	6
5	4.4	7.0	0.3	177	6
6	4.5	6.7	0.3	187	4
7	4.7	6.6	0.3	183	3
8	4.8	6.4	0.4	215	3
9	4.9	5.9	0.3	187	7
10	5.0	6.6	0.4	185	4
11	5.1	5.7	0.3	188	4
12	5.6	5.9	0.4	223	6
13	5.8	6.7	0.2	219	3
14	5.9	5.8	0.5	226	5
15	6.0	5.8	0.2	220	2
16	6.1	6.1	0.4	220	6
17	6.1	6.3	0.4	222	2
18	6.2	6.4	0.3	173	5
19	6.3	6.0	0.2	219	4
20	6.4	6.0	0.2	220	2
21	6.4	5.7	0.4	223	7
22	6.5	6.3	0.4	197	8
23	6.7	7.0	0.6	69	8
24	6.8	6.1	0.4	204	7
25	6.8	6.3	0.2	204	4
26	6.8	6.0	0.6	221	2
27	6.9	6.0	0.3	205	6
28	6.9	5.8	0.3	221	5
29	6.9	7.1	0.3	223	5
30	7.0	6.2	0.2	201	6
31	7.0	6.3	0.2	203	2
32	7.1	6.2	0.3	205	7

33	7.2	7.1	0.6	82	3
34	7.2	8.0	0.3	86	5
35	7.2	6.7	0.2	193	4
36	7.2	6.5	0.2	199	5
37	7.2	6.1	0.2	205	3
38	7.2	6.1	0.2	205	3
39	7.3	6.8	0.2	200	3
40	7.3	6.3	0.2	201	4
41	7.4	6.4	0.2	203	3
42	7.5	6.3	0.2	205	4
43	7.6	7.8	0.3	85	5
44	7.6	6.5	0.5	205	8
45	7.8	7.2	0.4	94	5
46	7.8	7.0	0.5	95	9
47	7.8	7.1	0.5	193	6
48	7.8	6.0	0.2	205	5
49	7.8	6.2	0.3	207	4
50	7.9	7.2	0.4	113	7
51	7.9	6.1	0.3	204	7
52	8.0	6.1	0.4	271	7
53	8.1	7.4	0.4	191	4
54	8.2	6.6	0.5	103	6
55	8.3	6.9	0.3	122	3
56	8.4	6.9	0.3	193	6
57	8.5	7.0	0.2	112	4
58	8.8	5.6	0.5	203	5
59	8.9	6.8	0.6	193	5
60	8.9	7.1	0.3	243	2
61	9.1	8.1	0.6	104	9
62	9.2	6.3	0.3	186	5
63H	9.4	7.9	0.2	106	5
64	9.4	7.3	0.3	121	6
65	9.5	7.8	0.4	61	4
66	9.9	6.5	0.4	238	5

67	10.7	6.5	0.2	201	8
68	11.1	6.5	0.2	221	5
69	11.2	7.1	0.6	116	8
70	11.3	6.9	0.3	121	8
71	12.3	5.8	0.6	34	6
72	12.3	6.7	0.3	216	4
73	12.4	7.8	0.7	213	5
74	12.8	6.4	0.6	227	9
75	13.3	8.0	0.2	222	6
76	13.5	6.4	0.2	295	5
77	13.7	6.7	0.7	227	7
78	13.8	6.0	0.3	290	2
79	13.9	6.2	0.3	231	8
80	14.3	7.2	0.4	219	8
81	14.6	6.8	0.5	229	2
82	14.7	6.7	0.6	222	4
83	14.9	8.1	0.6	255	7
84	15.1	7.8	0.4	238	5
85	15.2	6.4	0.4	236	3
86	15.3	6.1	0.3	229	4
87	15.9	7.7	0.8	228	3
88	17.5	6.7	0.3	237	4
89	20.0	7.6	0.6	158	8
90	20.0	6.7	0.3	23	4
91	21.0	6.9	0.4	20	3
92	22.5	6.8	0.3	150	5
93	22.6	7.5	0.6	16	7
94	22.7	6.6	0.3	192	3
95	23.1	7.9	0.4	204	5
96	23.5	7.5	0.2	157	2
97	24.0	7.3	0.3	152	9
98	24.0	8.3	0.6	210	8
99	24.1	7.8	0.7	206	4
100	24.2	7.0	0.5	157	3

101	24.3	8.2	0.6	192	4
102	24.4	7.9	0.5	196	4
103	24.6	7.2	0.5	193	8
104	24.7	7.0	0.2	149	7
105	24.8	7.8	0.3	203	5
106	26.0	7.4	0.7	138	4
107	30.5	8.3	0.8	233	6
108	37.1	7.8	0.2	202	2
109	42.5	8.4	0.6	267	5
110	46.2	8.1	0.7	264	8
111	47.0	8.0	0.8	282	8
112	47.3	7.8	0.4	204	6
113	48.3	7.9	0.5	257	9
114	48.4	8.4	0.5	190	4
115	50.7	8.0	0.8	268	7
116	52.5	7.9	0.7	282	6
117	53.0	7.8	0.6	272	8
118	54.0	7.9	0.5	278	7
119	54.1	7.8	0.5	255	8
120	58.3	7.4	0.8	271	3
121	58.8	8.4	0.5	269	6
122	59.2	8.1	0.7	265	9
123	60.7	6.3	0.7	213	4
124	62.2	8.2	0.5	255	7
125	66.2	7.9	0.6	259	3
126	69.4	8.0	0.2	211	7
127	76.7	7.9	0.3	192	5
128	79.2	7.9	0.6	257	4
129	80.5	8.0	0.5	172	10
130	83.6	8.1	0.6	256	6

Fig. 16. Apparent velocity versus P-S time of events.

(• AZIMUTHS 160 - 360 degrees

| AZIMUTHS 0 - 160 degrees).

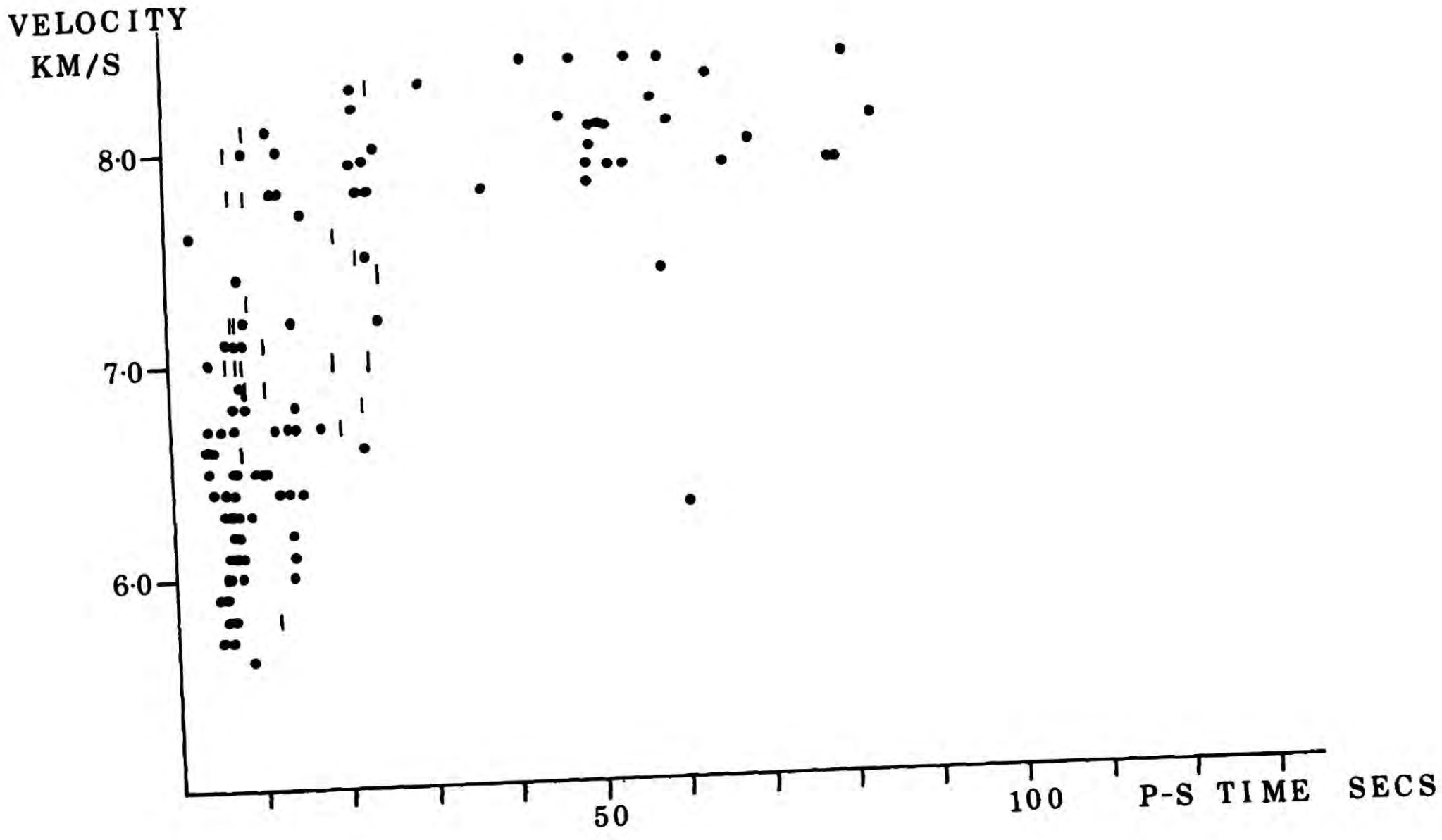
VELOCITY
KM/S
8·0
7·0
6·0
50
100
P-S TIME SECS

Fig. 17. Apparent velocity versus apparent azimuth of events.

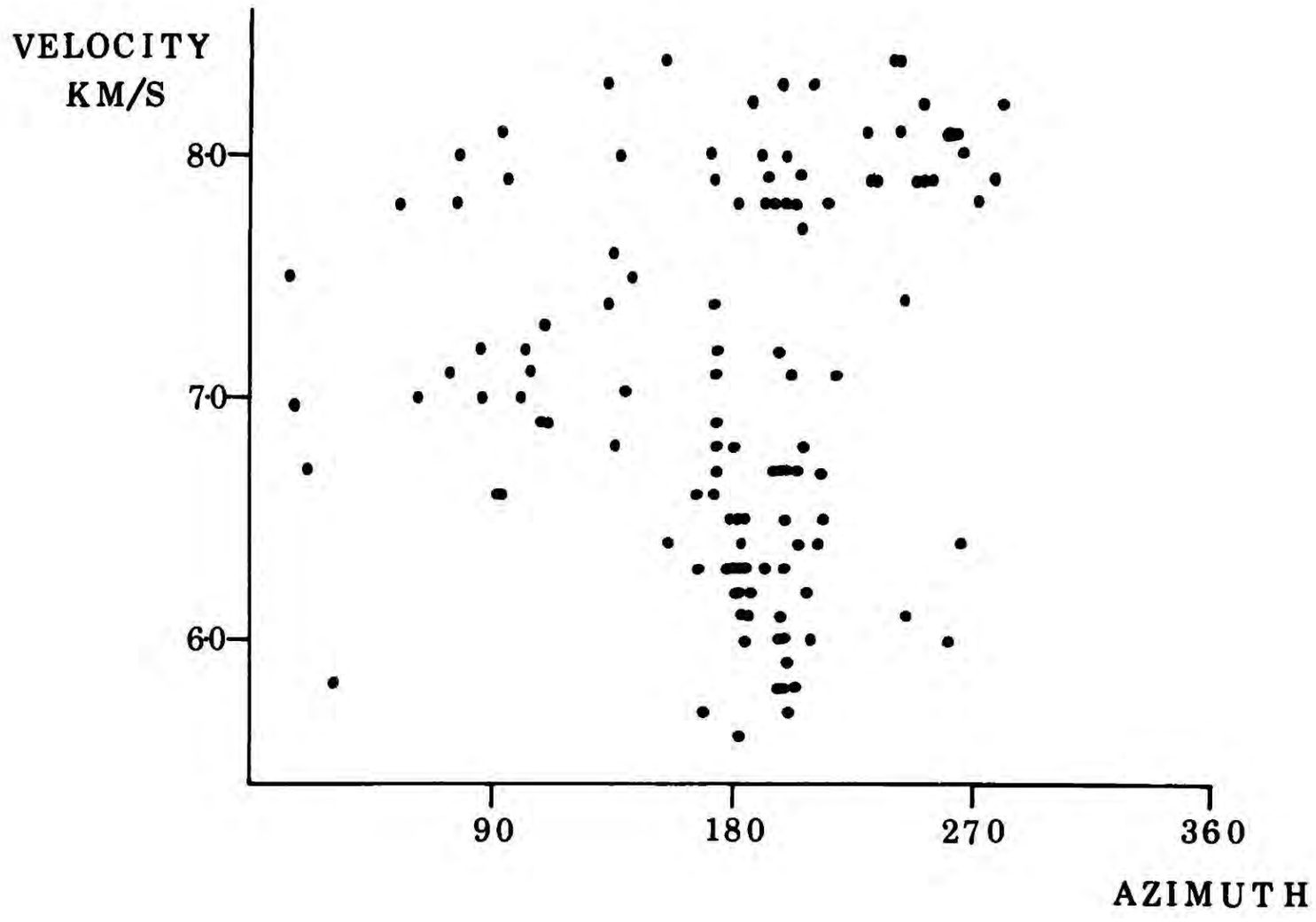
VELOCITY
KM/S
8·0
7·0
6·0
90
180
270
360
AZIMUTH

Fig. 18. Location of Events.

Events originating beyond 200 km have Sn arrivals indicated as Good, Fair, Poor.

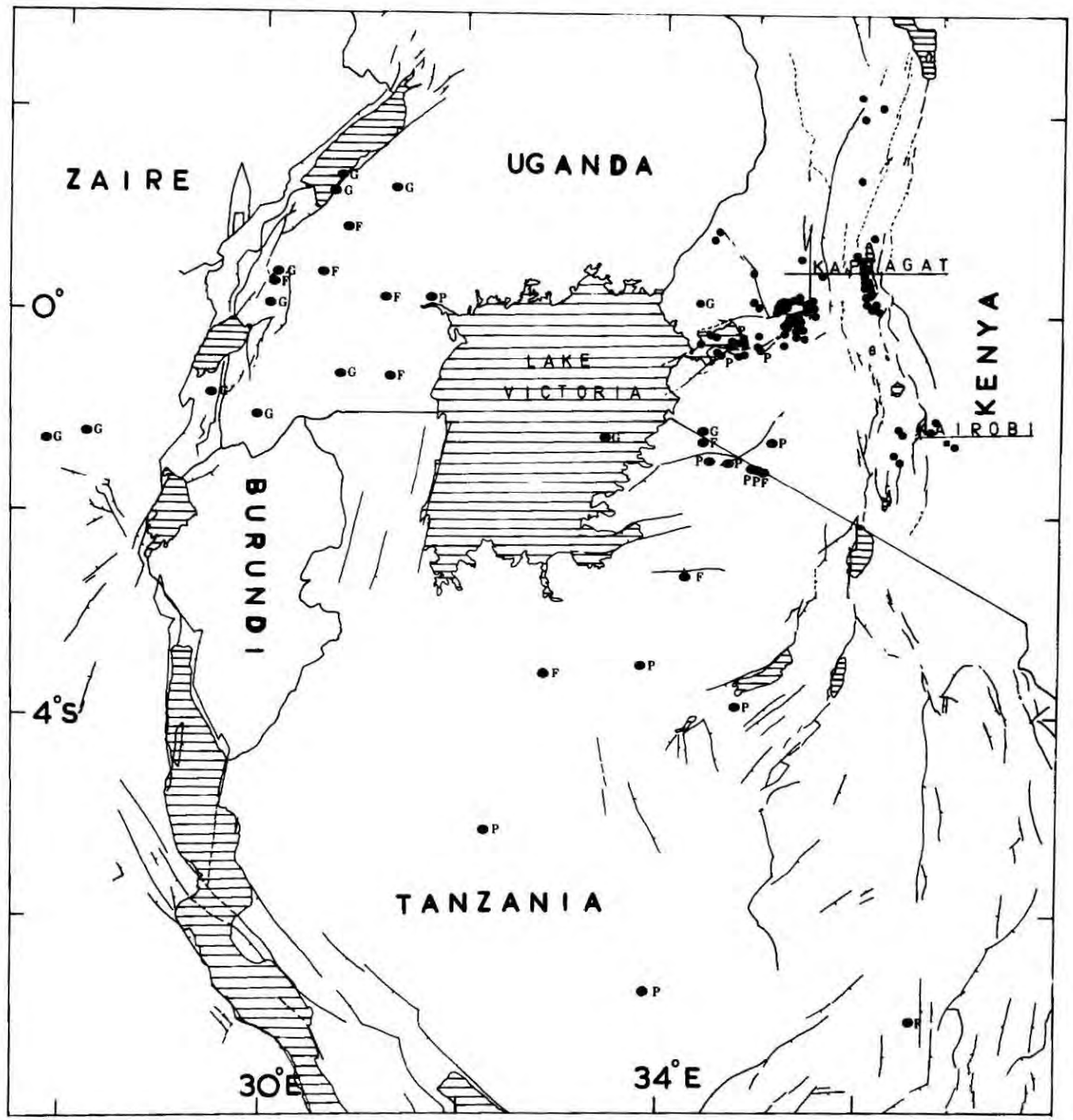
ZAIRE
UGANDA
KENYA
LAKE VICTORIA
BURUNDI
TANZANIA
NAIROBI
0°
4°S
30°E
34°E

due solely to approximation of a curved to a plane wavefront. Theroetical values of δ_{ik} were calculated for point sources at 50 and 100 km with apparent velocities across the array of 6.4, 7.3 and 8.2 km/s in each case. The azimuth of approach ranged from 0 through to 360 degrees in steps of 10 degrees.

By solving equation (7) as

$$\delta_{ik} = A_i + B_i \sin(\Theta_k + \phi_i) + \delta^1_{ik}$$

by the method of least squares in the presence of δ^1_{ik} it was found that the maximum value of A_i was found to be less than 1.5 milleseconds, while that for B_i was less than 0.3 milleseconds, which are negligible. Hence the e_{ik} calculated from the plane wavefront analysis were used in the analysis of the pit residuals for the determination of a site correction for all ten seismometer pits.

The onset time residuals for all the events are plotted for each seismometer site, together with the curves fitted to the residuals (Figs. 19-23). A_i, B_i and ϕ_i are tabulated together with their 95% confidence limits (Table 4).

The seismometers are set on laterally homogeneous phonolite overlying the basement, from which it would be expected that the values of A_i should be small. This is indeed the case as no value exceeds $\pm$ 0.012 seconds and all except that for Y2 are less than $\pm$ 0.007 seconds. Since the A_i do not correlate well with the site altitudes (Fig. 24), it is assumed that the height corrections applied in the main analyses are approximately correct.

The B_i terms are all less than 0.02 seconds, and hence the structure beneath the array is assumed to be horizontally layered, since a dipping layer would cause the B_i to be large. This agrees with the geological interpretation which allows for a very gently northward dip of the basement complex beneath the Uasin Gishu plateau (JENNINGS 1964). Over the array dimensions, this dip will not be more than 1 or 2 metres

Fig. 19 - 23.

Onset time residuals for seismometers, with fitted sine curves.

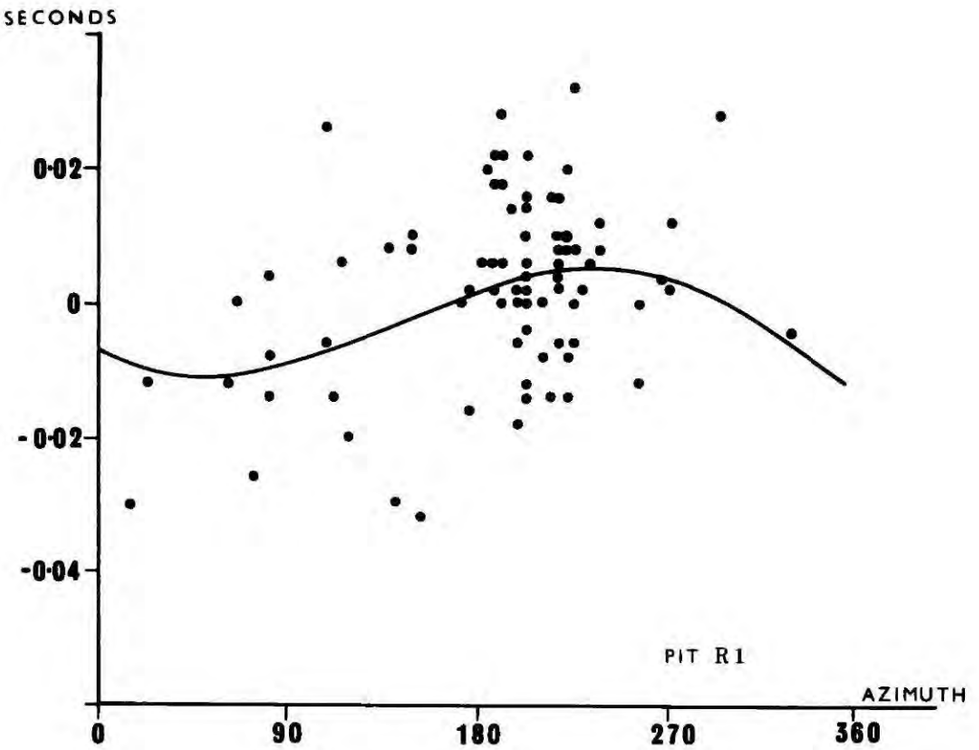
SECONDS
0·02
0
-0·02
-0·04
PIT R1
AZIMUTH
0
90
180
270
360

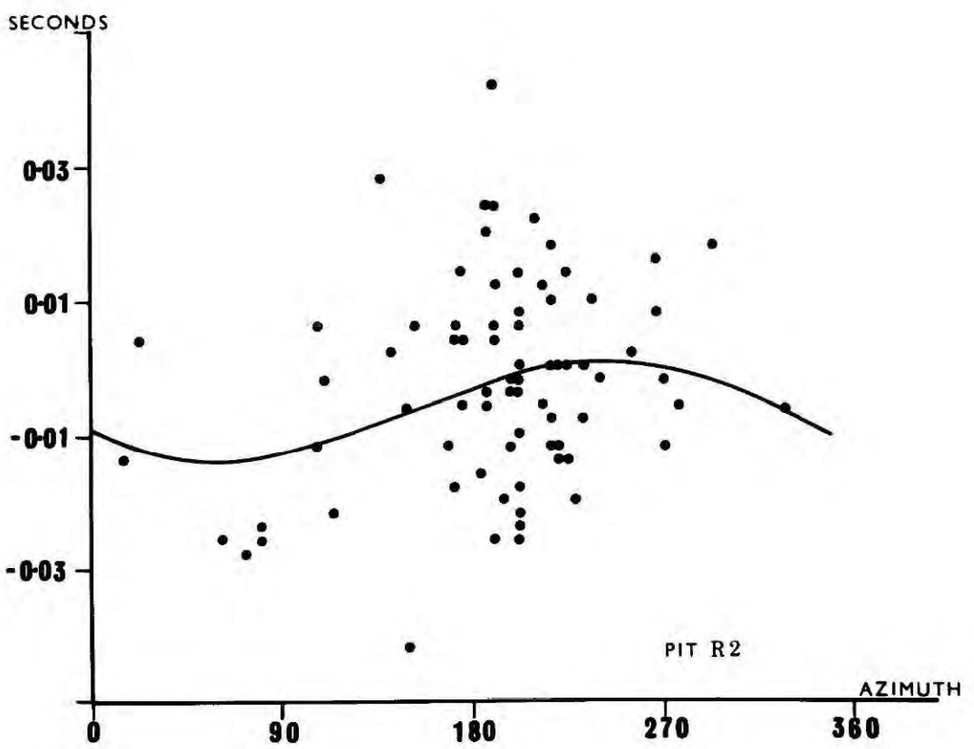
SECONDS
0·03
0·01
-0·01
-0·03
PIT R2
AZIMUTH
0
90
180
270
360

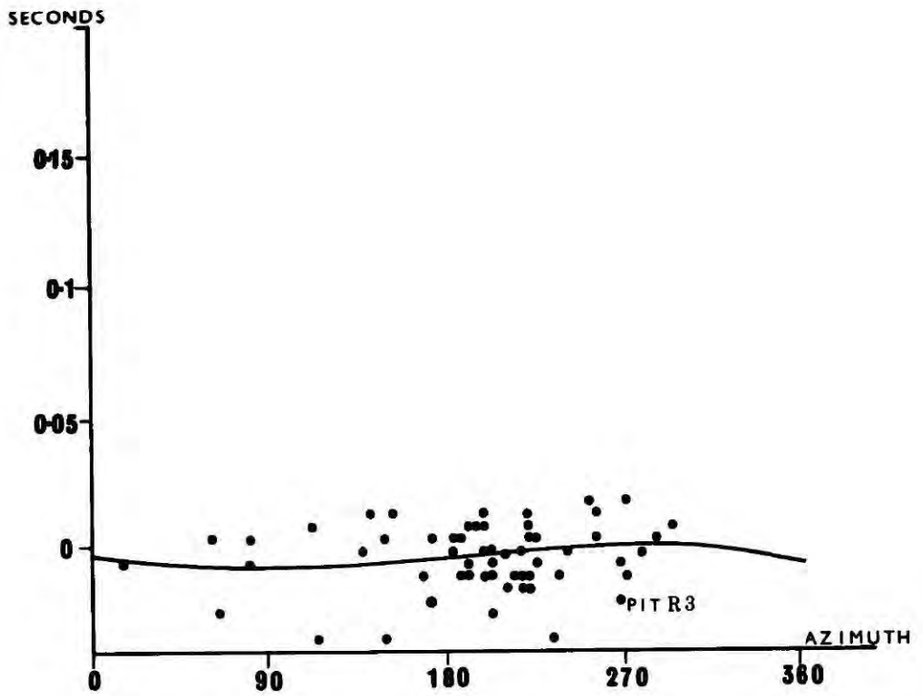
SECONDS
0·15
0·1
0·05
0
PIT R3
AZIMUTH
0
90
180
270
360

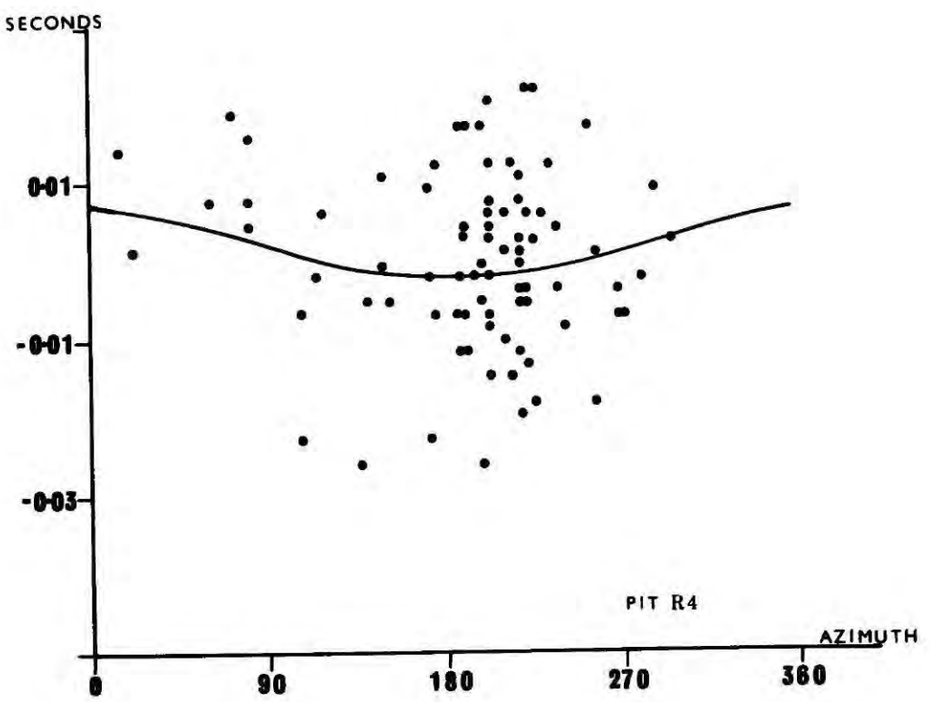
SECONDS
0·01
-0·01
-0·03
PIT R4
AZIMUTH
0
90
180
270
360

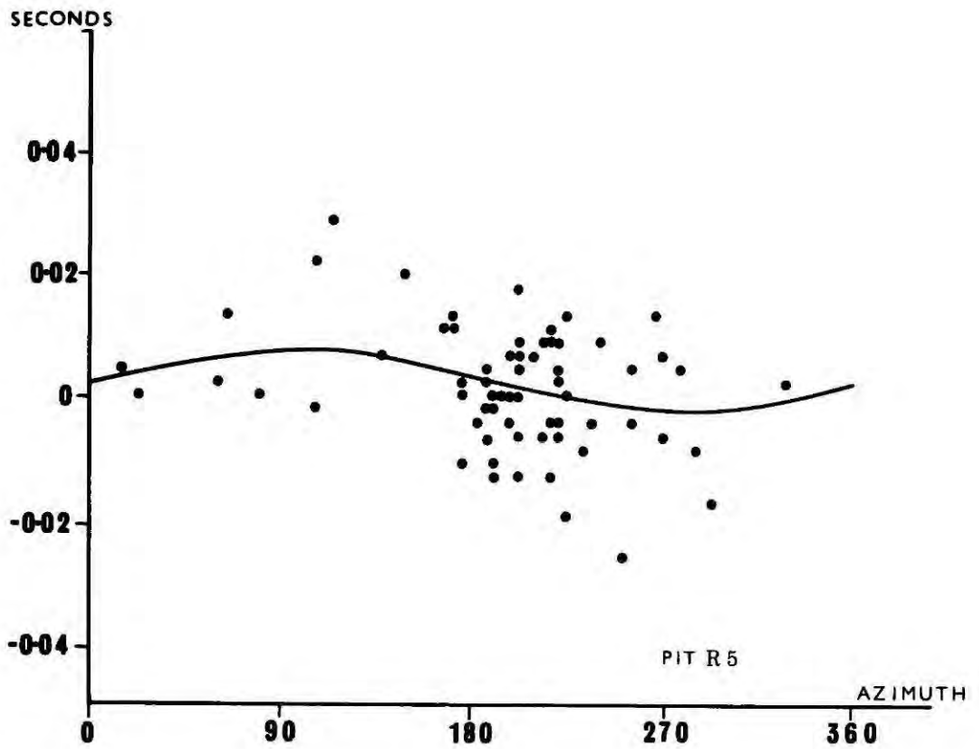
SECONDS
0·04
0·02
0
-0·02
-0·04
PIT R5
AZIMUTH
0
90
180
270
360

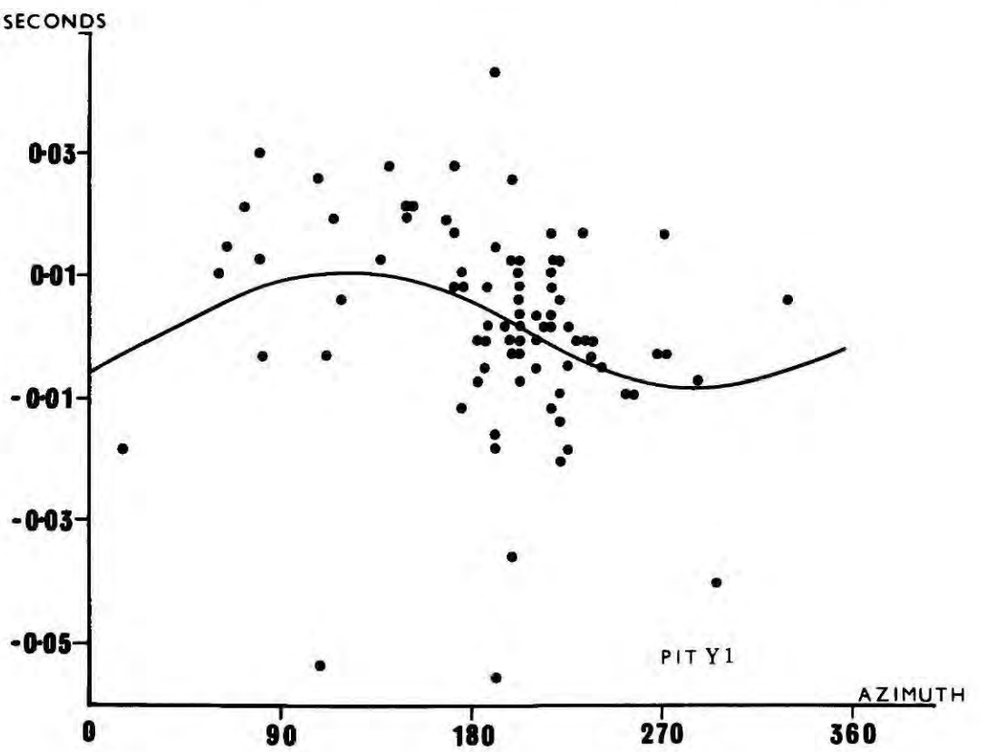
SECONDS
0·03
0·01
-0·01
-0·03
-0·05
PIT Y1
AZIMUTH
0
90
180
270
360

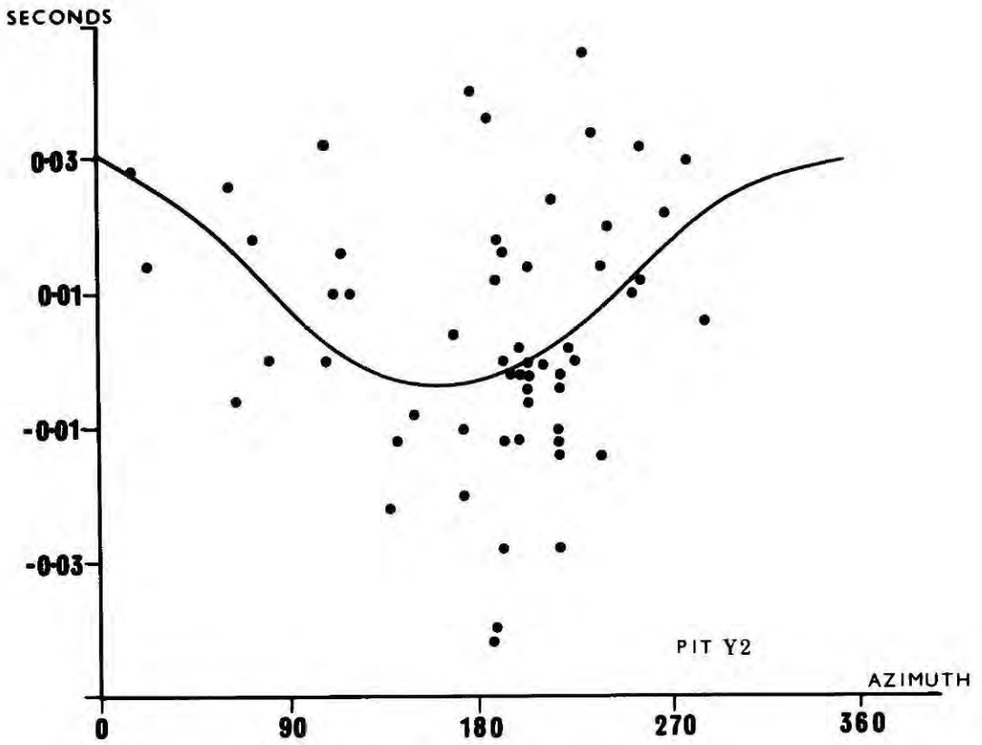
SECONDS
0·03
0·01
-0·01
-0·03
PIT Y2
AZIMUTH
0
90
180
270
360

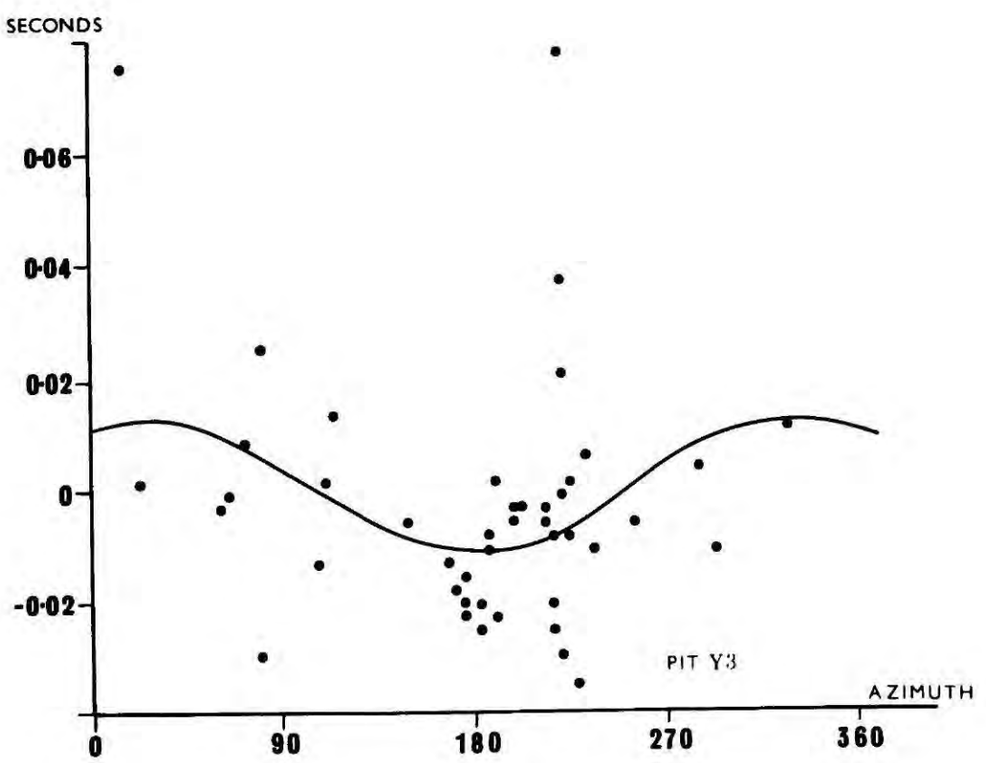
SECONDS
0·06
0·04
0·02
0
-0·02
PIT Y3
AZIMUTH
0
90
180
270
360

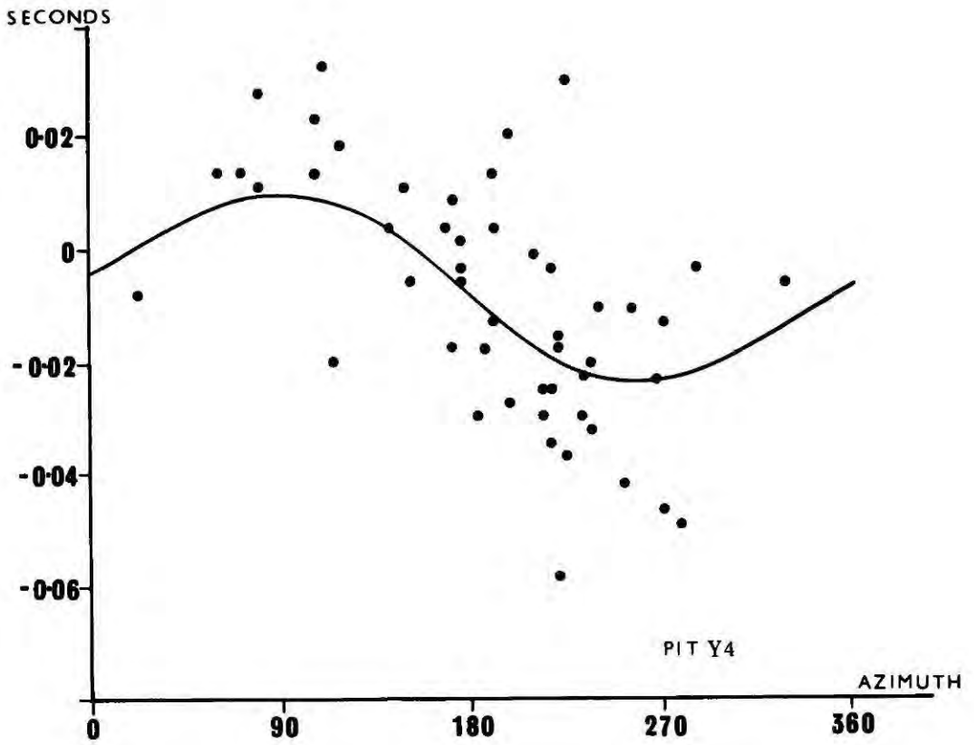
SECONDS
0·02
0
-0·02
-0·04
-0·06
PIT Y4
AZIMUTH
0
90
180
270
360

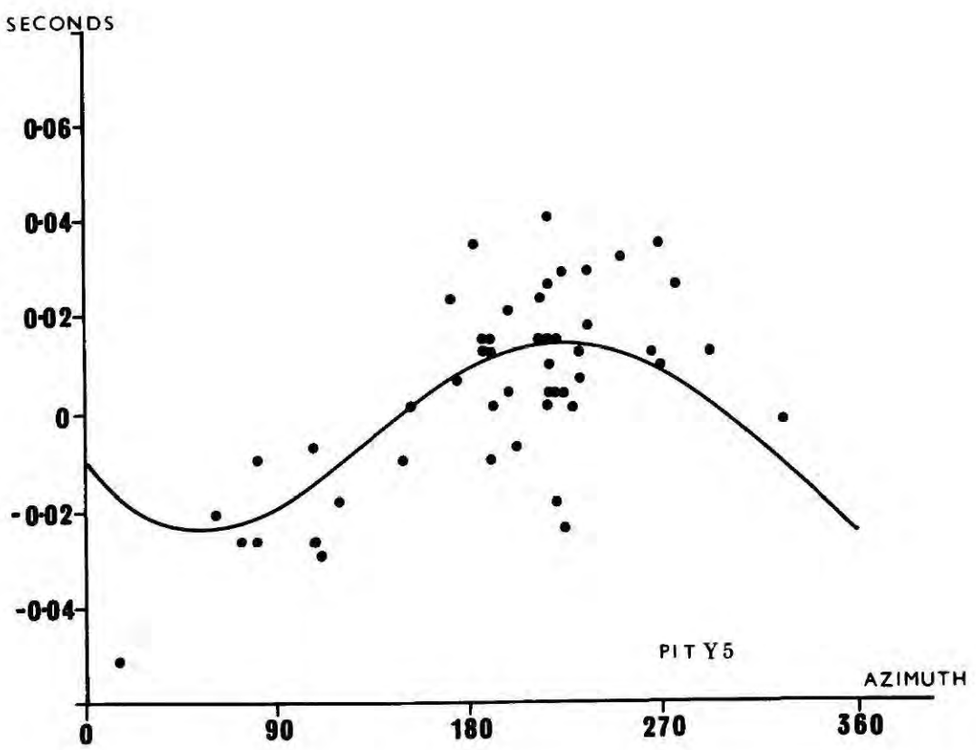
SECONDS
0·06
0·04
0·02
0
-0·02
-0·04
PIT Y5
AZIMUTH
0
90
180
270
360

TABLE 4

ARRAY SITE CORRECTIONS

(ERRORS ARE 95% CONFIDENCE LIMITS)

PIT	A (seconds)	B (seconds)	Ø (degress)
R1	-0.002 ± 0.004	0.008 ± 0.006	217.4
R2	-0.006 ± 0.005	0.007 ± 0.006	209.7
R3	-0.004 ± 0.007	0.002 ± 0.007	187.2
R4	0.002 ± 0.004	0.004 ± 0.006	74.2
R5	0.004 ± 0.004	0.005 ± 0.005	354.1
Y1	0.002 ± 0.005	0.009 ± 0.006	330.8
Y2	0.012 ± 0.007	0.017 ± 0.009	103.5
Y3	0.002 ± 0.008	0.013 ± 0.011	94.4
Y4	-0.006 ± 0.008	0.017 ± 0.009	5.4
Y5	-0.004 ± 0.007	0.019 ± 0.008	224.6

Fig. 24. D.C. term A of onset time residuals as a function of seismometer elevation with respect to the cross-over point.

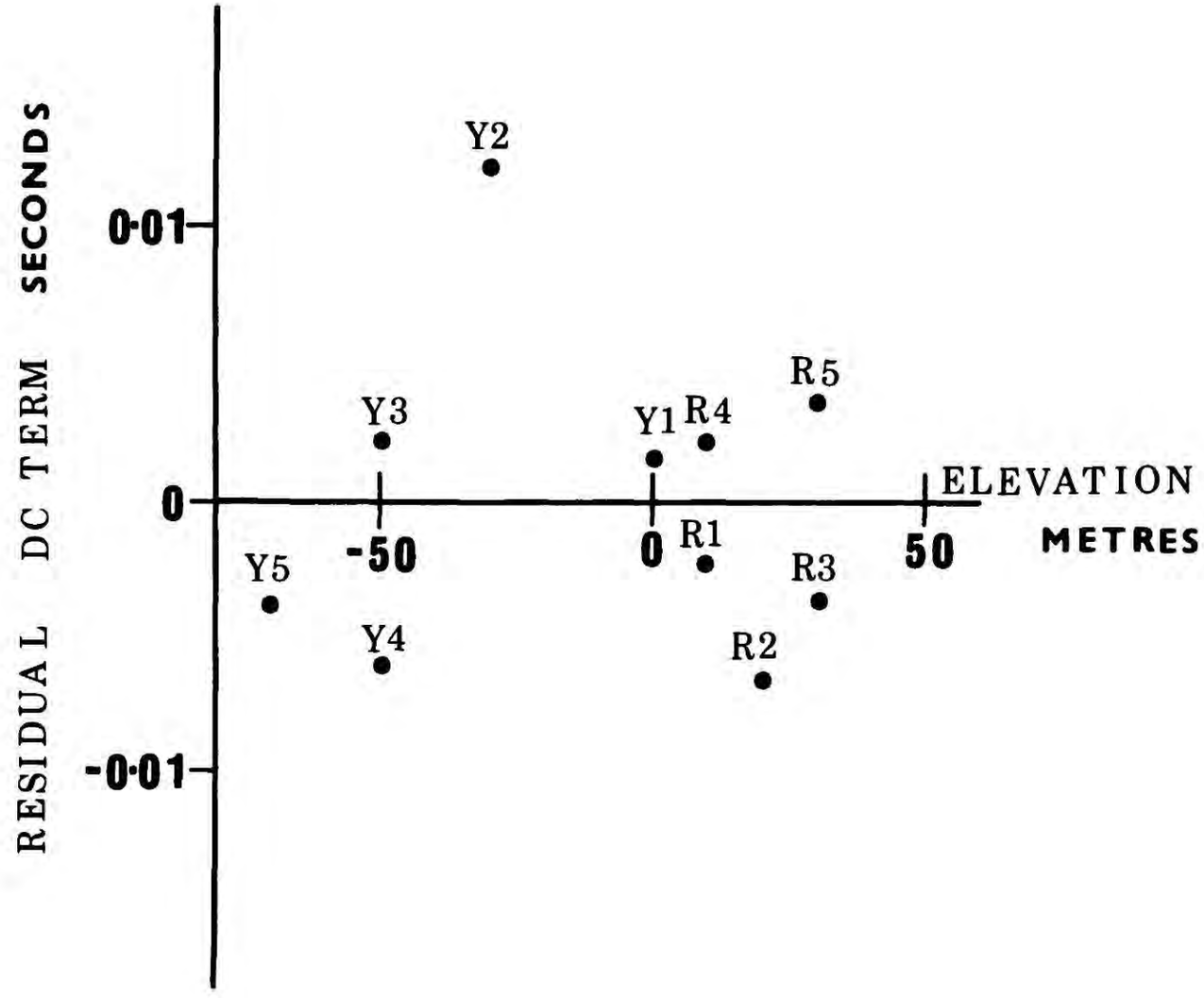
RESIDUAL DC TERM SECONDS
0·01
0
-0·01
-50
0
50
ELEVATION
METRES
Y1
Y2
Y3
Y4
Y5
R1
R2
R3
R4
R5

in 5 km, and hence not evident. The lack of any uniform azimuth variation in structure is confirmed by the scatter in values of the phase angle ϕ_i.

From the fact that the site correction terms are very small, a further non-linear analysis (as initially discussed in 3.1.7) was considered unnecessary.

CHAPTER 4

INTERPRETATION OF THE DATA.

Apparent ground velocities of local and regional events may be interpreted in terms of crustal velocities. Restriction on distance and azimuth of the events can then provide a comprehensive picture of crustal structure in the vicinity of the array. From the analysis of second arrivals an increased amount of information regarding crustal velocities, crustal thickness and focal depth of event may be determined. However, local and regional events at Kaptagat were characterized by a large number of interfering arrivals (Fig. 14) and second arrival analysis proved difficult and of insufficient accuracy for detailed interpretation. However it was used to check the crustal model derived from the first arrival analysis.

4.1. APPARENT VELOCITIES.

If an arrival has been critically refracted, the apparent velocity across the array will be related to the velocity of the headwave refractor at the critical distance from the array. Thus apparent velocities provide information about local structure. Lateral inhomogeneities in the regional structure will not be evident. In a horizontally layered model the apparent velocity equals the velocity of the refractor at the critical distance (Fig. 25a). If the refractor has a regional dip in the vicinity of the array, the apparent velocity will vary continuously with azimuth. Recognition of such a variation allows the mean dip as well as the mean velocity of the headwave refractor to be measured. The maximum velocity occurs for the updip arrival, while the minimum velocity occurs for the down dip arrival (Fig. 25b). For a refracted arrival the apparent azimuth of approach will be displaced away from the strike of the dipping layer (NAIZI 1966). Thus the variation in apparent velocity with apparent azimuth will not be strictly uniform. However, to a first approximation the velocity may be taken as varying sinusoidally as

$$V = V_o + V \sin (\emptyset + \theta)$$

where V_o is the velocity of the headwave refractor

θ the azimuth of approach

$\emptyset$ a constant phase angle

and $\theta_d = 90 - \emptyset$ the direction of dip.

If the arrival is not critically refracted the apparent velocity can be related to a crustal velocity only if the focal depth of event and hypocentral distance can be determined. This is also true for a direct arrival from an event originating within a crust in which velocity increases with depth. However, hypocentral distance may be determined as a function of crustal velocity from a knowledge of the P-S time of event. From a statistical analysis of event focal depths, it is therefore possible to relate apparent velocities to crustal velocities when the first arrival is not critically refracted.

Fig. 25. Three ideal models and the relation of apparent velocity to structure.

a) Horizontal layer: V_A is equal to velocity of headwave refractor at critical distance from observation point.

b) Dipping layer : V_A depends on azimuth of approach.

V_A = Vmax for updip arrival.

V_A = Vmin for downdip arrival.

c) Diffraction : V_A is related to position of diffracting point and velocity of medium between the diffracting point and the observation position.

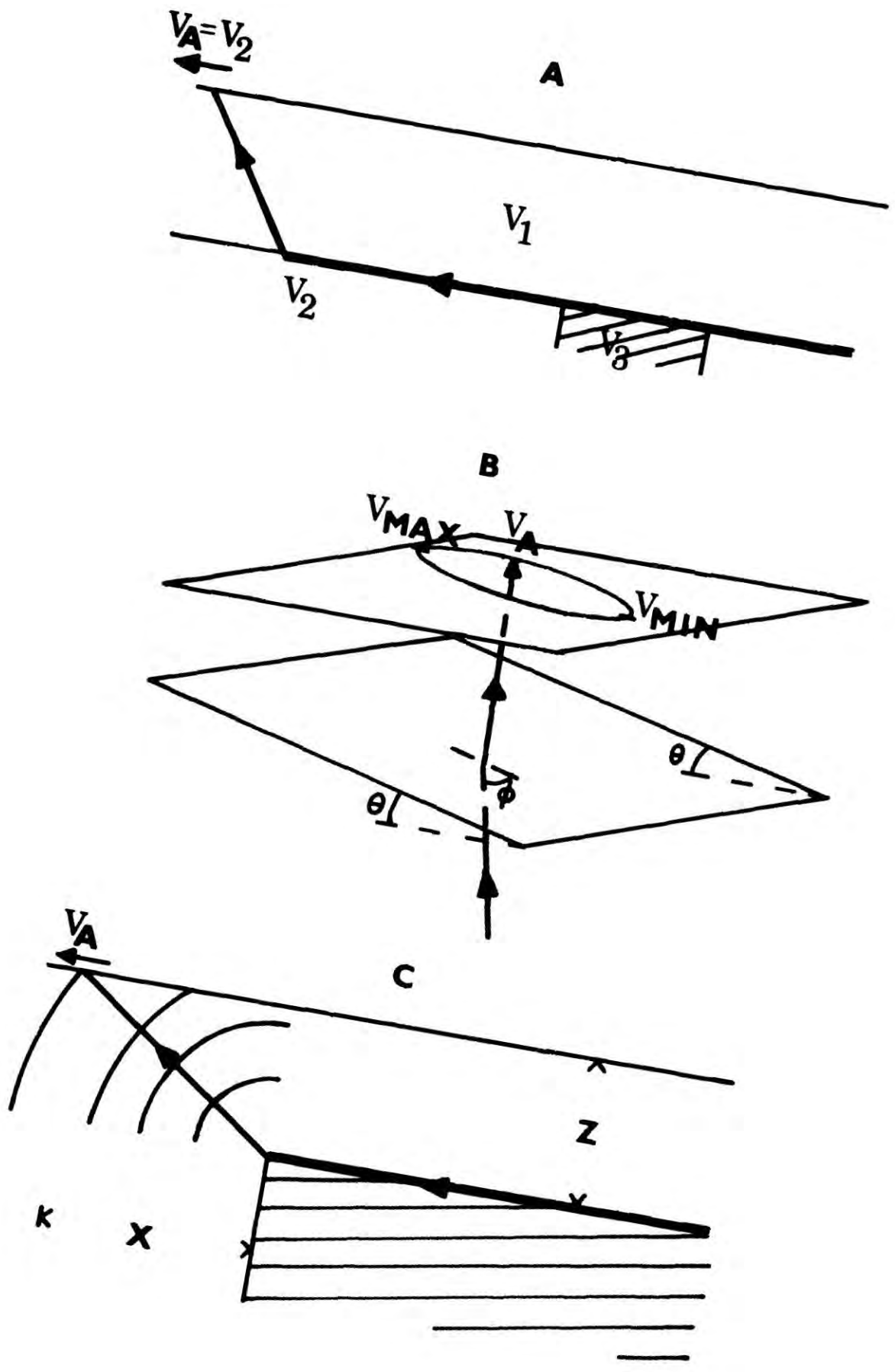
$V_A = V_2$
A
V_1
V_2
V_3
B
V_{MAX}
V_A
V_{MIN}
θ
θ
ϕ
V_A
C
Z
K
X

If an arrival has been diffracted off some structural boundary in the vicinity of the array, then the apparent velocity across the array will be related only to the position of the diffracting edge and the velocity of the medium beneath the array. It will be independent of the velocity of the diffracting material (Fig. 25c). However, the amplitude of a diffracted arrival will fall off rapidly with distance from the array to the diffracting edge. Such an arrival is unlikely to be observed, unless the diffractor is very close to the array.

If there is a low velocity layer within the crust, then no headwave arrival can be observed from such a layer.

4.2. SURFACE LAVAS.

From geological evidence (2.1) and the analysis of the pit residuals (3.5.3), it is concluded that the surface volcanics beneath the Kaptagat array form an approximately horizontal layer above the basement complex. The P-wave velocity in the volcanics is concluded to be 4.5 km/s (BACKHOUSE 1972), while the thickness beneath the array is of the order of 170-200 metres.

Since the lavas form a horizontal layer beneath the array station, their presence will not affect the apparent velocity across the array of the deep crustal arrivals. However, the P-S time of an event will be larger than if the volcanics were not present. But, for a headwave arrival from the basement complex immediately beneath the lavas, likely to pass through a maximum of 300 metres of phonolite, the P-S time through these lavas will be no more than 0.05 seconds. This value is negligible in comparison with the P-S time errors (3.4.1) and hence the surface volcanic layer may be neglected in the analysis of apparent velocities and P-S times.

4.3. STRUCTURAL BOUNDARY.

The Kaptagat array is located 10 km west of the Elgeyo escarpment, the western boundary fault of the Gregory Rift in the vicinity of latitude 0.5N. The array is situated on Tertiary volcanics, which in turn overlie basement rocks, exposed both to the west and to the east of Kaptagat. The basement complex forms part of the Precambrian Mozambique belt adjoining the Tanganyika craton which has acted as a stable block from 1850 $\pm$ 250 my ago (CLIFFORD 1970). The large volumes of Tertiary to Recent volcanics, the uplift of the Kenya dome, the high geothermal and seismic activity, all connected with the Eastern Rift structure, suggest that this is a dynamic region of the crust, as opposed to the static Precambrian region to the west of the Rift.

KHAN and MANSFIELD (1971) computed Bouguer values for more than 1500 gravity observations in Kenya, using a density of 2.67 $gm/_{cc}$

From a comparison of the regression lines for the plots of Bouguer anomaly versus elevation for stations within and outside the Gregory Rift, they inferred that different densities must be evident in the two zones. The difference in the slope of the regression lines is too great to be accounted for by surface densities alone and an abnormal crustal structure beneath the Rift is indicated. Gravity profiles across the Rift have been interpreted in terms of a mantle derived crustal intrusion existing beneath the Rift itself (SEARLE 1970, KHAN and MANSFIELD 1971, BAKER and WOHLENBERG 1971). The seismic refraction line of GRIFFITHS et al (1971) confirmed that anomolously high velocity material exists within the crust along the axis of the northern part of the Gregory Rift. If this intrusion is of finite lateral extent, as indicated by the interpretations of the Bouguer anomalies, then there is likely to be

either 1) a gradational change

or 2) a sharp structural boundary

between the crustal structure beneath the Rift, and the crustal structure

of the Tanganyika craton and Precambrian Mozambique belt on the western flank of the Rift. If apparent velocities can be related to crustal velocities, a change in velocity distribution with azimuth from the array would therefore not be unexpected, since Kaptagat lies 10 km from the Rift margin. This distance is likely to be less than the critical distance for headwave arrivals from the Moho, or an intermediate layer.
For example:-

The critical distance for an 8.0 km/s arrival

= 42.6 km

and the critical distance for a 6.6 km/s arrival

= 39.0 km

for the Afric Model of GUMPER and POMEROY (1970) (MODEL 2).

The critical distance for a 7.5 km/s arrival

= 33 km

for GRIFFITHS et al (1971) model of the axial crustal structure of the Rift (MODEL 7).

4.4. DIVISION OF THE DATA.

A preliminary analysis of Fig. 17, the apparent velocity versus azimuth plot, suggests that the data can be divided into two azimuthal zones.

21% of the events originate between azimuths 0 and 160 degrees. In this group, only one event has an apparent velocity of less than 6.6 km/s, while 96%, with P-S times of greater than 3.0 seconds, have velocities between 6.6 km/s and 8.3 km/s. Of the events originating between 160 and 360 degrees, 44% have velocities of less than 6.6 km/s, while the remaining 56% have velocities greater than this value.

However, before such an apparent difference in velocity distribution can be confirmed, allowance for the different P-S times of the events must be taken into account.

24 of the 27 events originating between azimuths 0 and 160 degrees have P-S times lying between 7.5-12.5 and 20-27.5 seconds. 26 events from azimuths 160 to 360 degrees lie in the same P-S time ranges. In the former case 4% of the events have velocities of less than 6.6 km/s. In the latter, 42% of the events have velocities of less than 6.6 km/s. Such a percentage difference may be due to

1) different focal depth distributions in the same crustal structure

or 2) different crustal structures between the two azimuthal zones.

But no matter what the cause, there is a marked difference in velocity distribution between the two zones.

All the events with P-S times of greater than 3.0 seconds between 0 and 160 degrees, originate within or to the east of the Gregory Rift (Fig. 18). The coincidence of the geological and geophysical evidence considered in 4.2, together with the difference in velocity distribution, suggests that there is a difference in crustal structure between the two azimuthal zones. Thus the interpretation of the data is initially divided

into two parts, related to the two azimuthal zones. The particular events originating close to the boundaries of the two zones will be considered in more detail once the initial model is determined.

CHAPTER 5

THE WESTERN GROUP OF EVENTS

(AZIMUTHS 160-360 DEGREES).

5.1. APPARENT VELOCITIES AND P-S TIMES.

The apparent velocities of the western group of events will be interpreted in terms of the simplest crustal structure with which the data is consistent.

Two initial assumptions will be made

1) that the structure is continuous in the vicinity of the array, throughout the range of azimuths of the western group of events

and 2) that there is a most probable focal depth, which remains constant over the range of local event epicentral distances considered in the analysis.

Apparent velocities may be related to crustal velocities at the critical distance from the array, which is likely to be less than 45 km from Kaptagat for any headwave arrival (4.3). Assumption (1) is considered reasonable, from the fact that an arc of radius 45 km, between azimuths 160 and 360 degrees from Kaptagat lies totally within the Kapsabet plateau, a structurally stable block bounded to the east, south and west by major faults. (2.1).

Assumption (2) is less viable in that the most probable focal depth of event depends entirely upon the local dynamic crustal properties at the epicentre. However, 90% of the events originate from within the Tanganyika shield and Mozambique belt, and it is reasonable to suppose that the dynamic crustal properties do not vary substantially over these Precambrian systems. The remaining 10% of the events originate from within and beyond the Western Rift, and focal depth is

not critical in the analysis of regional events.

The scatter in the data can be related to deviations from the two assumptions mentioned above.

The crustal model produced is unlikely to be unique, and further geologically realistic models, with which the data is consistent will be considered.

Apparent velocity versus P-S time plots have been drawn for three simple structural models, assuming a constant focal depth of event. (Fig. 26).

1) A horizontal homogeneous single layered crust.
2) A horizontal single layered crust with velocity increasing with depth.

and 3) A horizontal, homogeneous two layered crust with

a) the event focus in the upper layer

and b) the event focus in the lower layer.

All these models overlie a horizontal, homogeneous Moho.

In order to interpret the data in terms of a simple structural model, the plot of apparent velocity versus P-S time for the western group of events has been blocked into three regions A, B and C (Fig. 27). (Events with P-S times greater than 25 seconds, have been omitted from the diagram, to indicate more clearly the distribution of events with small P-S times).

Fig. 26. Three velocity versus P-S time plots, assuming a constant focal depth in horizontally homogeneous models.

a) A single layered crust.

b) A single layered crust, with velocity increasing with depth.

c) A two layered crust with

   a) event focus in the upper layer

   b) event focus in the lower layer.

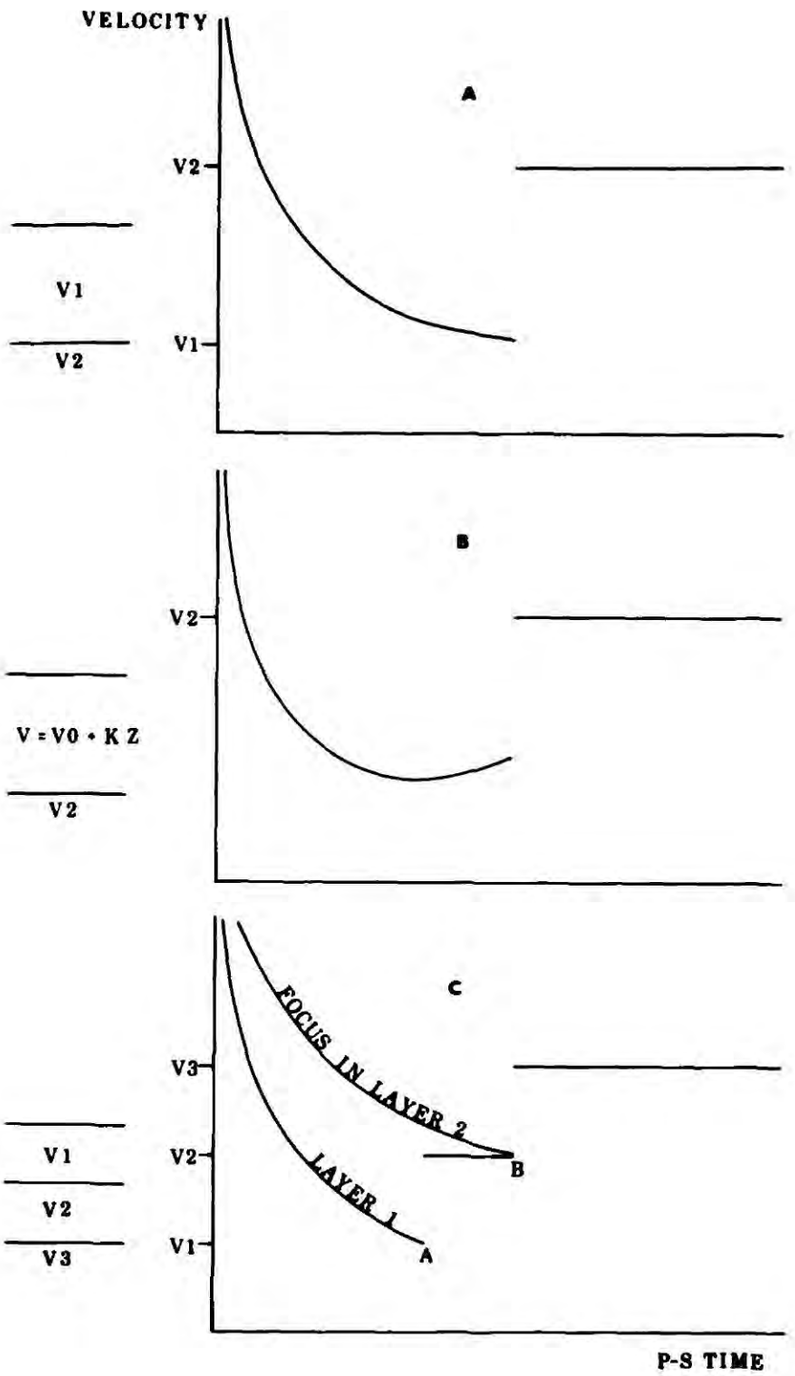
VELOCITY
A
V2
V1
V1
V2
B
V2
V = V0 + K Z
V2
C
FOCUS IN LAYER 2
V3
V1
V2
V2
V3
LAYER 1
B
V2
V1
A
P-S TIME

Fig. 27. P-S time vs apparent velocity plot for events originating in the western azimuthal zone omitting those events with P-S times greater than 25 seconds.

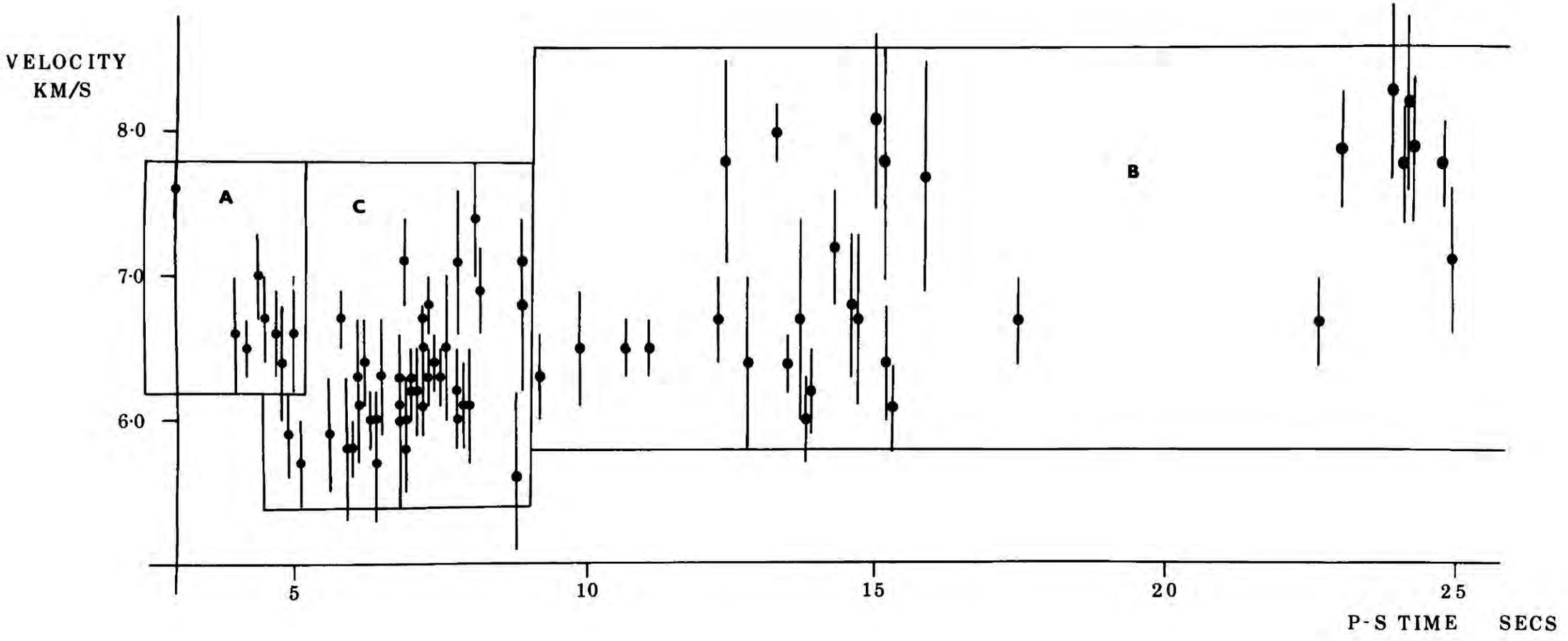
VELOCITY
KM/S
8·0
7·0
6·0
A
C
B
5
10
15
20
25
P-S TIME SECS

5.2. DIRECT ARRIVALS.

From a comparison with Fig. 26, the events in Block A of Fig. 27, are likely to be direct arrivals. The apparent ground velocity of these events will depend on

1) the focal depth of event

and 2) the velocity of the medium beneath the array.

The events with P-S times between 4.0 and 5.0 seconds all originate between azimuths 177 and 215 degrees. They are consistent with the earthquakes being associated with crustal movement in the vicinity of the Nyando fault, to the south of the Kapsabet block. Their epicentral distances will differ by no more than approximately 10 km, while the azimuthal spread is of the order of 25 km. The total area within which these events occur is thus likely to be no more than 250 km^2. Over such an area it is probable that the events originate from a small focal depth range, especially so if they are associated with movement on the same fault. If a most probable focal depth is assumed for all the events of Block A, then it is possible to determine the velocity of the medium beneath the array.

Fig. 28 is a plot of the range of focal depths versus various values of the medium velocity. That focal depth with the smallest distribution about the mean occurs at 16.4 km. With this value the velocity of the basement material beneath the array is calculated as 5.9 ± 0.2 km/s.

This value is confirmed from the following analysis. In calculating the apparent velocity and azimuth of approach of an event, using the curved wavefront formulation, a third unknown is the epicentral distance (3.1.). 14 events from the western group with P-S times of less than 8.1 seconds, were found to have $\sum_{i=1}^{n-1} e_i^2 / n - 1 \leq 0.003$ seconds, e_i, is the observed minus calculated onset time of arrival at

Fig. 28. Plot of range of focal depths versus various values of medium velocity for the events of Block A. (Fig. 27).

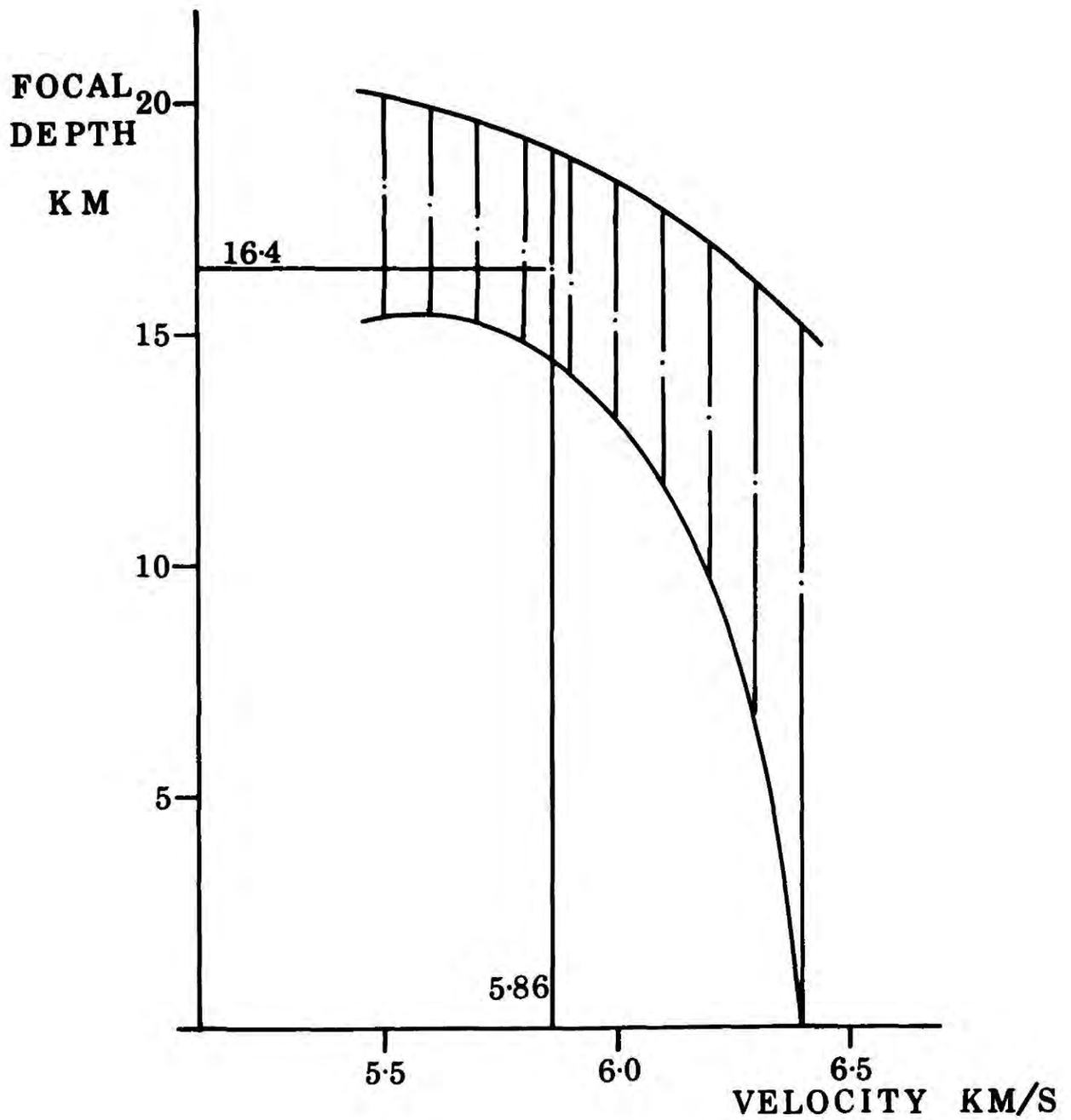
FOCAL
DEPTH
KM
20
16·4
15
10
5
5·86
5·5
6·0
6·5
VELOCITY KM/S

the i^{th} seismometer relative to Y1, while n is the number of operative seismometers. For these events the value of Δ, the epicentral distance was critically dependent in determining the minimum value of $\sum_{i=1}^{n-1} e_1^2$ This enabled a relation between P-S time and epicentral distance to be calculated. A straight line has been fitted by a least squares method through the origin and data points (Fig. 29) corresponding to a P-S time - Δ relation for a surface focus event. This asymptotic approximation is justified for distances greater than 50 km, when the epicentral and hypocentral distance differ by no more than 3% for a focal depth of 16 km. This difference falls to less than 1% at a distance of 65 km.

It is found that

$$T_{ps} = (0.126 \pm 0.006)\ \Delta$$

But

$$= \left(\frac{Vp - Vs}{Vp\ Vs}\right)\Delta$$

If the ratio $R = Vp/_{Vs}$ is assumed as 1.74 (3.3.1).

$$Vp = 5.9 \pm 0.3 \text{ km/s}$$

This value is confirmed to some extent by the fact that no arrivals have been observed with velocities statistically less than 5.9 ± 0.3 km/s, while 32% of the arrivals from Block C (Fig. 27) have velocities less than or equal to 6.0 km/s.

Fig. 29. P-S time versus epicentral distance plot for 14 events analysed on curved wavefront analysis.

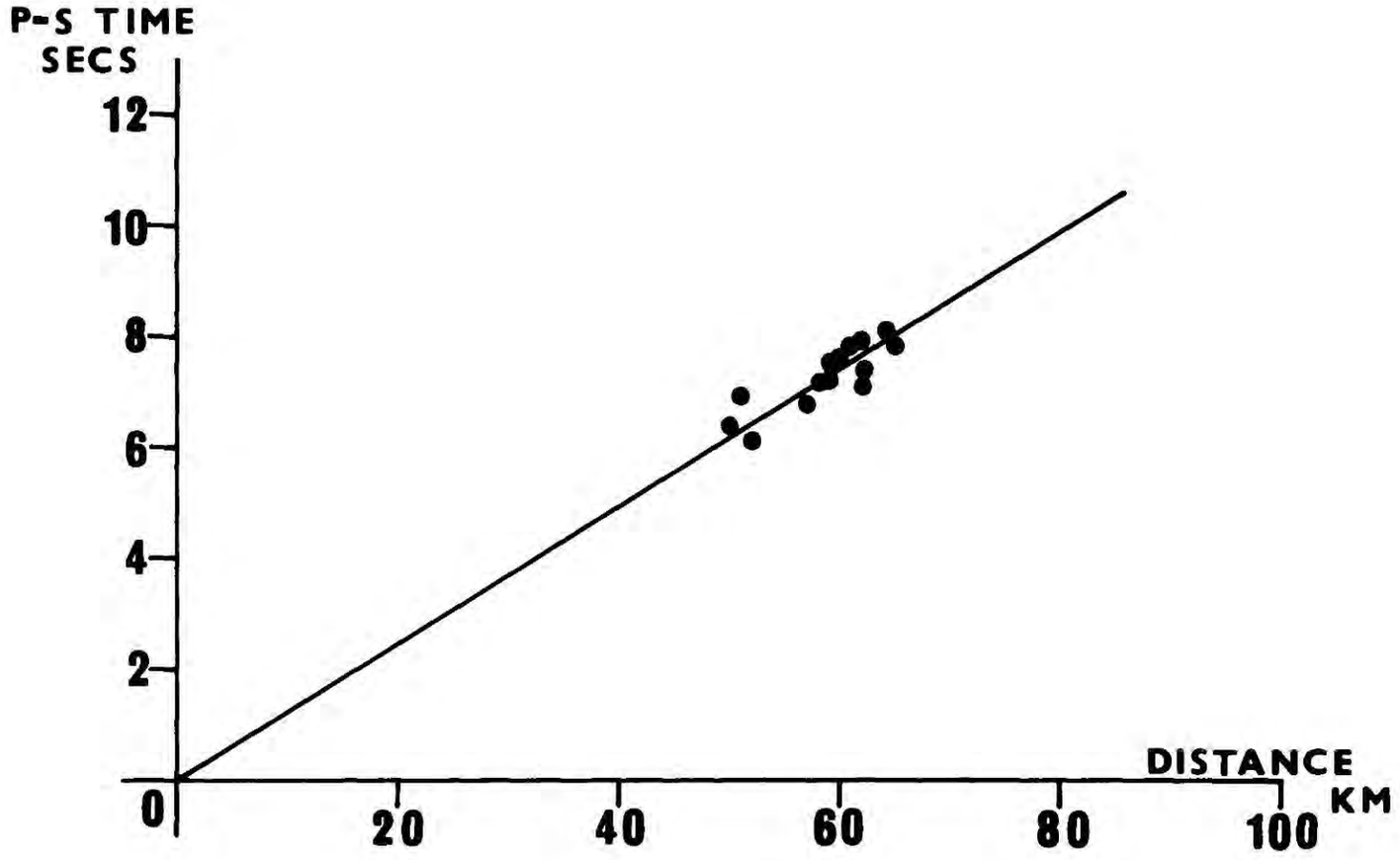
P-S TIME
SECS
12
10
8
6
4
2
0
20
40
60
80
100
DISTANCE
KM

5.3. REFRACTED ARRIVALS.

From comparison with Fig. 26, the events in block B (Fig. 27) are likely to be refracted arrivals. On plotting a histogram of the number of events versus apparent velocity (Fig. 30) (including those events with P-S times greater than 25 seconds) two main peaks are apparent at 6.5 and 7.9 km/s.

5.3.1. THE MOHO.

Those events causing the peak at 7.9 km/s are assumed to be Moho arrivals. Their P-S times are all greater than 12.0 seconds, and they originate from between azimuths 172-278 degrees.

The width of the peak at 7.9 km/s may be related to

1) The distant events having a higher apparent velocity than the near events.
2) an azimuthal variation of velocity due to a dipping Moho

or 3) the error increase for high velocity signals crossing the small array.

Due to the curvature of the earth, the first arrivals from distant events will have travelled a path reaching a few kilometres into the upper mantle. Their apparent velocities across the array are likely to be higher than for the local Moho arrivals, due to a decreased angle of incidence at the Moho. For an epicentral distance of 800 km, this increase in velocity will be no more than 0.02 km/s and hence negligible. However, since the ray paths for more distant events do penetrate into the upper mantle, a marked variation in the immediate upper mantle velocity would become evident in a variation in apparent velocity with increasing P-S time. The scatter in apparent velocities with increasing P-S time suggests that this is not the case.

A sharp change in the Moho structure would be evident in a

Fig. 30. Histogram of number of events versus apparent velocity for events of Block B.(Fig. 27).

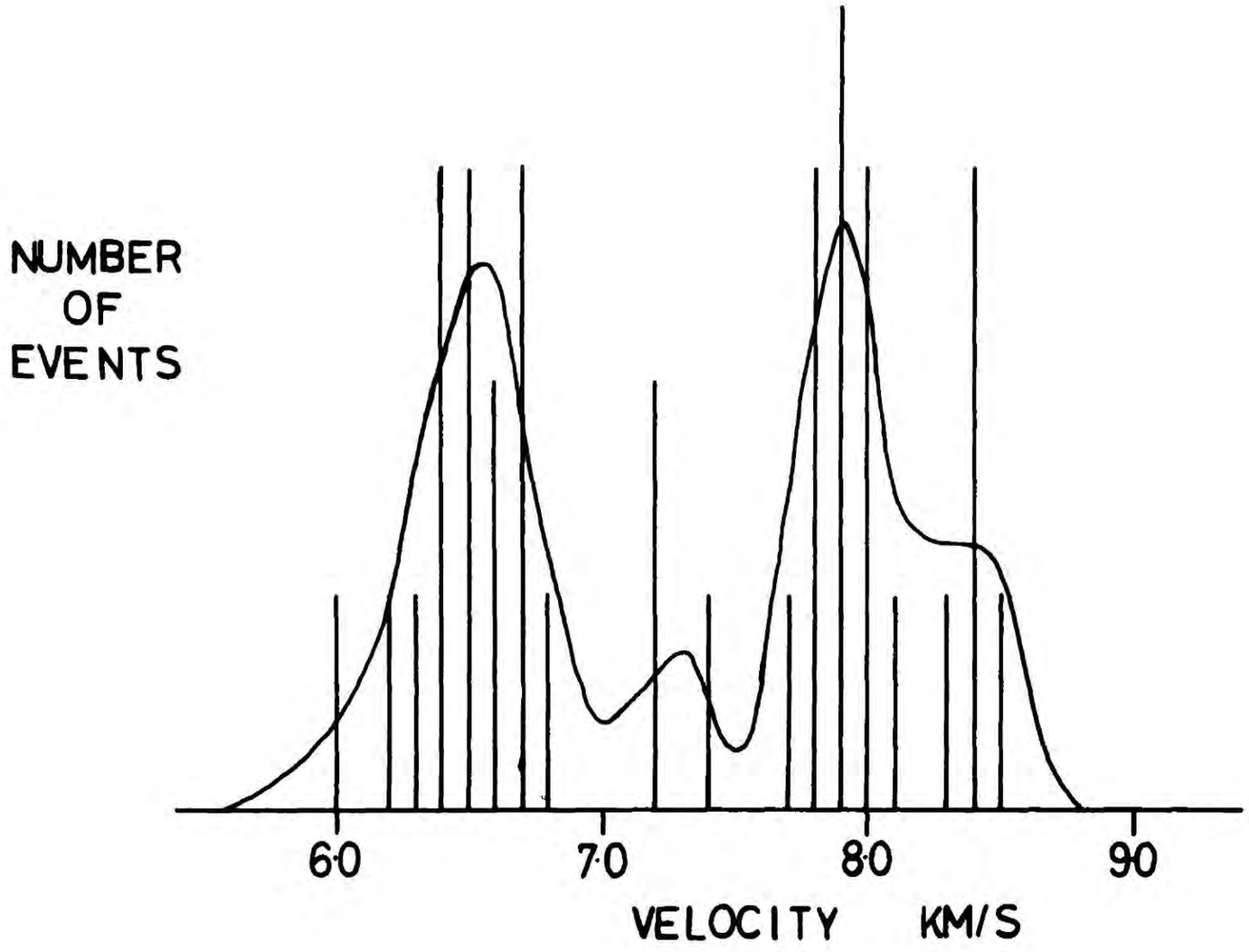
NUMBER
OF
EVENTS
60
70
80
90
VELOCITY KM/S

discontinuity of velocity with azimuth. This is also not apparent (Fig. 31). In order to determine if the Moho is dipping, an azimuthally varying sine function has been fitted by a least squares method through the first arrival velocities (Fig. 31) (see 4.1) causing the peak at 7.9 km/s (Fig. 30).

The azimuthal spread of the events is such that only $\frac{1}{3}$ of a wavelength is used in the fit. The lack of events originating from the NNW sector from Kaptagat, and the distinction between the western and eastern groups of events results in this loss of azimuthal control, which in turn results in large error limits on the velocity coefficients.

If is found that

$$V = (8.1 \pm 0.2) + (0.1 \pm 0.15) \sin(\theta + (45 \pm 50))$$

This results in a variation in velocity of 0.1 ± 0.15 km/s which is not significant at the 95% confidence limit level. The Moho is therefore regarded as horizontal in the vicinity of the array, and the crust beneath the station, horizontally layered.

The fact that the scatter in the apparent velocities is evenly spread over all the sampled azimuths and P-S times suggests that it is due to errors arising from the analysis of the apparent velocities. A weighted mean velocity of 8.0 ± 0.1 km/s is therefore taken as a velocity for the Moho on the western flank of the Gregory Rift. This suggests that normal Moho exists in the Lake Victoria region, a result consistent with S_n propagation across this area (MOLNAR and OLIVER 1969). In this analysis the S_n onset was designated as

GOOD	:	A definite onset (Fig. 14c)
FAIR	:	An unsure onset
POOR	:	A highly uncertain onset.

From Fig. 18 it is seen that the arrivals from due west of the array, originating in the vicinity of the Western Rift, in general have good S_n onsets, while those to the south are uncertain.

Fig. 31. Apparent velocity versus azimuth for events peaking at 7.9 km/s (Fig. 30) with fitted sinusoid.

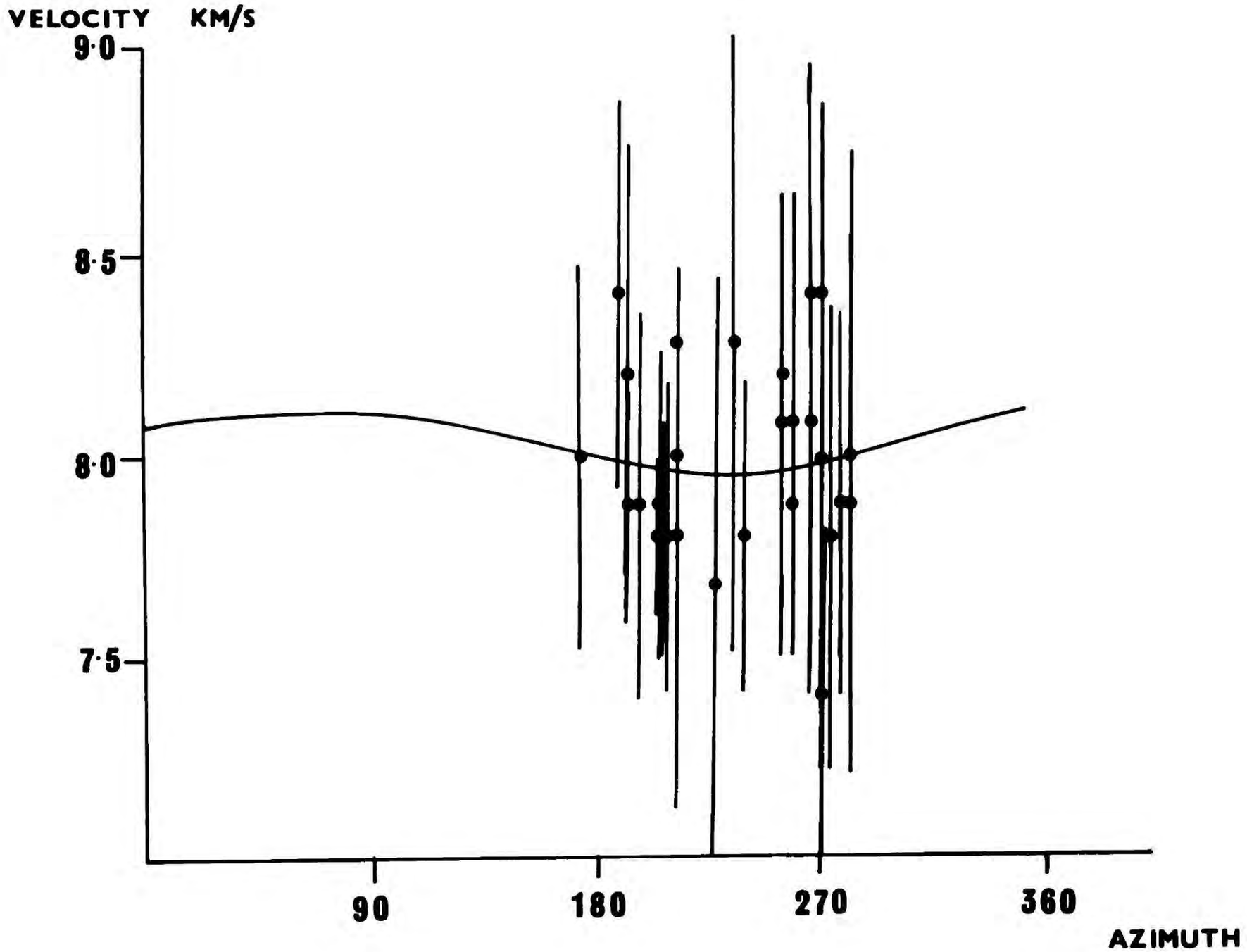
VELOCITY KM/S
9·0
8·5
8·0
7·5
90
180
270
360
AZIMUTH

This trend may possibly be related to

1) anomalous mantle material, as evident beneath the Gregory Rift, existing beyond the critical distance of a Moho arrival to the south of Kaptagat, but not to the west

or 2) the focal mechanisms of the events being consistent with large amplitude S_n arrivals from the west and poor arrivals from the south.

From the refraction study of GRIFFITHS et al (1971), along the axis of the Rift, a body of material with P-wave velocity 7·5 km/s is found to exist within 20 km of the Rift floor. This is presumed to be anomolous mantle material. The fact that the S_n phase does not propagate across the Rift in the presence of this anomolous material (GUMPER and POMEROY1970) suggests a similar attenuation for the arrivals to the south of Kaptagat. However, from an analysis of Fig. 18, this would imply that the anomolous material extended some 120 km to the west of the Rift immediately beneath the Moho. However a normal, horizontal Moho has been identified between azimuths 190-275 degrees, at the critical distance from Kaptagat, ie. to within 32 km of the Rift margin (see 6.3.4.). It would seem unlikely that there is such a marked change in the lateral extent of the anomolous mantle material evident beneath the Rift axis. This is consistent with a gravity interpretation in the region of Menengai (BAKER and WOHLENBERG 1971) which requires the anomolous material to be constrained beneath the Rift itself at least to a depth of 40 km. (Fig. 5).

Thus the second alternative would seem to be more plausible as an explanation of the decrease in amplitude of the S_n phase from west to south of the array.

5.3.2. THE CRUST.

The peak at 6.5 km/s (Fig. 30) indicates the presence of an intermediate layer in the crust with this velocity. The events are likely to be headwaves originating from a focus in the upper crust, due to their apparent velocities remaining approximately constant with increasing P-S time (Fig. 27). However a number of simple crustal models will be considered.

MODEL 1 A SINGLE LAYERED CRUST.

The events from block A, and the 14 events analysed on the curved wavefront analysis (5.2) are only compatible with a crustal velocity of at the most 6.2 km/s. This would necessitate the events in group B peaking at 6.5 km/s to have focal depths which increased with distance from the array to a depth of 56 km for the event with a P-S time of 17.5 seconds. The depth to the Moho would have to be at least 66 km, for Pg to be the first arrival for this event.

This latter value is considerably greater than the average crustal thickness of 36.2 km derived for Africa as a whole (GUMPER and POMEROY 1970). It is also greater than the average crustal thickness of 36 km for regions near the Rift System (BONJER, FUCHS and WOHLENBERG 1970; RYKOUNOV et al 1972). Hence a single layered model is not compatible either with a reasonable crustal thickness, or with a consistent focal depth range with increasing distance from the array.

MODEL 2 A SINGLE LAYERED CRUST, WITH VELOCITY INCREASING WITH DEPTH.

For a single layered model in which velocity increases with depth as

$$V = Vo + Kz$$

it is possible to relate the P-S time of an event, and the apparent ground velocity to

1) epicentral distance ; x

2) focal depth ; h

3) Vo

and 4) K

For such a model, the ray paths are circular (Fig. 32). The apparent ground velocity:

$$V_A = \left[\left\{ (x^2 + \frac{2Voh}{K} + h^2)\, k/_{2x} \right\}^2 + V_o^2 \right]^{\frac{1}{2}} \qquad 9$$

If the initial ray is upgoing (from point A in Fig. 32)

The P wave travel time:

$$Tp = 1/_K \log \left[\frac{(Vo + Kh)(Va + (Va^2 - Vo^2)^{\frac{1}{2}})}{Vo(Va + (Va^2 - (Vo + Kh)^2)^{\frac{1}{2}})} \right] \qquad 10$$

If the initial ray is downgoing (from point B in Fig. 35)

$$Tp = 1/_K \log \left[\frac{(Va + (Va^2 - Vo^2)^{\frac{1}{2}})(Va + Va^2 - (Vo + Kh)^{2\,\frac{1}{2}})}{Vo(Vo + Kh)} \right] \qquad 11$$

Assuming $Vp/_{Vs} = 1.74$ (see 3.3.1). Tps can then be determined.

For earthquakes originating at any point on a single raypath (e.g. A and B in Fig. 32) the apparent ground velocity will be the same. The hypocentral distance along the ray path is controlled by the P-S time of the event. For those events with apparent velocities less than the Moho velocity, it is possible to determine the epicentral distance and focal depth of each event for a selected value of Vo and K, by systematically varying x and h

$$\text{until } \Delta_i = (Tps(obs) - Tps(calc))^2 + (Va(obs) - Va(calc))^2$$
$$= 0$$

If x and h are 'stepped through' certain values, the optimum values of these two parameters will be reached when Δ_i reaches its minimum value.

It is then possible to determine the optimum values of Vo and K for all the events with sub Moho velocities if a number of constraints are

Fig. 32. Model of single-layered crust with velocity increasing with depth, showing two event ray paths.

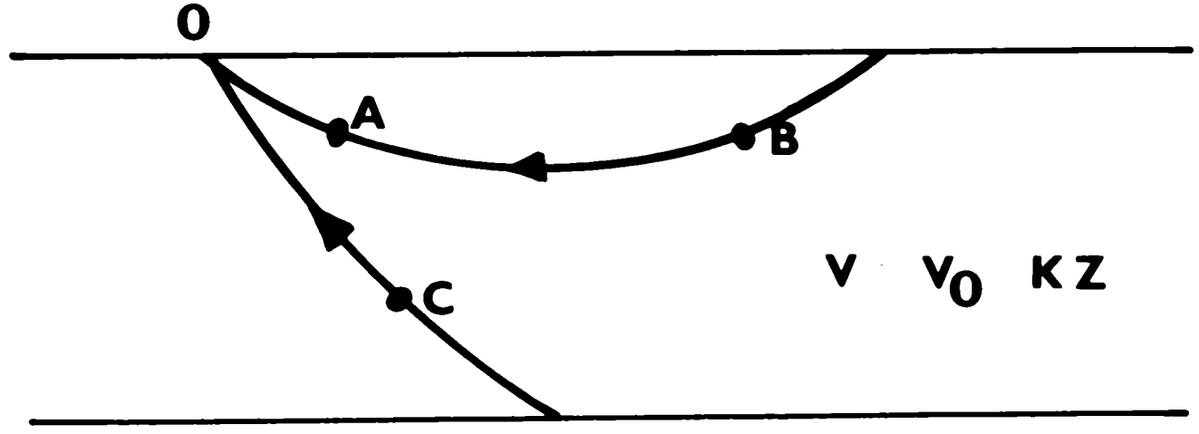
0
A
B
C
V V0 KZ

applied.

1) From equations 10 and 11

$$Vo \leqq Va$$

i.e. Vo must be less than, or equal to the minimum observed apparent velocity.

2) From equations 10 and 11

$$Vo + Kh \leqq Va$$

i.e. the velocity at the focus must be less than or equal to Va, for any event.

3) For any ray path, with any Vo and K, there is a maximum value of Tps, since all ray paths form arcs of circles bounded by a chord which is the surface (Fig. 32). Thus the maximum value of Tps(calc) for any ray path, must be greater than Tps(obs) on the same ray path.

4) The crust is of finite thickness.

Considering Fig. 32, it can be seen that any event with an initial upgoing ray path, as from point C, can have an apparent velocity

$$Vo \leqq Va \leqq \infty$$

In this case there is a different maximum value for Tps(calc) since such a ray path is bounded by the surface and the base of the crust. Again

$$\text{maxTps(calc)} \geqq \text{Tps(obs)}$$ for the same ray path.

For any event with an initial downgoing ray path, if it is to be a direct arrival

$$Vo \leqq Va \leqq Vo + Kz$$

where z is the thickness of the crust.

5) The values for Vo and K must be geologically reasonable.

i.e. there is a plausible range of values for each parameter

consistent with normal crust.

By varying Vo and K through specified ranges, the minimum value of $\sum_{\text{all events}} \Delta_i^2$ was determined. If the values of Vo and K were such that Va(obs) and Tps(obs) had to lie outside the constrained values of Va(calc) and Tps(calc), then still the minimum value of Δ_L was accepted, with the event focus either on the surface or at the base of the crust.

Assuming a crustal thickness of 45 km Vo was ranged from 5.05 to 6.05, while K was ranged from 0.0225 to 0.0585 in order to determine the minimum value of

$$\sum_{\text{all events}} \Delta_i^2$$

A plot of the standard error of the fit with the various values of Vo and K (Fig. 33) shows that a minimum value is reached. The orientation of the contours shows that the parameters Vo and K are not uniquely determined.

A small change in Vo can be compensated by a small change in K. The fact that a minimum does occur is due to constraint 4, the crust being of finite thickness. If there were a range of values of Vo and K for which none of the events or event ray paths intersected the crustal boundaries, then the model would be consistent with any of the combinations of Vo and K within this range. However by constraining the crust to be 45 km thick, it is found that some of the events are pushed to the crustal boundaries for all combinations of Vo and K.

The optimum values of Vo and K are taken to be those corresponding to the centre of the contours of the standard error map.

i.e. $V = 5.40 + 0.039z.$ 12.

With this model it is possible to locate the events on a simple epicentral

Fig. 33. Contoured standard error map for event P-S times and apparent velocities fitted to a crustal model with velocity increasing with depth. (Assumed minimum standard error at

$V_o = 5.4$ km/s

$K = 0.039\ \text{sec}^{-1}$)

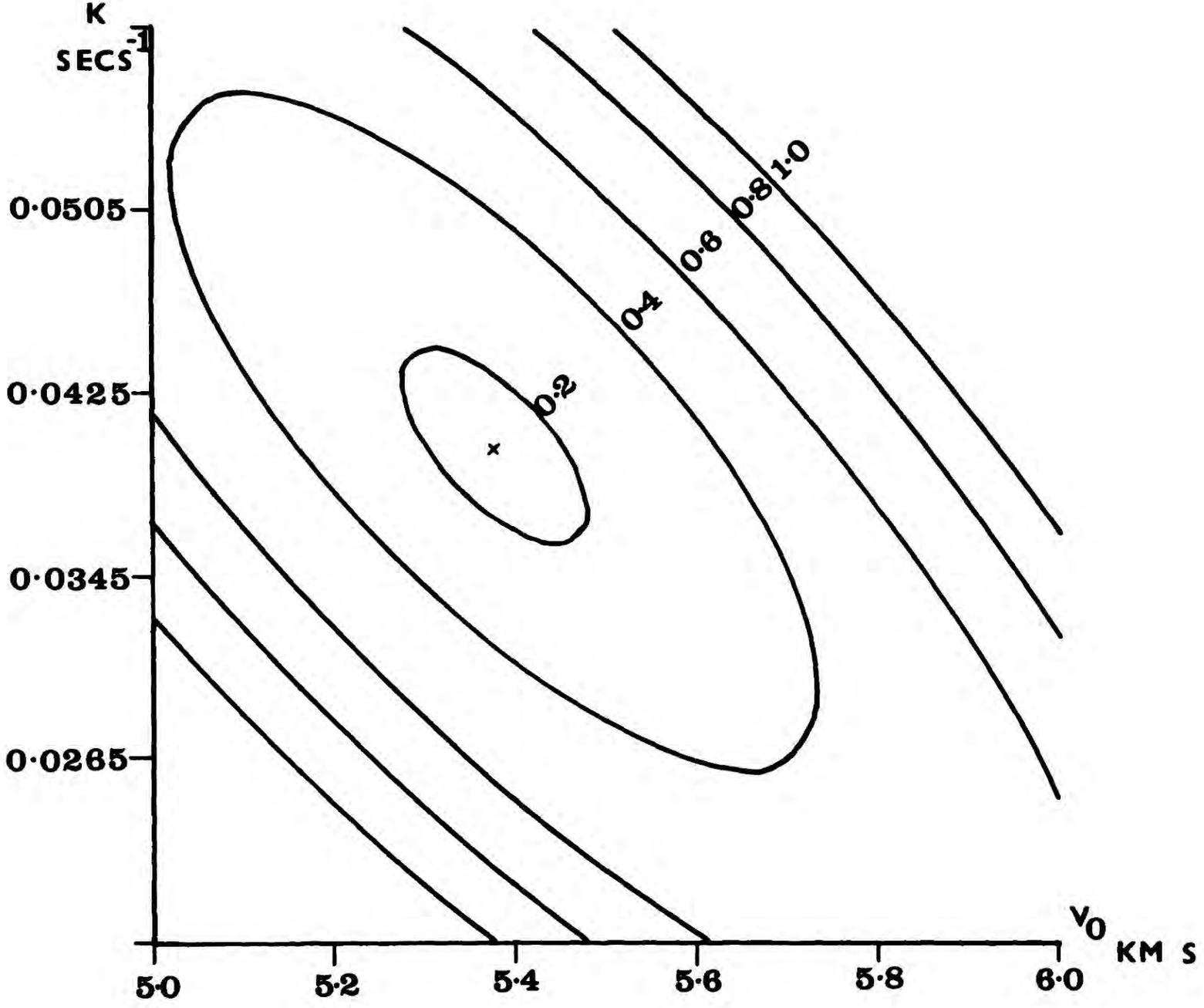
K
SECS⁻¹
0·0505
0·0425
0·0345
0·0265
0·2
0·4
0·6
0·8
1·0
5·0
5·2
5·4
5·6
5·8
6·0
V0 KM S

distance - focal depth plot as in Fig. 34. The mean focal depth has been averaged over a $\pm$10 km window. This can be seen to follow an arc falling from approximately 15 km at a distance of 25 km, to 30 km at a distance of 100 km (Fig. 35). The lack of events beyond this distance results in a loss of control on the mean focal depth. However, the few events from this region suggest that it does rise again. The crustal thickness proposed, 45 km, is greater than the mean value determined for Africa as a whole. However, a smaller value would both

1) push a number of events to the crustal boundaries

and 2) cause events with initial downgoing rays (as B in Fig. 32) to have ray paths which intersect the base of the crust.

This model thus produces a focal depth range which varies with distance from the array and also requires a fairly large crustal thickness, to be compatible with the observed data. The fact that the mean focal depth closely follows an arc, corresponding to a 6.5 km/s apparent velocity across the array (Fig. 35), again suggests that there is an intermediate layer in the crust with this velocity, and MODEL 2 is considered unlikely.

MODEL 3. A TWO LAYERED CRUST.

The azimuth spread of the events peaking at 6.5 km/s (Fig. 30) is from 186 to 290 degrees. No significant azimuthal variation in velocity is evident; a quantitative analysis being considered unjustified since 71% of these events occur between azimuths 210 and 240 degrees. Also there is no significant variation in velocity with P-S time. The scatter in the apparent velocities is thus initially assumed to be due to errors arising from the analysis of these velocities, as in the case of the Moho arrivals. The events peaking at 6.5 km/s are thus assumed to be headwave arrivals from an intermediate layer, which is horizontal at the critical distance from the array. This latter result is consistent with the presence of the horizontal Moho, and also with the near

Fig. 34. Epicentral distance - focal depth plot for events with sub Moho velocities, existing in a single layered crust with velocity increasing with depth.

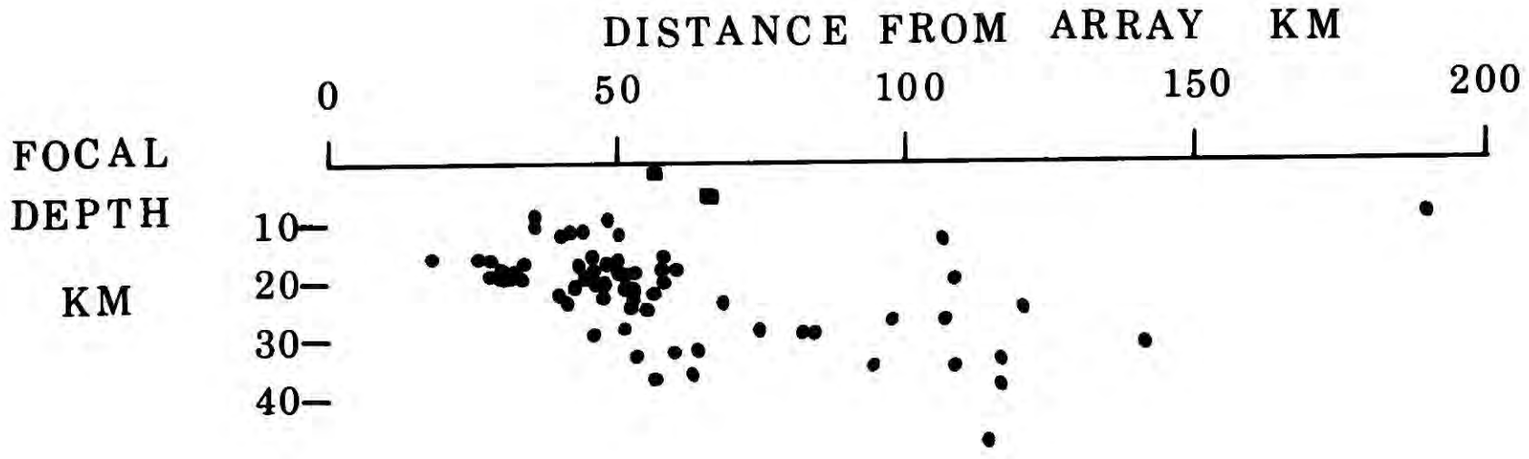
DISTANCE FROM ARRAY KM
0
50
100
150
200
FOCAL
DEPTH
KM
10
20
30
40

Fig. 35. Mean focal depths of events from Fig. 34 averaged over a $\pm$10 km window (circles). Solid line represents locus of event foci, which would have apparent ground velocities of 6.5 km/s.

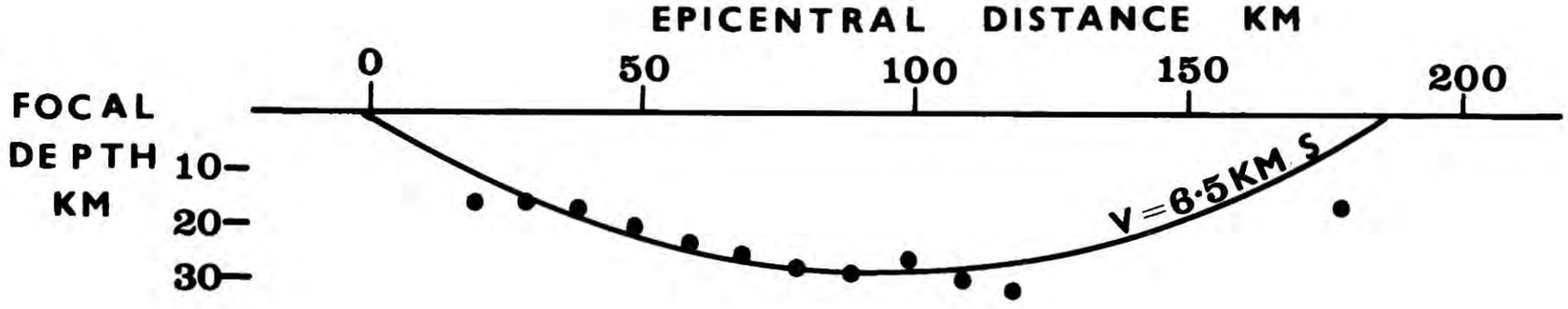
EPICENTRAL DISTANCE KM
0
50
100
150
200
FOCAL DEPTH KM
10
20
30
V=6·5KM S

horizontal surface of the basement complex (2.1).

The weighted mean of the first arrival velocities peaking at 6.5 km/s (Fig. 30) is 6.5 ± 0.3 km/s. Thus it is concluded that the crust to the west of the Gregory Rift is horizontally layered with a 5.9 ± 0.2 km/s layer overlying a 6.5 ± 0.3 km/s layer above an 8.0 ± 0.1 km/s Moho.

5.3.3. DEPTH TO LAYER BOUNDARIES AND FOCAL DEPTHS.

By considering the P-S times of the breaks in the plot of velocity versus P-S time (Fig. 27) as at A and B in Fig. 26(c), it is possible to compute the depths to the layer boundaries.

INTERMEDIATE LAYER.

For a constant focal depth of event, the depth to the intermediate layer can be determined exactly from noting when the P-S time of the P^* arrival is equal to that of the Pg arrival. i.e. the focal depth must be less than the depth to the intermediate layer.

75% of the events in block C (Fig. 29) have apparent velocities of less than 6.5 km/s and thus must have originated in the upper crustal layer. Hence it is possible to determine a focal depth distribution for those events originating in this upper layer from an analysis of the P-S times and apparent velocities of these events.

The most probable focal depth occurs at 16 km, consistent with that derived from the events of block A (see 5.2). If this most probable focal depth is assumed to remain constant at all distances from the array (see 5.1), with the break A (Fig. 26(3)) occuring at a P-S time between 7 and 11 seconds (Fig. 27), a depth to the intermediate layer may be calculated as 18 ± 2 km.

All the events from block C (Fig. 27), have velocities less than

8.0 km/s, implying that they have all originated within the crust.

All of these events are located within the Kavirondo Rift region. Knowing that 18 km of the 5.9 km/s material overlies the 6.5 km/s layer, it is possible to determine a focal depth distribution throughout the crust for this area (Fig. 36). In summing the number of events in the first, second and third ten kilometers of the crust, and relating these sums to those determined in the southern part of the Gregory Rift, (RYKOUNOV et al 1972), it is seen that there is an almost identical relation for the first to the second ten kilometre zone (Fig. 36). However fewer deep crustal events would appear to occur relative to the number in the top 10 km, in the Kavirondo region. A relative rather than absolute comparison was made between the two regions since

1) the time interval over which the data was collected was different in the two analyses

and 2) only those events with good first arrival onsets were considered in this analysis.

The scatter in the velocities of the events causing the peak at 6.5 km/s in block B (Fig. 27) can now also be related to variations in focal depths above and below the intermediate layer discontinuity. (See 5.3.2 (model 3)).

THE MOHO.

If the most probable focal depth of 16 km is taken together with the break B (Fig. 26 (3)) occuring at 18 $\pm$3 seconds(Fig. 27), a depth to the Moho can be computed as 35 $\pm$ 3 km. This value is to some extent confirmed by the fact that no event from block C has a focal depth of greater than 35 km.

The structure of the seismograms made the analysis of second arrivals difficult (see 4). However, identification of the onset time

Fig. 36. Focal depth distribution throughout crustal model 3 for events in Block B. (Fig. 27).

— · — · represents focal depth distribution in northern Tanzania (RYKOUNOV et al 1972).

— — — represents calculated distribution relative to top 10 km distribution in northern Tanzania.

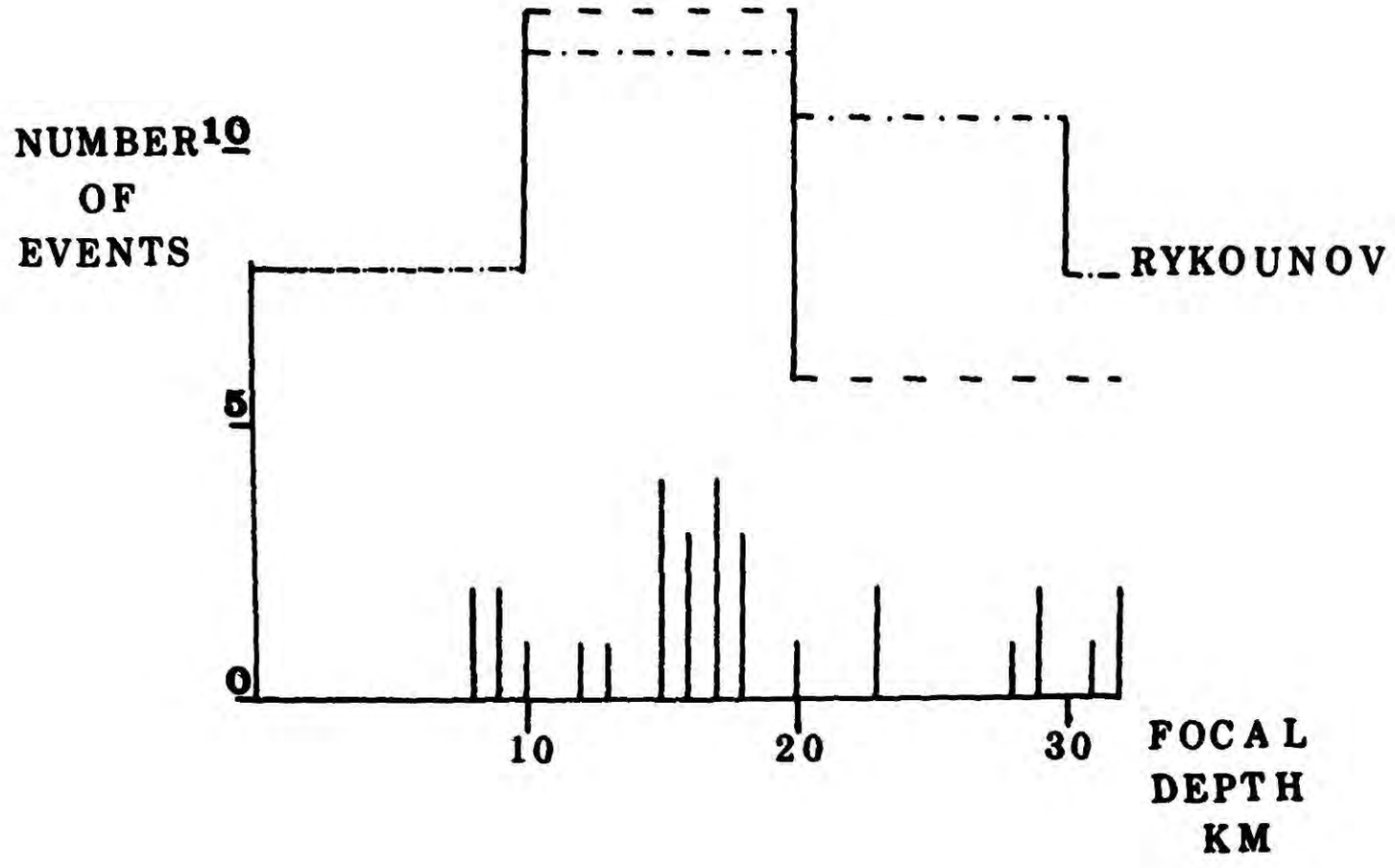
NUMBER OF EVENTS
10
5
0
RYKOUNOV
10
20
30
FOCAL DEPTH KM

of Pm, the Moho reflection, for local events can provide a check on crustal thickness.

For regional events

1) the focal depth of event is unknown

and 2) a variation in crustal thickness will not substantially affect the travel time of Pm.

Hence analysis of Pm, for events originating beyond approximately 200 km, will not provide a good control on crustal thickness.

For those events with P-S times of approximately 6 seconds, large amplitude arrivals were evident, occurring slightly after the initial high amplitude structure (Fig. 37a). As the P-S time of the events increased, so the delay of this arrival decreased with respect to the initial onset time, until it merged with initial P-wave structure (Fig. 37b), with subsequent difficulty of identification. It was assumed that this arrival was Pm. Its onset time was picked for 25 events and its delay relative to the initial onset time, versus P-S time of event plotted (Fig. 38).

The scatter in the data points is likely to be due to

1) varying focal depth of event
2) incorrect reading of the Pm and S onset

and 3) the arrival picked possibly not being Pm on all the records.

However, a theoretical curve for P-Pm time versus P-S time of event for a focal depth of 16 km in the crustal model produced correlates well with the data points (Fig. 38). RICHTER (1958), has quoted a Russian as saying 'For lack of material we restrain ourselves from any kind of conclusion.' In this instance, it may be said that an arrival did occur on the records consistent with that arrival being Pm on the crustal model produced. However, due to the difficulty of identification of Pm, the presence of that arrival does not strictly confirm the crustal thickness of 35 km.

Fig. 37. Two events from western azimuthal zone, indicating Pm arrival.

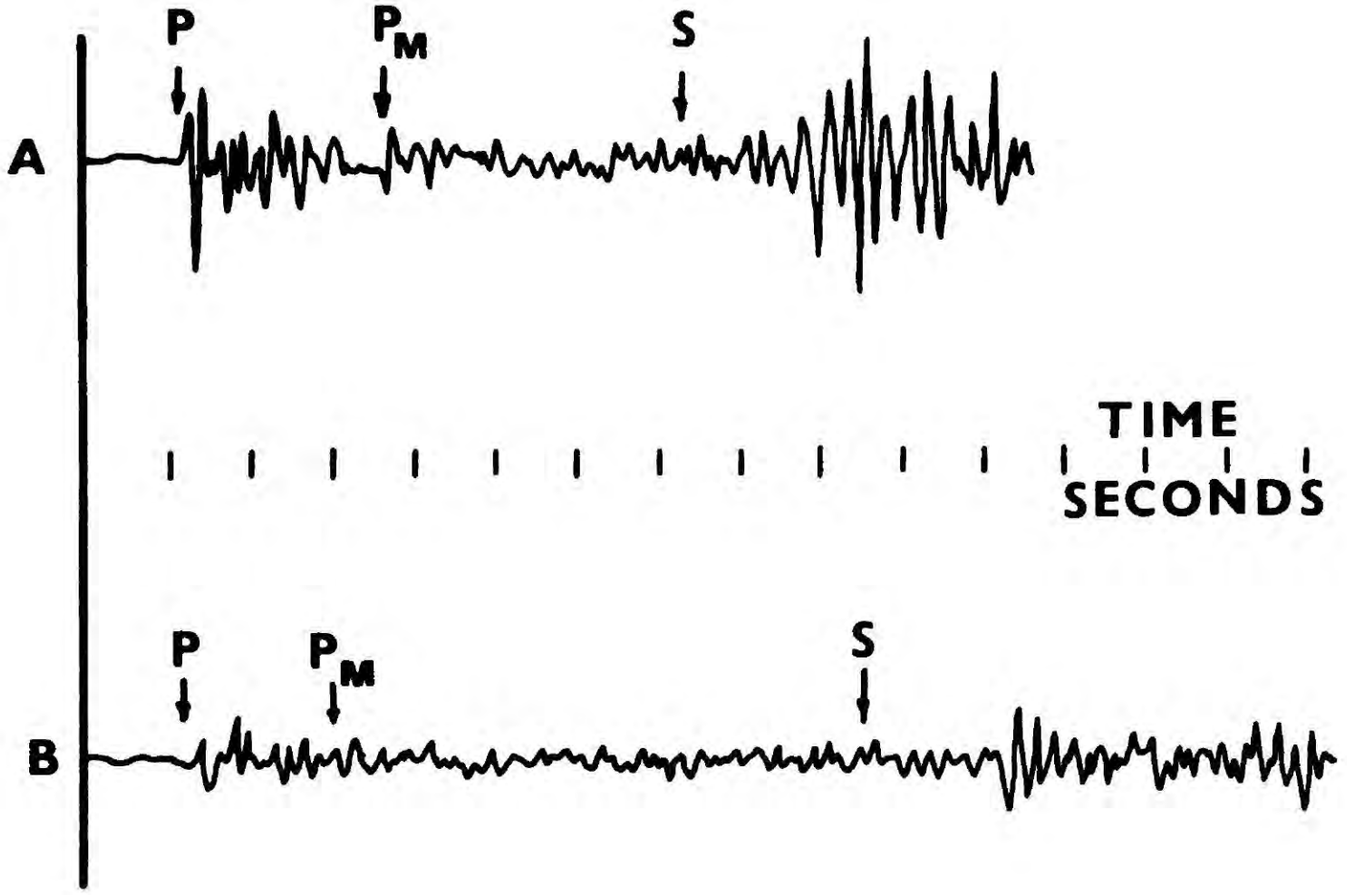
P
P_M
S
A
TIME
SECONDS
P
P_M
S
B

Fig. 38. P-Pm time versus P-S time for local arrivals. Solid line represents theoretical curve for event focal depth of 16 km within two-layered crustal model. (Fig. 44).

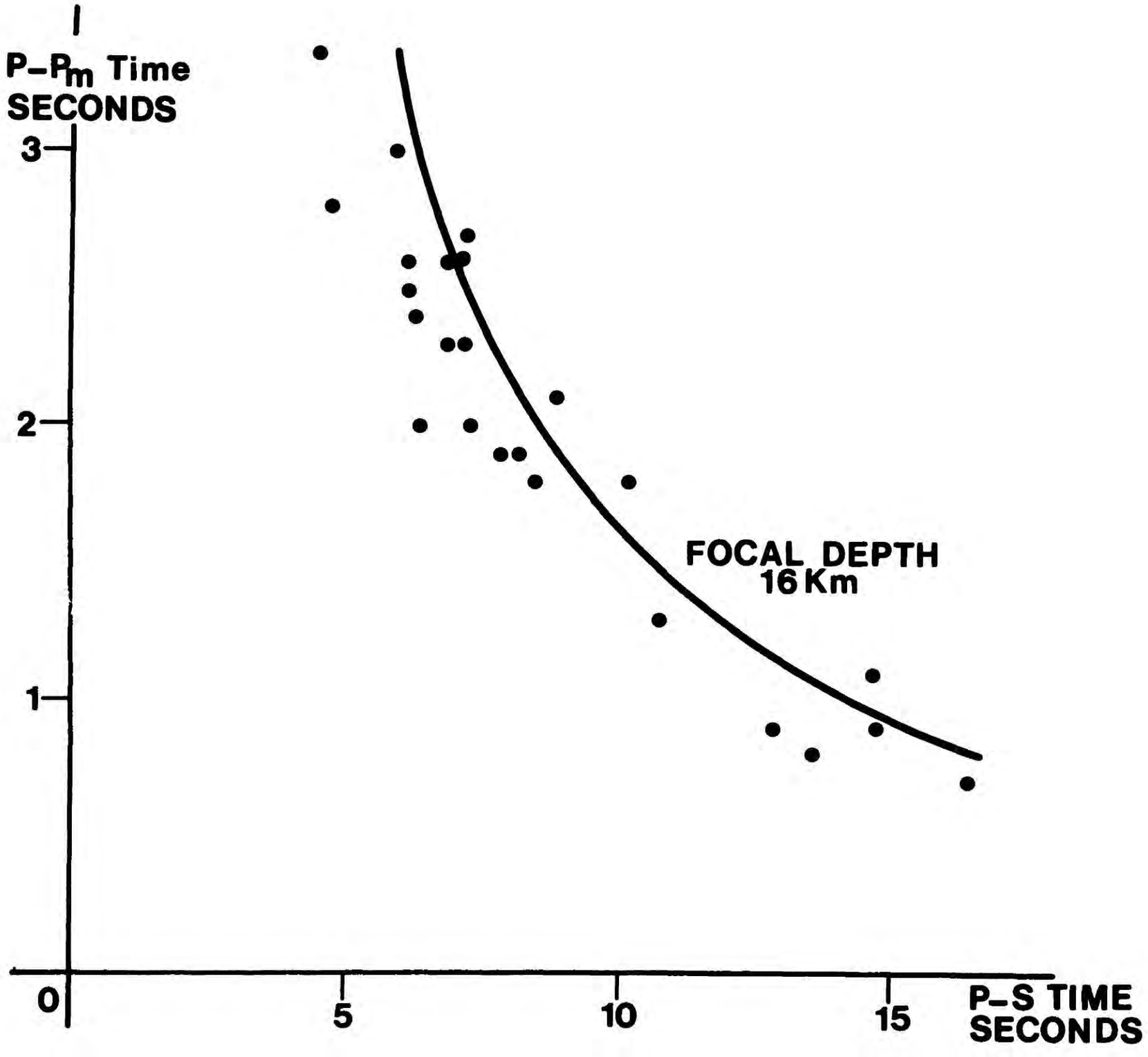
P–Pm Time
SECONDS
3
2
1
0
5
10
15
P–S TIME
SECONDS
FOCAL DEPTH
16 Km

5.4. SYNTHETIC SEISMOGRAMS.

A synthetic seismogram programme has been written (see Appendix) to compute the onset times, apparent velocities and amplitudes of all P, S and mode conversion arrivals incident on the surface from a point source located at depth in a uniform horizontally layered model. The method used is to expand the initial spherical wavefront into a planewavefront formulation, and then to evaluate the integrals resulting from the elastic wave equation in the asymptotic approximation of small wavelengths compared to the dimensions of the model. The displacement at the surface is then associated almost solely with the displacement along the ray path from source to receiver.

It will be stated in Appendix 1 that the synthetic seismograms should not be equated exactly with records of real seismograms. This is due to

1) the breakdown of the theory even in the case of an ideal crustal model, at distances near and beyond the critical distance

and 2) the real crust being considerably more complex than the input theoretical model.

Rather, the results should be considered as a guide in the identification of the arrivals on a real record.

A short discussion of the amplitudes of arrivals to be expected from MODEL 3, is followed by a qualitative comparison of the synthetic and real seismograms associated with the western azimuthal zone (160 - 360 degrees).

5.4.1. RESULTS.

The crustal model (MODEL 3) was input as data. The condition imposed in the theory, that the wavelength of the seismic ray must be small compared with the dimensions of the model, restricts the choice of focal depth. For a dominant frequency content of about 3 $c/_s$, the wavelength of the source function will be approximately 2 km, in the model considered. Therefore, when the focus is placed near a crustal boundary, the resultant arrival amplitudes are likely to differ markedly from the true arrival amplitudes from such a model. However, the onset time of the arrivals will be identical.

Fig. 39 represents a plot of the amplitude of five major P-phase arrivals with distance from the source.

Again, point I) relating to the breakdown of the theory near and beyond the critical distance should be raised. CERVENY (1966) has shown that the amplitude of the reflected wave does not reach its maximum value directly at the critical point (as follows from geometrical ray theory) but beyond it. In this analysis, reflection and transmission coefficients have been considered independent of the frequency of the incident wave. This is not so. CERVENY (1966) has shown that the maximum amplitude of the reflected waves occurs at increasing distances from the source for decreasing frequencies. The maximum value also decreases with a decrease in frequency. He found that for a crustal model similar to the one used in this analysis, the maximum amplitude of Pm decreased by approximately $^1/_7$ of an order of magnitude from the geometric ray theory case to the numerically integrated elastic wave solution case for a wave of frequency 3 $c/_s$. Bearing this fact in mind, Fig. 39 will be discussed.

The arrival containing the greatest amount of energy beyond the critical distance for a Pn arrival, is the Moho reflection, Pm. Its amplitude is approximately an order of magnitude greater than those of the two refracted arrivals and the direct wave. For the model

Fig. 39. Theoretical amplitudes (assuming unit amplitude source) versus epicentral distance, for five major P-arrivals computed on crustal model of Fig. 44 for an event focal depth of 10 km.

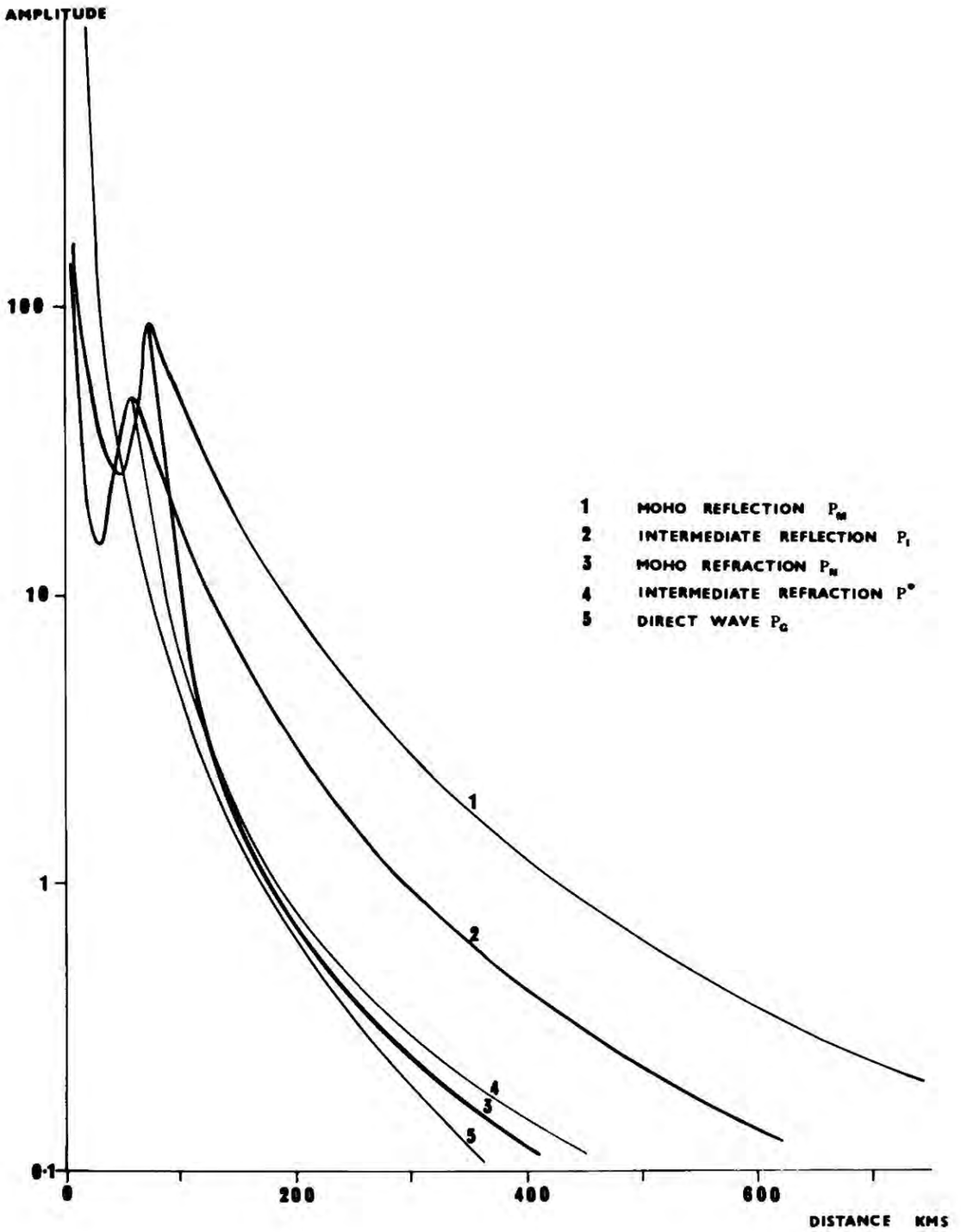
AMPLITUDE
100
10
1
0·1
0
200
400
600
DISTANCE KMS
1 MOHO REFLECTION P_M
2 INTERMEDIATE REFLECTION P_I
3 MOHO REFRACTION P_N
4 INTERMEDIATE REFRACTION P^*
5 DIRECT WAVE P_G
1
2
3
4
5

chosen, the amplitude of the intermediate reflection is approximately midway between that of the refracted and direct arrivals, and the Moho reflection. For a higher velocity contrast across the intermediate boundary, the amplitude of P_I would be increased at all distances from the source. Up to the critical distance for a Pn arrival, the four major arrivals Pg, P_I, P* and Pm have amplitudes which all lie approximately within 1 order of magnitude. Since their travel times differ by no more than about 3 seconds, it would be expected that the initial structure of the local records would be very complex, with the probability of interference between the various arrivals. For a reflected arrival, the apparent ground velocity is greater than the velocity of the medium immediately beneath the reflecting boundary at distances less than the critical distance. As the epicentral distance increases so the apparent velocity tends to the velocity of the medium above the interface. Thus, for example, between the critical distance for P* and Pn, the apparent velocity for $P_I < 6.5$ km/s while that for Pm > 8.0 km/s, for the model considered. Even though the relative amplitudes are similar, it should be possible, through velocity filtering techniques to determine which arrival is which. However, due to the marked interference effects at small epicentral distances, the possibility of distinguishing the various arrivals by their apparent velocities is not as certain as might at first be expected.

For example, considering P, S and mode conversion arrivals at a distance of 55 km including amplitudes differing by three orders of magnitude, 60 arrivals are evident within the first 9.63 seconds with velocities ranging from 3.47 - 13.57 km/s. Since these arrivals are likely to suffer interference effects across the dimensions of the array, the resultant apparent velocity of for example, two interfering arrivals may bear no apparent relation to the true apparent velocities of each individual arrival. However, in such cases there is likely to be a change in apparent azimuth from the true azimuth. There is

thus some means of detecting as to whether an apparently unique arrival onthe array records is in fact composed of two or more phases.

5.4.2. SYNTHETIC AND REAL SEISMOGRAMS FROM THE WESTERN AZIMUTHAL ZONE.

Seismograms of P arrivals occurring up to 10 seconds after the direct arrival have been computed for events with epicentral distances of 100, 210, 290, 365, 485, 590 and 710 km for a constant focal depth of 10 km in MODEL 3 (Fig. 40). (The amplitudes are not drawn to the same scale across the 7 records.)

At 100 km, the five major arrivals Pg, P*, Pn, P_I and Pm occur within the first 1.2 seconds of the record, with resultant difficulty of identification on a real record.

At 210 km a number of groups of arrivals of similar amplitude appear to be fairly evenly spaced throughout the first 10 seconds of the record. These are associated with

1) Pn
2) P*
3) P_I, Pg and (PmP_I) (a double reflection).
4) (PnPm) (a reflected refraction).
5) PnPm with an initial reflection off the free surface.

and 6) $PnPmP_I$ (a triple reflection).

The Moho reflection is markedly evident at this distance.

The records from events occurring at epicentral distances of 290 km and beyond show a characteristically similar structure, with three main groups of arrivals

1) Pn
2) P* and Moho reflections (LCLG)
3) Pg and Intermediate reflections (UCLG)

Fig. 40. Synthetic seismograms of P arrivals occuring up to 10 seconds after direct P arrival, for events with increasing epicentral distances and a constant focal depth of 10 km in crustal model of Fig. 44.

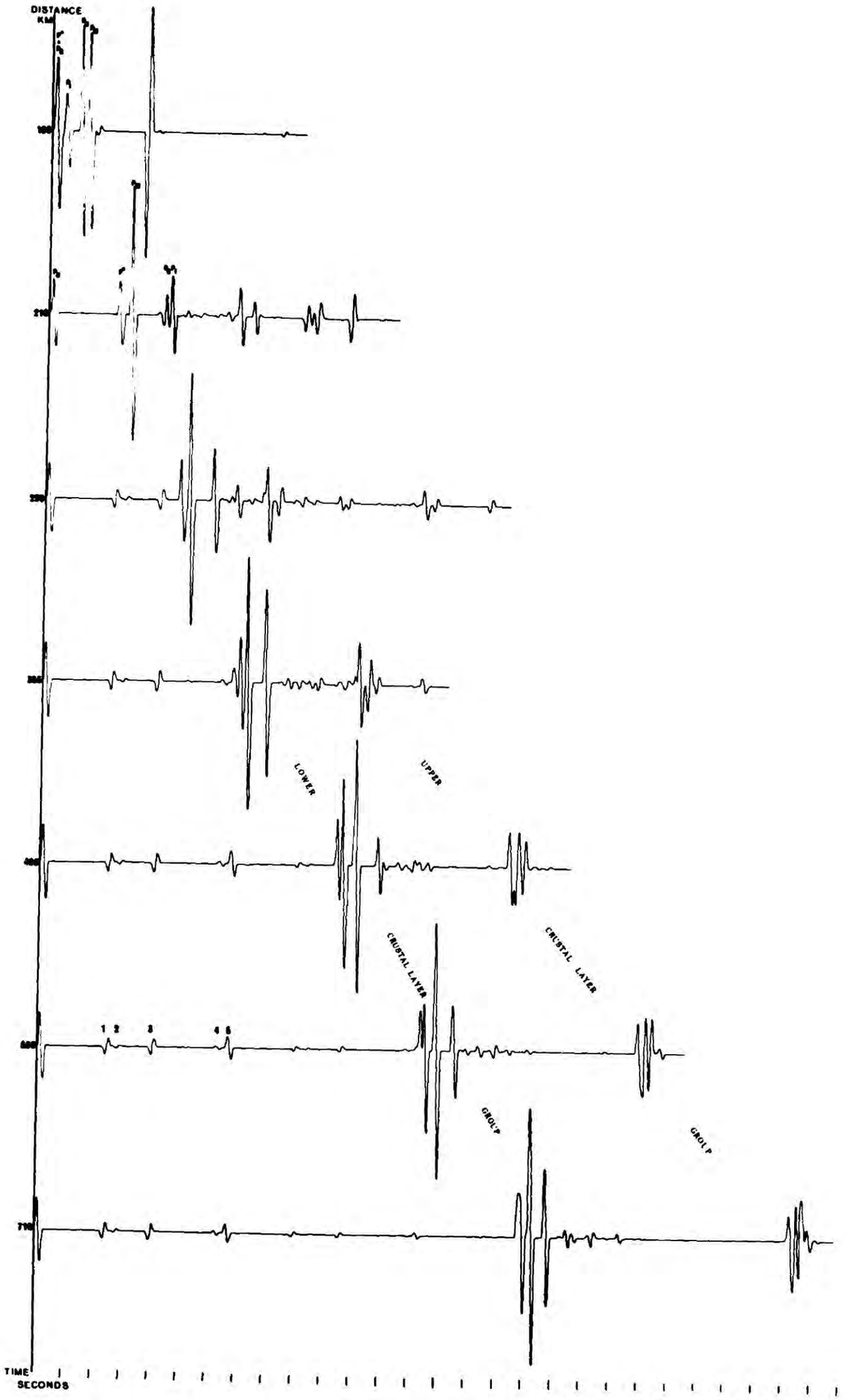
DISTANCE
KM
LOWER
UPPER
CRUSTAL LAYER
CRUSTAL LAYER
1 2 3 4 5
GROUP
GROUP
TIME
SECONDS

As the epicentral distance increases, so the apparent velocities of the arrivals in each of groups 2) and 3) tend to the same intermediate layer velocity and upper layer velocity. Thus if these two groups can be determined and the group velocity calculated, the basic crustal velocity model may immediately be deduced.

Also evident on these distant records are certain small amplitude arrivals that always occur with the same time delay with respect to the initial Pn arrival.

These are direction coded (see Appendix 3)

1 : 122011

2 : 2201211

3 : 2201121

4 : 12201121

5 : 220112211

They all have an apparent ground velocity of 8.0 km/s. If they can be identified with advanced velocity filtering techniques, then with a known crustal model, comparison of the onset times of these arrivals on records from the same azimuth, can lead to an accurate focal depth determination. Alternatively, if the focal depth is known from an analysis of one event recorded at different seismic stations, identification of these arrivals can provide a further check on crustal layer thicknesses.

It can be seen that information gained from one record can provide more information about a crustal model than the same amount of information gained from a number of records. For example, if the first arrivals from three events from the same region are analysed, less information is forthcoming about the crust than if three arrivals from the same event are analysed. However, as stated, the identification of second arrivals is a more difficult process than the simple results quoted here would suggest. McCAMY and MEYER

(1964) developed an elegant velocity filtering technique involving statistical correlation of arrivals. However, their results indicated a profusion of secondary arrival correlations and extreme variations in apparent velocities, apparently precluding the identification of a velocity-depth function.

In comparing the synthetic seismograms (Fig. 40) with real seismograms from the same epicentral distances (Fig. 41), it is firstly seen that the real seismograms are far more complicated than theory would suggest. This is most probably due to

1) mode conversion arrivals
2) a fluctuating velocity-depth profile

and 3) the presence of the volcanics above the basement beneath the array station.

It will be shown than mode conversion from both P to S and S to P on reflections from the layer boundaries, produces further large amplitude arrivals.

Instead of the simple two layered crustal model considered, the velocity depth relation probably fluctuates throughout the crust about the profile produced. Thus a considerable number of extra small amplitude arrivals will occur, which are likely to interfere in general destructively, but possibly constructively, producing a more complex record than predicted. The presence of the volcanic layer beneath the array station will produce extra arrivals with a number of reflections in this layer, associated with each major (and minor) arrival. Since the layer is only of the order of 170-200 m thick, it cannot be included in the synthetic seismogram model. This is because the dimensions of the model must be large in comparison with the wavelength of the seismic wave.

The various P arrivals appear to have more relatively equal amplitudes than expected. However, the refracted and direct arrivals

Fig. 41. Real seismograms of events originating from western azimuthal zone with increasing epicentral distance computed from P to S time, the crustal model of Fig. 44 and a constant focal depth of 10 km.

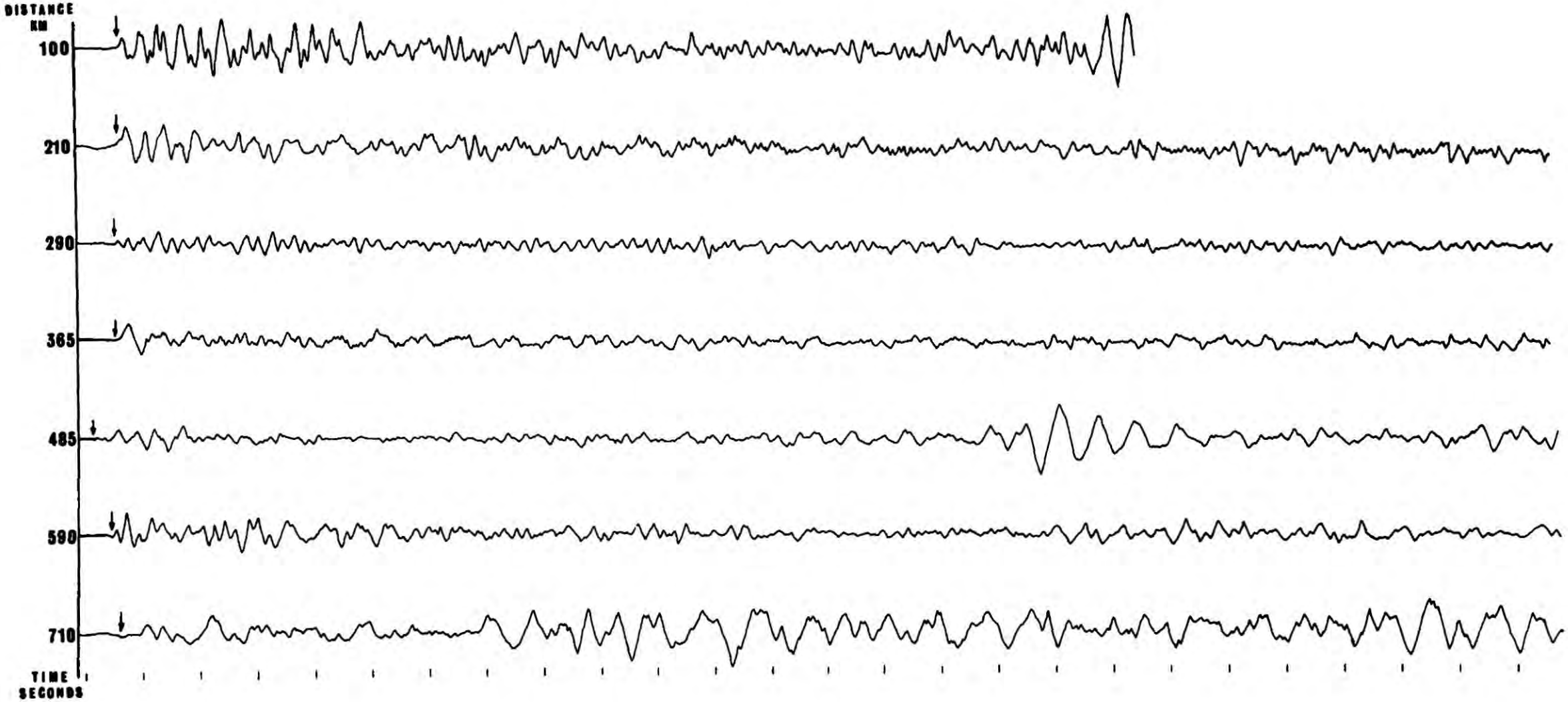
DISTANCE
KM
100
210
290
365
485
590
710
TIME
SECONDS

are likely to have similar amplitudes at large distances from the array. The reflection amplitudes calculated on the plane wave theory, have been shown to be too large (CERVENY 1966) even for the high frequency content local events. As the frequency content tends to lower values of the frequency at greater distances from the array, so the reflection amplitudes become even less.

For the event with an epicentral distance of 485 km, there is remarkably good correlation between the two large bursts of energy corresponding to the reflection groups with velocities of 6.5 and 5.9 km/s, although again, the relative theoretical amplitudes would appear not to correspond exactly with the relative real ones.

The event originating at 710 km from the array is characterized by a large amplitude arrival approximately 6 seconds after the initial onset. This is not evident on the theoretical record. But although the first arrivals will be dependent only on the structure between the source and the array, the later arrivals may be affected by structure at some considerable distance from the first arrival ray-path. In the case of the Kaptagat array station, the structural boundary postulated in 4.3, between the Rift and the shield crust which is concluded to exist to the west of the array, is likely to produce anomolous reflections and diffractions as second arrivals, for events originating in the normal shield crust to the west.

Three synthetic seismograms have been computed for a near surface, intermediate and deep focus event (3, 12 and 27 km respectively) in the crustal model, MODEL 3. (Fig. 42) In the first case, the source is close to one of the crustal boundaries. The resulting amplitudes will thus deviate from the expected amplitudes due to the asymptotic approximation (see 5.4) becoming invalid. But, again it must be emphasized that the seismograms only give an indication of the relative amplitudes of the various arrivals.

These three seismograms also include S waves and mode

Fig. 42. Three synthetic seismograms, including mode conversion arrivals, for events with different focal depths in the model of Fig. 44.

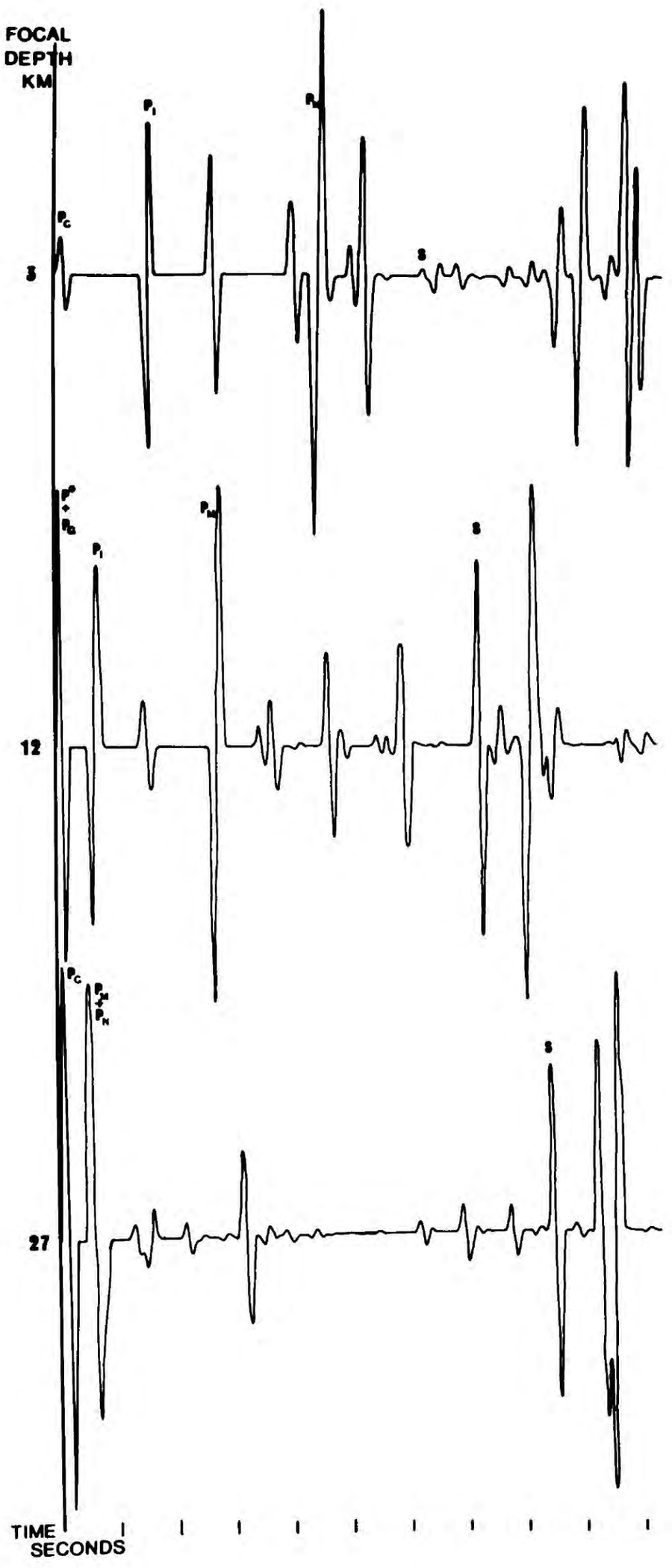
FOCAL
DEPTH
KM
8
12
27
TIME
SECONDS

conversion arrivals. (Their epicentral distances are equivalent to those of three real seismograms Fig. 43). Both the near surface and intermediate focus events are characterized by high amplitude structure throughout the records. The deep focus event is characterized by initial high amplitude arrivals Pg, Pn and Pm, followed by a largely low amplitude section until the onset of the pure S arrivals. The difficulty in estimating crustal thickness from an analysis of Pm from earthquakes of unknown focal depth is immediately apparent. Although there is a slight variation in epicentral distance over the three events ($\pm$ 5 km about the intermediate focus event), the onset time of the Pm arrival after the initial onset, differs by as much as 4 seconds over the three records.

It is seen that mode conversions can produce large amplitude arrivals. For example, the S-P intermediate layer reflection for a near surface focus event has an amplitude approximately half that of the intermediate P-P reflection, P_I. In general it appears that S-P reflections are of larger amplitude than the P-S reflections, but both are of smaller amplitude than the equivalent pure reflections.

The difficulty in velocity filtering of second arrivals is again apparent, from an analysis of the near surface focus seismogram. 6 large amplitude arrivals occur within 1.2 seconds, 4 seconds after the initial onset.

These correspond to the coded arrivals (see Appendix 3).

DIRECTION	P-S CODE	VELOCITY
21	21	6.41 km/s
21	12	6.29
121	121	6.63
121	112	6.64
2211	1111	9.90
12211	11111	10.48

Fig. 43. Three real seismograms with computed near surface, intermediate and deep focal depths from the western azimuthal zone. Computed epicentral distances correspond to

a) 50 km

b) 55 km

c) 60 km.

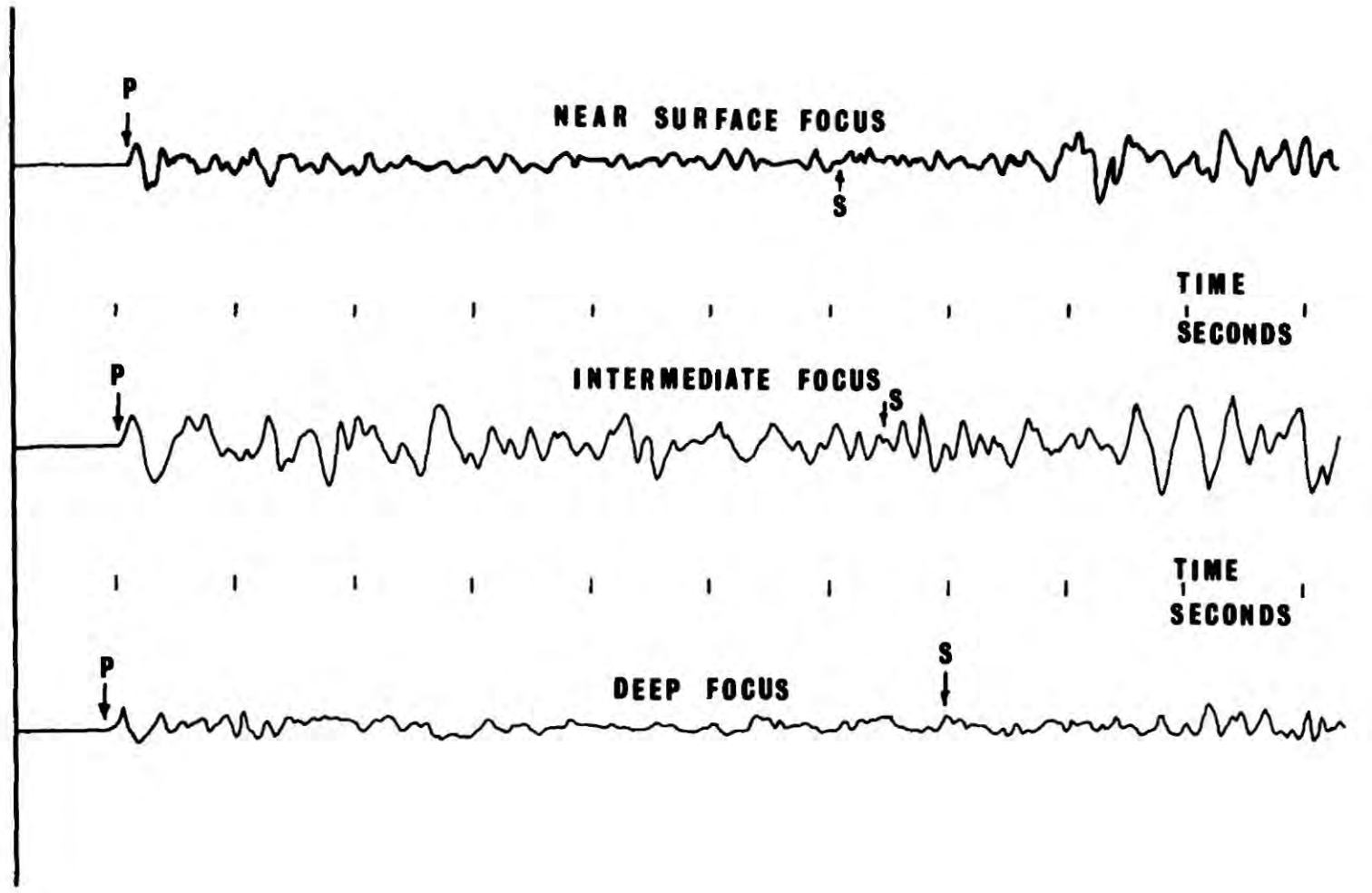
P
NEAR SURFACE FOCUS
S
TIME
SECONDS
P
INTERMEDIATE FOCUS
S
TIME
SECONDS
P
DEEP FOCUS
S

Over the dimensions of the array, the onset times of these arrivals will vary with respect to one another. Interfering phases may peak on velocity filtering at velocities which bear no relation to the individual velocities of the six arrivals.

Three events with epicentral distances of 50 - 60 km (Fig. 43) have calculated near surface, intermediate and deep foci. Since the focal depths were evaluated from analysis of the first arrival velocities, which were subject to errors of up to ± 0.4 km/s in these three cases, the focal depths may also be subject to large errors.

On comparing the three events with their respective synthetic counterparts, it is seen that the real records are again very much more complicated than the theoretical results predict. It is thus difficult to identify the large amplitude arrivals.

However, the near surface focus event (Fig. 43) is apparently characterized by three groups of arrivals before the S-wave onset.

1) immediately following the first arrival
2) after approximately 1.5 seconds

and 3) after 4.5 seconds.

The initial group is not evident on the synthetic seismogram (Fig. 42). It may be composed of reflections of the first arrival in the volcanic layer, and also P*, which is not calculated on the theoretical seismogram for an epicentral distance of 50 km. This is because the distance travelled by P* in the headwave layer is very small, in which case $\text{Amplitude}_{\text{HEADWAVE}} \longrightarrow \infty$ (see Appendix A1). The second and third groups do have their counterparts in the P_I and the Pn group (Fig. 42).

The intermediate focus event is composed of a large number of high amplitude arrivals throughout the P-wave train, which although not directly correlated with the theoretical arrivals, are consistent

with the high amplitude structure of the synthetic seismogram. The large amplitude arrival appearing about 2.5 seconds after the initial onset is consistent with the Moho reflection in the model considered.

The deep focus event lacks the major structure of the other two records, which is again consistent with the theoretical results. However a number of large amplitude arrivals again appear after the initial onset, which are not theoretically predicted.

5.4.3. COMMENT.

The qualitative analysis outlined in 5.4 neither confirms nor disproves the crustal model, MODEL 3. It has merely been a very preliminary outline and comparison of the synthetic seismograms produced from that model, with some real records from which that model was determined.

Firstly, the model relates to the crustal structure only between the headwave critical points and the array station. The synthetic seismograms have been calculated assuming that structure reaches to the hypocentre. Secondly, the crustal model considered is consistent with the first arrival data, but unlikely to be unique to it. No other model has been considered in the synthetic seismogram analysis. In order to obtain some quantitative comparison, between synthetic and real seismograms, and thereby a further indication of the crustal structure, the amplitudes, onset times and apparent velocities of regional events must be determined. (Local events appear to contain a large number of interfering arrivals, which would be difficult to isolate). Finally, it would be useful to obtain numerically integrated seismograms (without the need of the assymptotic approximation outlined in 5.4) to determine the effect on earthquake arrivals of the volcanic layer beneath the basement.

5.5. FURTHER MODELS.

It was stated that 'the simplest crustal structure' with which the data is consistent would be determined (5.1). However, this implies total subjectivity on the part of the scientist, in choosing the accepted and eliminated models. The accepted model is unlikely to be unique, and further models with which the data is consistent must be considered.

The data has been interpreted in terms of an homogeneous two-layered crustal model (MODEL 3). However, two factors cast doubt on the validity of such an interpretation.

1) the seismograms obtained are more complex than would be expected from a two layered crust.

and 2) Laboratory experiments make it extremely unlikely that the upper crust is a constant velocity layer, even if the composition is constant (BIRCH 1960; 1961).

BIRCH (1955) considers, in fact, that a more realistic view of crustal composition, in closer conformity with visible basement structure, is of a mosaic of intrusions of different kinds, metamorphosed sediments and volcanics, even to depths of 10 km or more in places. All of this structure is likely to have been faulted and broken into blocks of various shapes and sizes. Thus lateral variations and gradiants in the physical properties of the crust are likely to lead to a fluctuating velocity-depth function, with a gradual increase in velocity with depth, due to increasing pressure with depth.

However

1) the accuracy of the data limits the determination of the small scale fluctuations
2) it also limits the identification of any gradual increase in velocity with depth over small vertical regions within the crust.

and 3) the method used of interpreting apparent velocities in terms

of crustal velocities, does not directly allow for the determination of velocity reversals within the crust.

Thus the two-layered crustal model produced is as complex a structure as can be directly determined from the data. But is the data consistent with any other geologically-reasonable crustal model?

In considering MODEL 2 (5.3.2), a single layered crust with velocity increasing with depth, it was found that the mean focal depth of event followed an arc, consistent with a 6.5 km/s apparent velocity across the array (Fig. 35). This suggests that a 6.5 km/s layer exists in the crust, if there is to be a consistent focal depth range at all distances from the array.

The data has been interpreted, in terms of a homogeneous 5.9 km/s layer overlying the intermediate discontinuity. However, it would also be consistent with an upper crustal layer in which velocity increased with depth.

If the same velocity-depth relation is assumed as in equation 12, then it is seen that the most probable focal depths of the events originating up to 45 km from the array is still 16 km (Fig. 35). The depth to the intermediate discontinuity would have to increase slightly to 20 km for the first headwave arrivals from the 6.5 km/s layer to have P-S times of 9 seconds (see 5.3.3).

If Vo and K were to be increased, events □ (Fig. 34) would be pushed above the surface. If they were to be decreased

1) The velocity in the uppermost crust would be very low compared with other shield regions

and 2) the large numbers of arrivals with P-S times between 6 and 8 seconds, would become headwave arrivals from the 6.5 km/s layer, which is not the case.

Such a model with P-wave velocity increasing from 5.4 km/s

on the surface to 6.2 km/s above the 6.5 km/s layer is not inconsistent with the data. The mean velocity of about 5.6 km/s for the top 10 km of the crust is low for normal shield, although DOPP (1964) does assume a similar velocity for an upper crustal layer in the Western Rift. It can be seen that further models with K decreasing as Vo increases, assymptotically tend to the simple model (MODEL 3).

A slight increase of velocity with depth within the error limits of $\pm$ 0.3 km/s imposed on the upper crustal layer velocity, would not be inconsistent with the data. Such an increase would be compatible with increasing crustal density with depth, due to a positive pressure gradiant with depth.

Only a linear function relating velocity to depth has been considered. A continuous function, $v = f(z)$, which increased slowly throughout the upper crust, within the limits outlined above and then rapidly increased to about 6.5 km/s, but continuously (i.e. with no intermediate discontinuity) would also fit the observed data.

This would obviate the necessity for having a sharp crustal boundary within the crust, but rather a gradational contact between the upper and lower crustal media.

It can be seen that a number of increasing velocity with depth models fit the data, but they become indistinguishable in the present analysis due to the accuracy of determination of the apparent velocities and P-S times of the events.

From a time-term analysis of seismic refraction data from shots fired in the Irish Sea, BLUNDELL and PARKS (1969) indicate the presence of a 7.3 km/s layer at a depth of 24.4 km below the surface. It is overlayed by a layer of velocity 6.14 km/s. A small number of arrivals from the western group of events have velocities of the order of 7.0 km/s, which have been assumed to originate from the base of the crust. The P-S times of these events lie between 6.0 and 10.0

seconds. If these arrivals are headwaves from a lower crustal layer, then such a layer can only exist within the bottom few kilometres of the crust, and be a critical refractor to those events originating immediately above it. For an event focal depth of 16 km, the minimum depth of such a layer is 25 km if it is not to mask the 6.5 km/s arrivals from the intermediate layer for events with P-S times of less than 18 seconds. Such a layer would still have to be underlain by normal Moho to explain the wide azimuthal range of the 8.0 km/s.

A layer equivalent to the high velocity crustal layer observed beneath the Irish Sea may therefore exist beneath the crust to the west of the Eastern Rift, but since the results are consistent with the normal shield crust model (MODEL 3), its existence cannot be confirmed. Further seismic refraction work, or second arrival analysis would be likely to confirm or disprove its presence.

To explain the discrepancy between the velocities for Pg observed for earthquakes and explosions, GUTENBERG (1954, 1955) postulated a low velocity channel within the crust. Since that time, a number of crustal velocity reversals have been suggested; in the Gulf of Maine (STEINHART et al 1962), in the Alps (O'BRIEN 1964, 1965) and more spectacularly in Western Germany (FUCHS and LANDISMAN 1966). In the latter region, a layer of P-wave velocity 5.5 km/s is considered to exist approximately 10 km beneath the surface, under a layer of velocity 5.9 km/s.

The presence of such a low velocity layer to the west of the Gregory Rift cannot be confirmed from the present analysis, but it would not be inconsistent with the data. It would result in a slight increase in the depth to the intermediate 6.5 km/s layer and a subsequent increase in the depth to the Moho. LANDISMAN and MUELLER (1966) postulated that earthquakes would be likely to originate from a sialic low velocity channel. The depths of foci on the eastern flank of the Rhinegraben commonly lie at depths of 15-20 km (HILLER et al 1967)

which places the hypocentres in the low-velocity channel. The remarkably similar focal depths on the western flank of the Gregory Rift could thus be connected with a similar low velocity channel, but, as stated, its presence is by no means confirmed.

The original two layered, crustal model (Fig. 44) will be used in any subsequent analysis.

Fig. 44. Crustal model deduced from the western azimuthal zone group of events.

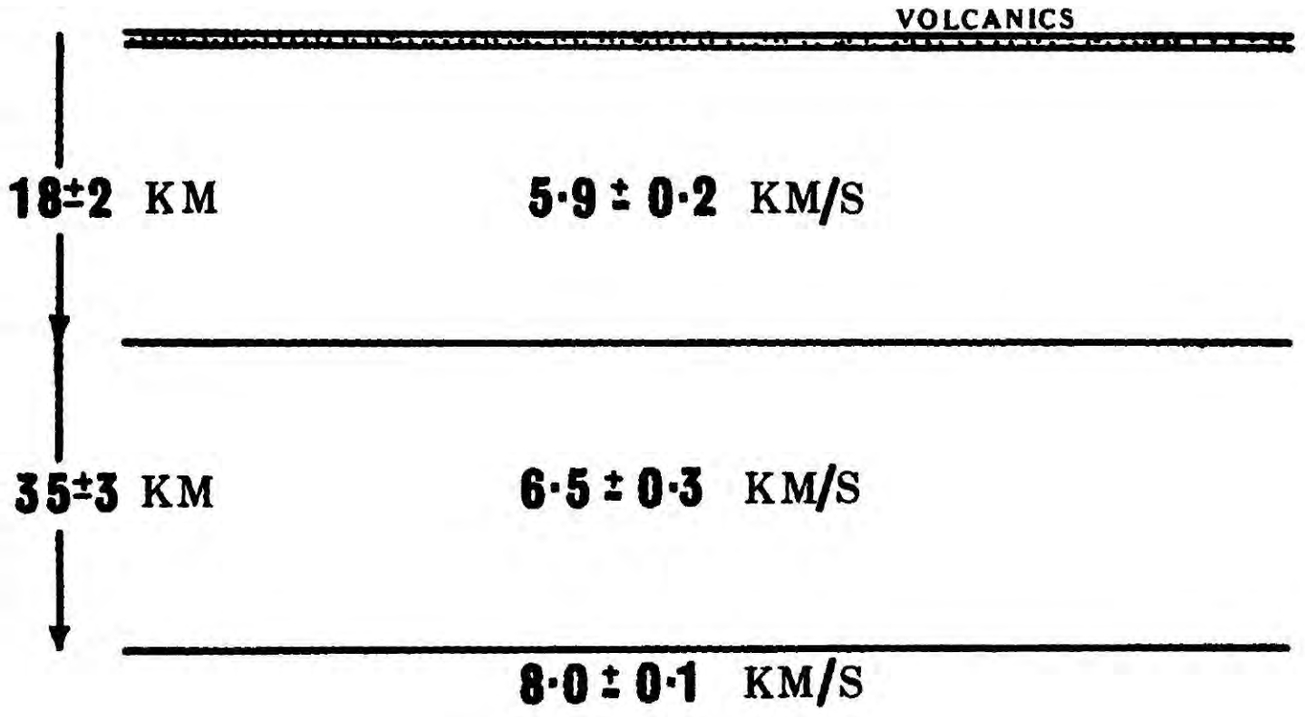
VOLCANICS
18±2 KM
5·9 ± 0·2 KM/S
35±3 KM
6·5 ± 0·3 KM/S
8·0 ± 0·1 KM/S

5.6. DISCUSSION.

All the apparent velocities of the western group of events are compatible with the crustal model produced (Fig. 44). The crustal and Moho velocities are similar to those found in the Canadian Shield (BRUNE and DORMAN 1963). They are also similar to those determined for the Rhodesia - Transvaal Shield in Southern Africa (WILLMORE et al 1952; GANE et al 1956; HALES and SACHS 1959). This latter region is similar to the Tanganyika Shield in remaining stable from 1850 $\pm$ 250 my ago. The crustal velocities determined from this analysis are all related to the structure of the Mozambique Belt, confirming that this is typical of normal shield in the vicinity of Kaptagat. DOPP (1964) observed crustal velocities from the western Rift similar to those predicted beneath Kaptagat. This fact, together with the presence of normal Moho on the western flank of the Gregory Rift, and the satisfactory propagation of Sn across the Lake Victoria downwarp suggests a continuity of the Precambrian shield crust between the Western and Eastern Rifts.

RYKOUNOV et al (1972) produced a crustal model for the southern part of the Gregory Rift in northern Tanzania (MODEL 5) (fig. 4.16) almost identical with that determined from this analysis. BONJER, FUCHS and WOHLENBERG (1970) found that a similar structure (MODEL 6(a)) was required to the east of the Gregory Rift to be consistent with the spectral response ratios of long period body waves recorded at Nairobi. The similarity in the crustal velocities to the east, south and west of the Gregory Rift suggests a further continuity of the crust outlining the central to southern region of the Rift Valley. This is consistent with these areas being characterized by the common Precambrian structure and metamorphism of the Mozambique Belt (McCONNELL 1972).

CHAPTER 6

THE EASTERN GROUP OF EVENTS

(AZIMUTHS 0 to 160 degrees)

6.1. LOCATION.

As stated in 4.2, the presence of the surface lavas beneath the array may be neglected, both in the analysis of P-S times and the apparent velocities of the events.

The events between azimuths 0 and 160 degrees have been located as in Fig. 45, using the model of Fig. 52. Variation in the focal depth of event from the surface to 20 km will cause an error in epicentral distance of no more than $\pm$ 6 km. The events congregate into three regions

1) a group lies along the axis of the Rift, immediately to the east of Kaptagat.
2) three events originate from the region south of Lake Rudolf.
3) a group originates from a region north of Lake Magadi.

In between these three groups, two quiet zones are apparent. However, only events with good first arrival onsets were considered, and this analysis should not be interpreted as a seismicity investigation.

Also included in Fig. 45 are a number of events which originated outside the Rift's western margin, considered in the analysis of the western group.

Fig. 45. Epicentral location of eastern group of events, including a number of events originating to the south of Kaptagat, included in the analysis of the western group. (Solid lines at azimuths 170 and 190 degrees, indicate the eastern most event ray paths sampling the intermediate and Moho boundaries, predicted from analysis of the western group of events).

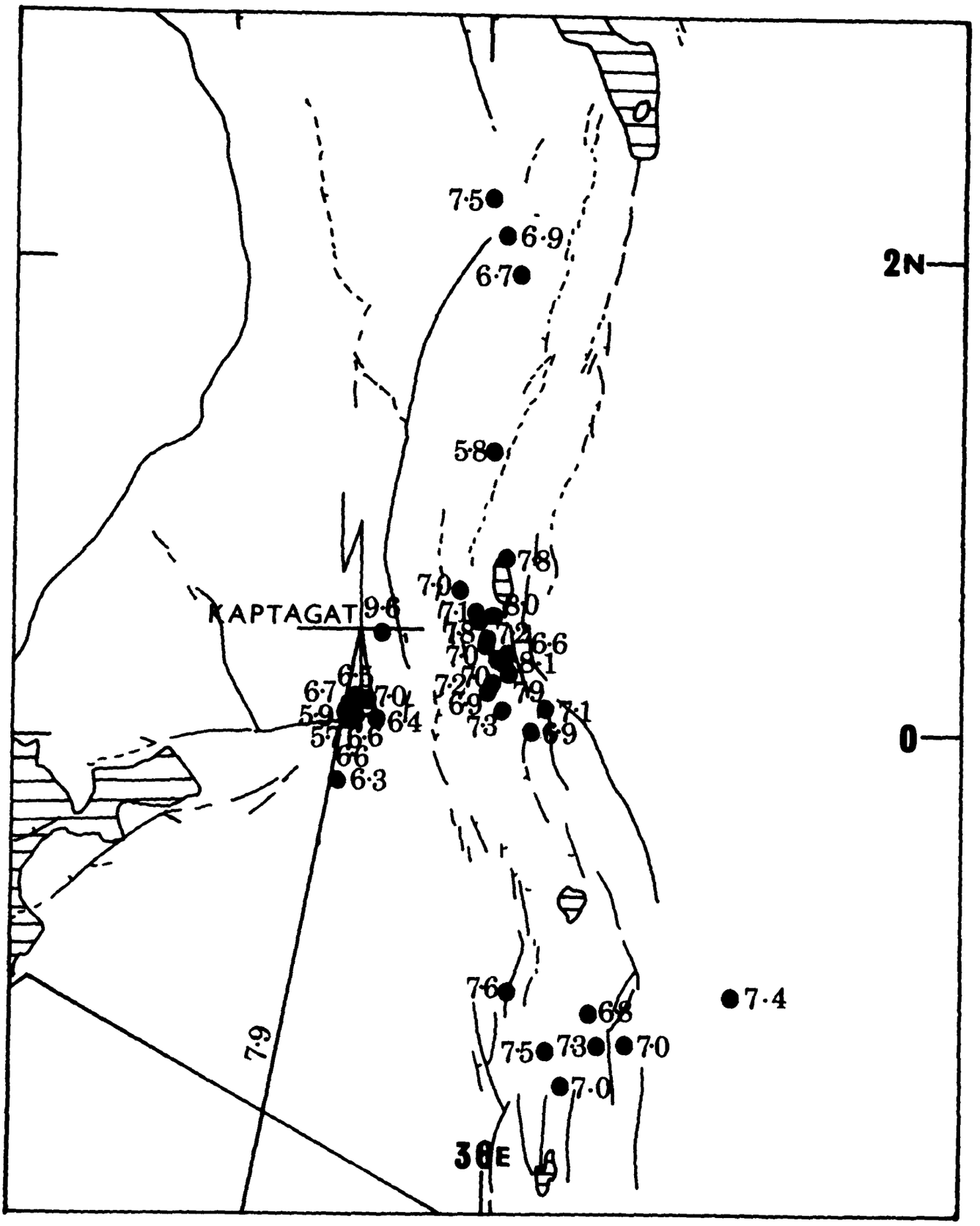
KAPTAGAT
2N
0
7·5
6·9
6·7
5·8
7·8
7·0
9·6
7·1
8·0
7·8
7·2
6·6
7·0
8·1
6·7
7·0
7·2
7·0
7·9
6·9
7·1
5·9
6·4
7·3
6·9
5·7
5·6
6·6
6·3
7·6
6·8
7·4
7·5
7·3
7·0
7·0
7·9
36E

6.2. APPARENT VELOCITIES.

The apparent velocities across the array have been plotted versus P-S time as in Fig. 46.

It is seen that only one event, originating to the north of the array, has a velocity of less than 6.6 km/s. Of the remaining events all have velocities between 6.6 and 7.6 km/s, except four having velocities ranging from 7.8 to 8.1 km/s in the group immediately to the east of Kaptagat.

Firstly, is it possible that the shield crust to the west of the Rift is continuous across the Rift zone?

The critical distance for a Moho headwave Pn is 42 $\pm$ 3 km, while for an intermediate headwave P* it is 38 $\pm$ 3 km. Pn will become the first arrival for a surface focus event for epicentral distances greater than 150 km.

The apparent velocity of 5.8 km/s for the event originating to the north of Kaptagat at a distance of approximately 100 km, suggests that the event has a near surface focus, the first arrival being the direct arrival.

The events originating from the two groups, south of Lake Rudolf and north of Lake Magadi, with epicentral distances of approximately 200 km would be expected to have Pn as the first arrival, velocity 8.0 km/s. Their velocities are substantially lower than this value. This fact together with an apparent variation in the velocities between 7.6 and 6.8 km/s, suggests that the structure through which the rays pass is not horizontally layered crust.

The first arrival velocities of the events originating immediately to the east of Kaptagat can apparently be explained on a normal shield crust model if they originate from the lower crust. In this case a decrease in focal depth from 18 to 30 km will increase the first arrival velocity from 6.5 km/s to 7.2 km/s, after which the Moho headwave

Fig. 46. Apparent velocity versus P-S time of eastern azimuthal zone events.

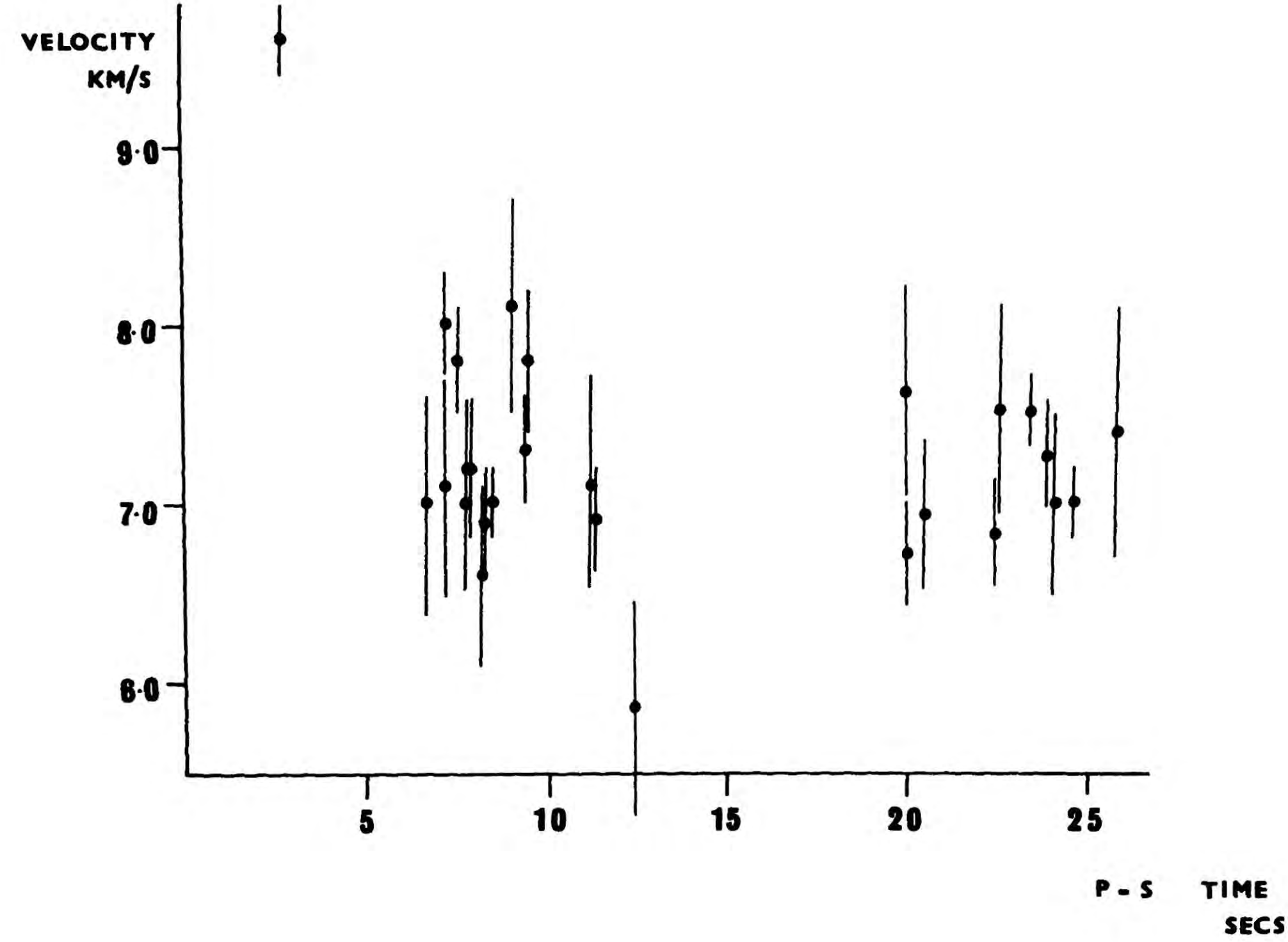
VELOCITY
KM/S
9·0
8·0
7·0
6·0
5
10
15
20
25
P - S TIME
SECS

becomes the first arrival with a velocity of 8.0 km/s, for a P-S time of 8.0 seconds (Fig. 47).

However, one of the 8.0 km/s apparent velocities is associated with the first arrival from the Lake Hannington shot of GRIFFITHS et al (1971). If this first arrival is the Moho headwave, then the Moho must reach to within 7 km of the Rift floor. It would then be impossible to observe velocities of less than 8.0 km/s from events with similar azimuths and P-S times, which is not so. The velocity of about 8.0 km/s for the three earthquakes originating from the same group, in comparison with the Lake Hannington shot, is unlikely to be associated with the Moho. To postulate all the hypocentres in the lower half of the crust is in marked contrast to the focal depth distribution to the west of the Rift and also to the south in northern Tanzania. In these regions the greater number of events occur at depths of less than 20 km.

Omitting those arrivals with velocities of about 8.0 km/s and that with a velocity of 5.8 km/s and assuming there is no marked decrease in focal depth from outside to within the Rift zone, is it possible to associate the arrivals with headwaves from the intermediate layer? Since the velocities are all greater than 6.5 km/s, the intermediate layer would have to dip to the east. The apparent velocity of a refracted arrival would then be azimuthally dependent, the maximum value occurring normal to the strike of the updipping layer. From Fig. 45 it is apparent that the minimum apparent velocity of the eastern group of events, occurs immediately to the east of the array.

It is thus necessary to assume that there is a marked difference in structure between the normal shield crust to the west of the Rift, and the crust beneath the Rift zone itself in order to interpret the apparent velocities in terms of a simple structural model. A simple modification of the horizontal layering of the shield crust does not provide a model consistent with the data.

Fig. 47. Model showing increase of apparent velocity with increasing focal depth for an event originating within the structure of Fig. 44, with a P-S time of 8 seconds.

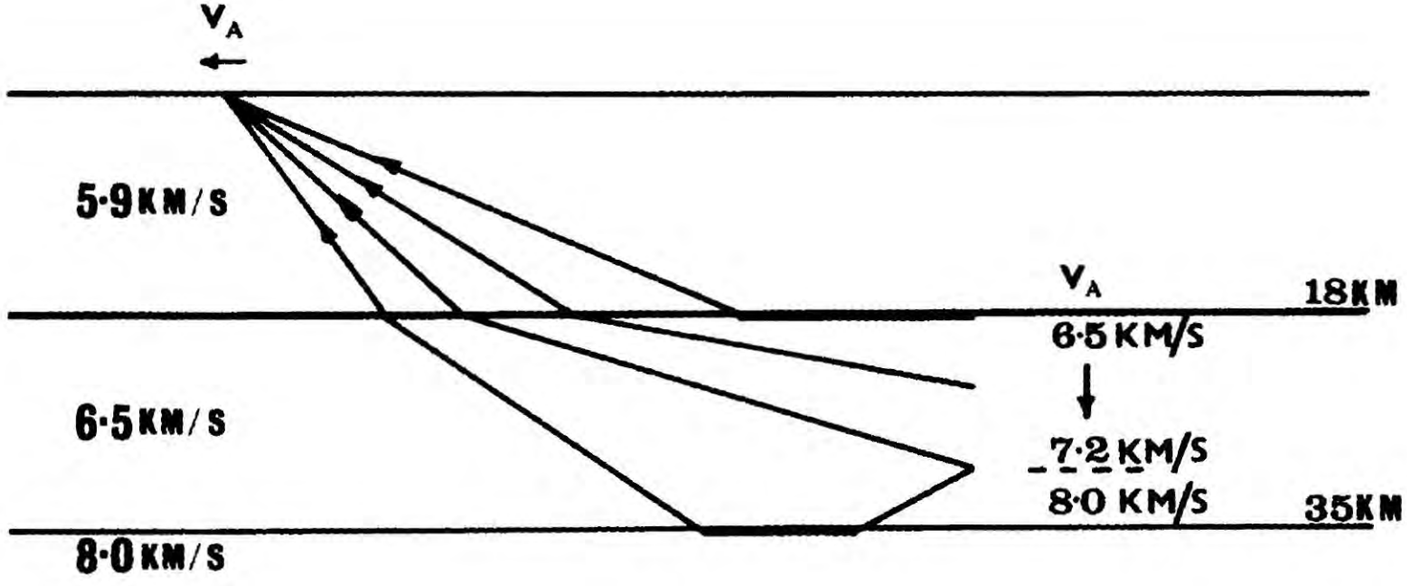
V_A
5·9 KM/S
V_A
18KM
6·5 KM/S
6·5 KM/S
7·2 KM/S
8·0 KM/S
35KM
8·0 KM/S

6.3. ANOMALOUS MATERIAL BENEATH THE RIFT ZONE

In concluding that there is a difference in structure between the crust on the flanks of the Rift and the crust beneath the Rift itself, one fact is immediately evident. Seismic waves from events originating within the Rift zone will have to pass across some structural boundary before they arrive at the array. They are likely to be affected in some way during the transition from the one crustal region to the other. However, in order to analyse the data it will be initially assumed that they are unaffected by the 'transition' zone. Once a model consistent with the data has been determined, the effect of passing from the Rift zone to the flanks will be considered in more detail. As in the case of the western group of events the data will initially be interpreted in terms of a simple uniform layered model.

6.3.1. TWO-LAYERED MODEL.

From shots fired in the Lake Baringo region, taken together with the seismic refraction results of GRIFFITHS et al (1971), it appears that rocks with a velocity of 6.3 - 6.4 km/s exist under approximately 3 km of volcanics beneath the Rift axis.

The first arrival velocities of the eastern group of events are all greater than 6.4 km/s (omitting that event with a velocity of 5.8 km/s) and are assumed to be associated with higher velocity material below the 6.3-6.4 km/s zone.

An azimuthally varying sine function has been fitted by a least squares method through the first arrival velocities of the eastern events, omitting those four with velocities of about 8.0 km/s and that with a velocity of 5.8 km/s (Fig. 48) (see 4.1).

It is found that

$$V = 7.3 \pm 0.3 + (0.3 \pm 0.2) \sin (\circ + 200 \pm 45) \text{ km/s}.$$

Fig. 48. Apparent velocity versus azimuth of eastern azimuthal zone events omitting those four with velocities of about 8 km/s, and that with a velocity of 5.8 km/s. Included is the fitted sinusoid.

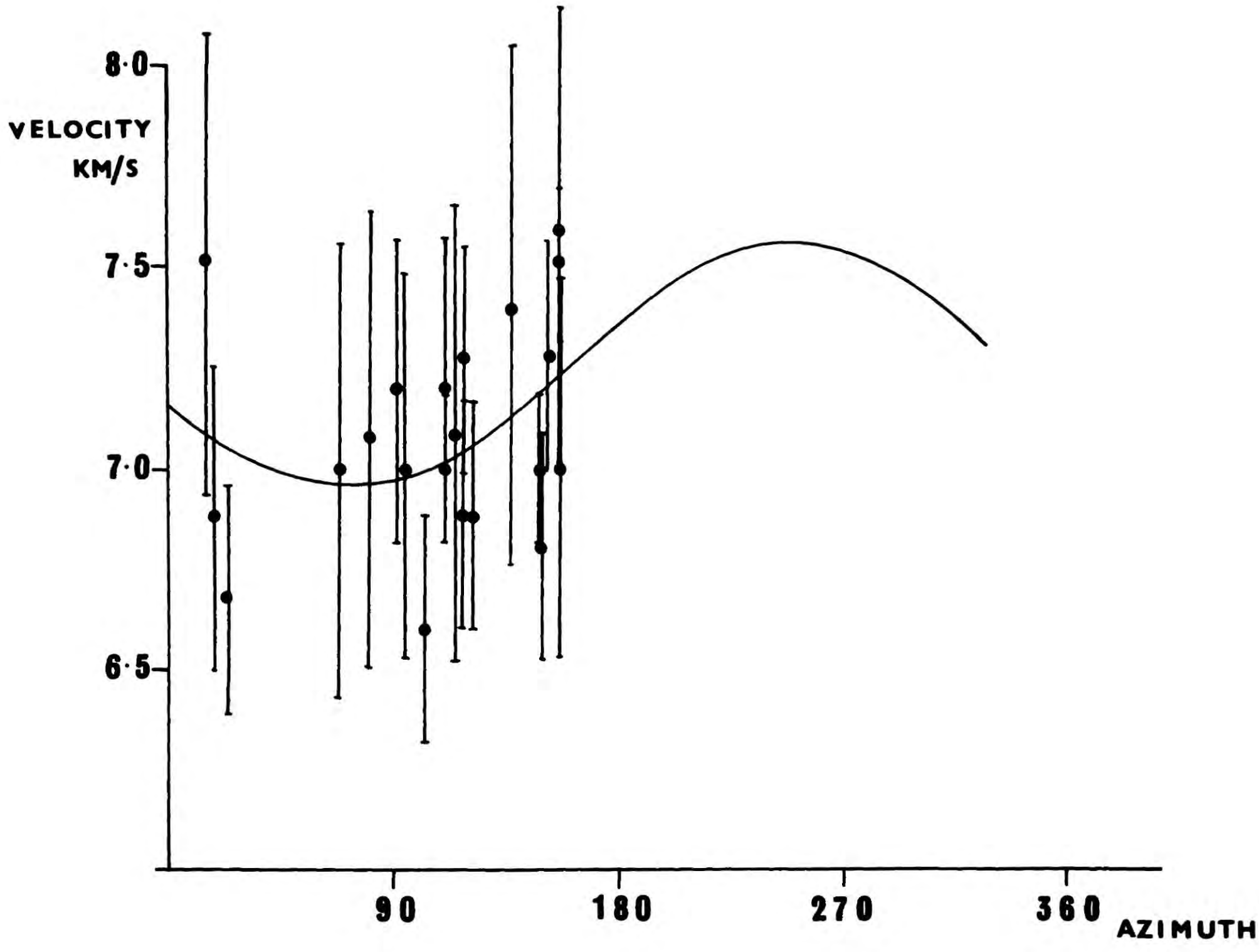
8·0
VELOCITY
KM/S
7·5
7·0
6·5
90
180
270
360
AZIMUTH

This result is consistent with the presence of a headwave refractor of velocity 7.3 $\pm$ 0.3 km/s dipping at 3 degrees to the west, with the strike at 160 degrees. This latter value correlates well with the trend of the Rift Valley, to the east of Kaptagat. Between 0.5N to 1.0S, it is 20 degrees west of north, while south of 1 degree south it is 20 degrees east of north, as it is from 0.5N to 2.0N.

6.3.2. DEPTH TO 7.3 km/s LAYER.

GRIFFITHS et al (1971), from their seismic refraction results postulated the existence of 7.5 km/s material at a depth of 18.5 km beneath the axis of the Rift, north of Lake Hannington. Is it possible for this layer to be equivalent to the 7.3 km/s layer predicted from this analysis?

The two values for the velocity of the anomolous layer cannot be statistically resolved. However lateral variations in velocity of the order of $\pm$ 0.2 km/s over distances of 50 to 100 km would not be unreasonable. In the present analysis, if the 7.3 km/s material is to be as deep as 18.5 km beneath the axis of the Rift, the focal depths of the group of events immediately to the east of Kaptagat must be at least as deep as 14.5 km. This is necessary if the first arrivals of the events with P-S times of approximately 8 seconds are to be headwaves from the 7.3 km/s layer. Such a focal depth appears consistent with the focal depth distribution determined for the western group of events. However, since there is a marked difference in crustal structure between these two zones; the western flank of the Rift is characterized by a stable Precambrian shield crust, the Rift itself is characterized by volcanic, geothermal and microseismic activity and the presence of high velocity material within the crust; there is no reason to suppose that the focal depth distributions will be similar.

From a microearthquake survey within the Gregory Rift, all the events analysed were consistent with having focal depths of less than 5 km (MOLNAR and AGGARWAL 1971). Although the high frequency of microearthquake signals will lead to rapid attenuation with increasing focal depth, such that no deeper focus events are likely to be seen, the marked drop to 14.5 km for the focal depths in this analysis appears unlikely. When it is seen that the focal depths of earthquakes from other regions underlain by a high velocity crustal layer and associated with both continental and oceanic rift systems, are also very near surface, the figure of 14.5 km seems even more unlikely.

From a refraction survey in western Iceland, BATH (1960) observed a 7.4 km/s layer at a depth of 18 km.

The earthquakes in Iceland, originating from a totally volcanic zone lying across the Mid-Atlantic Ridge are likely to be of volcanic and tectonic origin. From a microearthquake survey, including events up to magnitude 5 (WARD et al 1969) (similar to the magnitude of events considered in this analysis where M is of the order 2 - 4 (personal communication from LRA.ARNOLD)) 99% of the events had focal depths of less than 4 km.

The Rhinegraben is characterized by a 'rift-cushion' of velocity 7.6 - 7.7 km/s, 25 km below the surface which extends at least as far as 200 km outside the Rift margins. (MUELLER et al 1969). The Rift zone reaches elevations of at least 2 km (ILLIES 1969), similar to the uplift observed in Kenya. Relative movements between the graben and its shoulders are still in progress, the increase in vertical throw amounting to about 0.5 mm/y (MALZER 1967). The cessation of volcanic activity in the Pleistocene (ILLIES 1969) suggests that the present earthquakes are of tectonic origin associated with the crustal movement in the graben zone. There is a marked change in focal depth distribution from outside to within the graben itself. On the eastern flank, focal depths of 15 - 20 km are common

while in the graben proper depths of foci rarely exceed 8 km. (HILLER et al 1967).

Thus, whether the earthquakes originating from the Eastern Rift are of tectonic or volcanic origin, a near surface focal depth range would appear more consistent with known focal depths from similar, 'anomolous' regions than depths of about 14 km.

If a focal depth distribution of 5 $\pm$ 4 km is assumed, then the 7.3 km/s layer has to reach to within at least 10 $\pm$ 4 km of the Rift floor, which is substantially less than the 18.5 km to the 7.5 km/s layer suggested by GRIFFITHS et al (1971).

A two-layered model of 6.3 - 6.4 km/s matrial overlying a 7.3 - 7.5 km/s layer appears to be too simple a structure to explain both the apparent velocities observed in this analysis, and the results of the seismic refraction line.

GRIFFITHS REFRACTION LINE.

Before continuing with the present analysis, a brief resume of the seismic refraction line and GRIFFITHS (1972) reinterpretation of the results will be outlined.

The shotpoints and station positions are shown in Fig. 49. Reduced travel times for the arrivals from the Lake Hannington and Lake Rudolf shotpoints are plotted as in Fig. 50 a and b. Both figures are obtained from GRIFFITHS (1972). No end-to-end times were available but a difference in the overall extrapolated travel times of approximately 5.5 seconds suggests that the arrivals from the two shotpoints were from two different refracting horizons. GRIFFITHS et al (1971) found that any attempt to construct delay time profiles assuming the arrivals had travelled along the same refracting horizon led to improbable shot-point delays. Hence a two-layered model (MODEL 5)

Fig. 49. Shotpoints and recording stations of the seismic refraction line project of GRIFFITHS et al (1971).

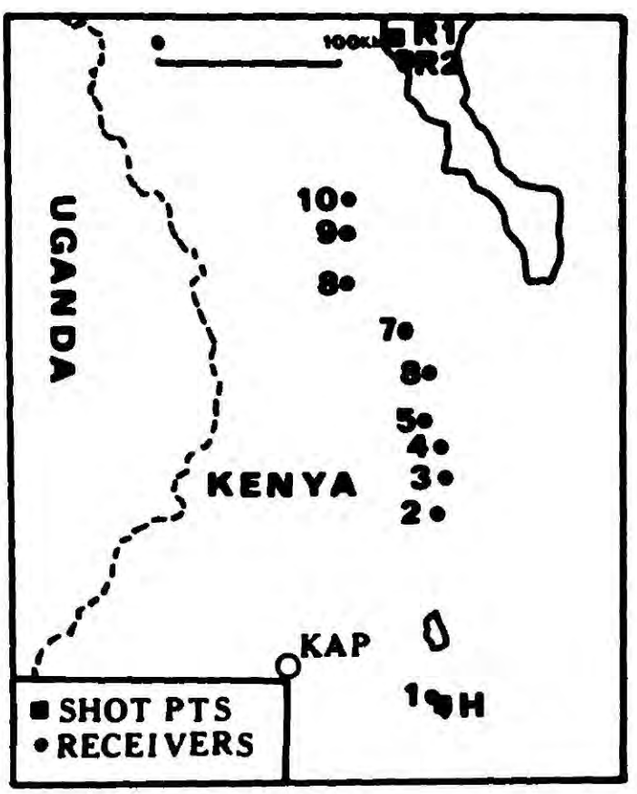
100KM
R1
R2
UGANDA
10
9
8
7
8
5
4
3
2
KAP
1
H
KENYA
SHOT PTS
RECEIVERS

was postulated.

GRIFFITHS (1972) indicated that the first arrivals from the Lake Hannington shot at stations 4, 5, 6 and 7 (Fig. 50a) were early for crustal arrivals, though only the arrival at station 5 seemed early enough to be a refraction from the high velocity layer. He suggested that rocks with a 6.7 km/s velocity could be present at a depth of about 10 km, giving travel times consistent with the data. The 7.5 km/s layer was postulated from the results of the Lake Rudolf shots. The observed delay times can be seen from the reduced travel time plot, to change in a more or less random way along the seismic line, by as much as $\pm$ 0.5 seconds. They show no correlation with the changes in Bouguer anomaly along the line mapped by KHAN and MANSFIELD (1971) and cannot be explained by reasonable velocity variations in the high velocity layer. Hence GRIFFITHS (1972) assumes that there is a highly irregular, possibly in part gradational contact between the 7.5 km/s layer and the overlying material.

6.3.3. THREE LAYERED MODEL.

For a surface focus event the first arrival will be a headwave from the 7.5 km/s for epicentral distances greater than 140 km on GRIFFITHS (1972) three layered model. The group of events immediately to the east of the array, have P-S times corresponding to epicentral distances of approximately half this value. If there is an intermediate layer, their first arrivals are therefore likely to be headwaves from this intermediate layer. Omitting those four events with velocities of 7.8 - 8.1 km/s, the remainder from this group have a weighted mean first arrival velocity of 7.0 $\pm$ 0.2 km/s. With the same focal depth range as assumed previously (5 $\pm$ 4 km), the depth to the 7.0 km/s apparent velocity layer must be no greater than 8 $\pm$ 4 km. The similarity in depth between the 6.7 km/s layer tentatively postulated by GRIFFITHS

Fig. 50. Reduced travel time plots for arrivals from Lake Hannington (a) and Lake Rudolf (b) from GRIFFITHS (1972).

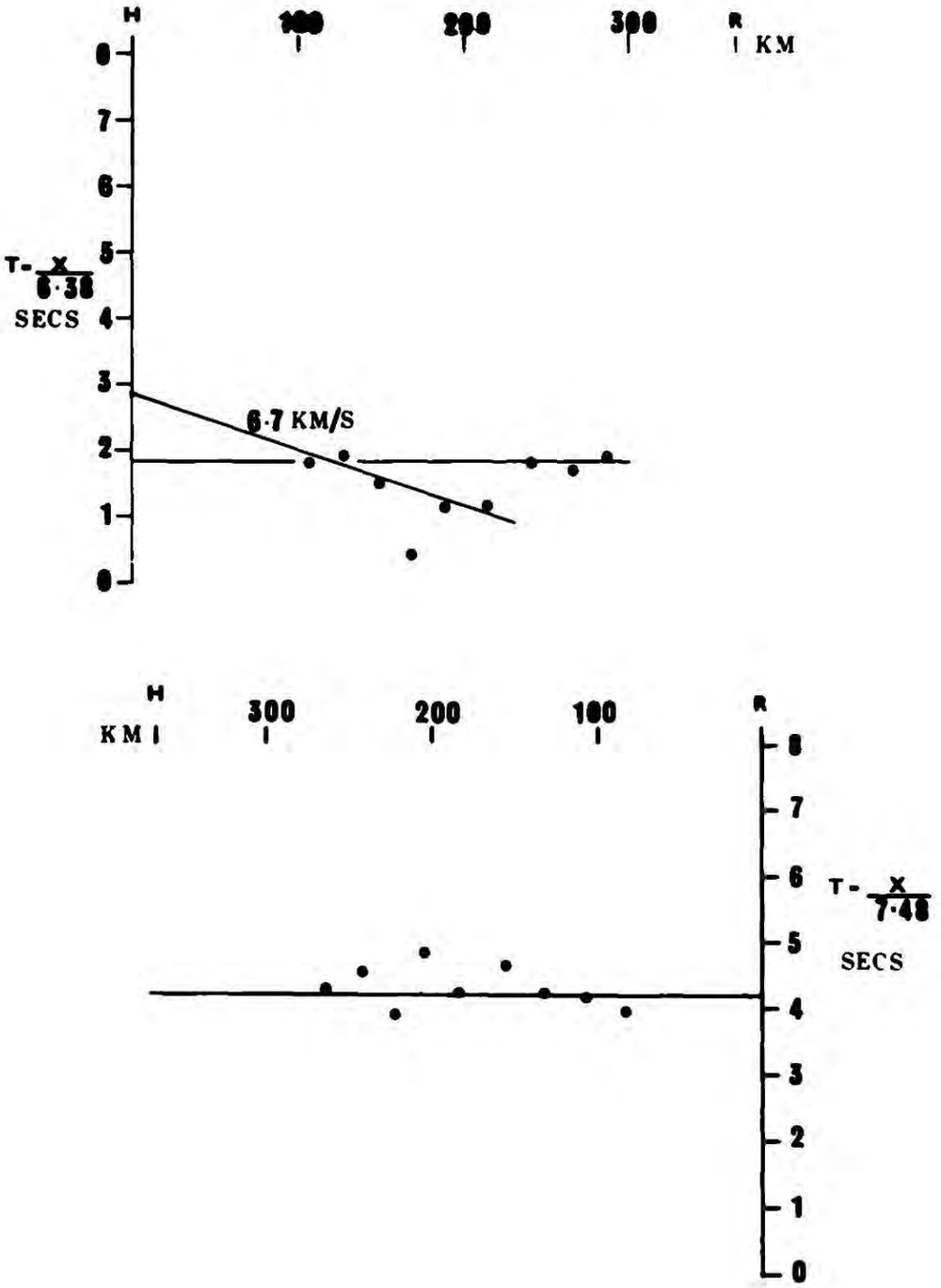
H
100
200
300
R
KM
7
6
5
T - X/6·38
SECS
4
3
6·7 KM/S
2
1
0
H
KM
300
200
100
R
8
7
6
T - X/7·48
5
SECS
4
3
2
1
0

(1972) and the 7.0 km/s apparent velocity layer predicted from this analysis with a geologically reasonable focal depth distribution suggests that the same layer is being observed in each case.

The difference in velocity between the two interpretations is likely to be due to either

1) a 6.7 km/s layer dipping eastwards from the margin of the Rift Valley towards the axis of the Rift
2) A marked lateral variation in velocity, between the material beneath the axis of the Rift and the material at the critical distance from the array

or 3) a 7.0 km/s layer dipping northward from Lake Hannington.

Since headwave arrivals from a layer 10 km beneath the surface of the Rift were not observed on the Lake Rudolf shot records, there can be no direct evidence for a dip on this layer.

However SEARLE (1970) has interpreted the axial positive Bouguer anomaly, mapped from 0.25N to 1.25S in terms of a massive basic intrusion of positive density contrast with respect to the neighbouring crust, existing beneath the graben floor. In the vicinity of the equator, its upper surface is about 6 km below the Rift floor, except beneath the axis where it reaches almost to the surface. It seems probable that the layer of velocity 7.0 km/s or 6.7 km/s is equivalent to the upper surface of this intrusion. In addition to the gravity interpretations, the indirect evidence of volcanic and geothermal activity centred on the axis of the Rift (SEARLE 1970), again suggests that this intrusion is likely to reach nearer to the Rift floor in this region, rather than at the flanks. Hence, if there is any dip on the upper surface it is more likely to be to the west, and not to the east as in case (1). In which case 7.0 ± 0.2 km/s may be taken as a lower limit to the P-wave velocity of this layer (see 4.1). As no further control is available on the angle of dip of this layer, the data will be

interpreted in terms of a simple horizontal layer of velocity 7.0 ± 0.2 km/s. Such a horizontal boundary would not be inconsistent with SEARLE's (1970) model of the intrusion in the vicinity of the equator, which has an approximately horizontal surface westward from the Rift axis.

The critical distance for a headwave arrival from the postulated 7.0 km/s layer is 17 km (see 6.3.4). The critical point due east of Kaptagat thus lies approximately 30 km west of the north-south refraction line. The difference in the velocities of 6.7 km/s and 7.0 km/s could be related solely to a lateral variation in velocity across a horizontal layer although such a variation would be large; 0.3 km/s in 30 km. However, if the 7.0 km/s velocity is indicative of the layer velocity, then the 6.7 km/s velocity material, which GRIFFITHS (1972) predicts might be present at approximately the same depth, could be indicative of the 7.0 km/s layer dipping to the north.

Due to the high structural complexity along the axis of the Rift as evident from

1) the large scatter in delay times from the seismic refraction results

and 2) the lower velocity first arrivals seen at distances beyond the higher velocity first arrivals from the Lake Hannington shot (Fig. 50a)

any calculation of dip on the 7.0 km/s layer is liable to be very inaccurate. However, a maximum possible dip of 6 degrees, from a depth of 6 km due east of the array, to a depth of 18 km, 150 km north of the shotpoint, is compatible both with the observed apparent velocities and the travel times of the seismic refraction arrivals. Such a model would also be more consistent with the event originating 100 km north-east of the array with an apparent velocity of 5.8 km/s. If the 7.0 km/s layer remained horizontal to the north of Kaptagat, the first arrival from this event would be expected to be a 7.0 km/s

headwave. Since the layer apparently dips northward, the first arrival from this event would be likely to be the direct arrival passing horizontally through the 5.9 km/s material beneath the array station.

The first arrival velocities from the two groups to the north of Lake Magadi and to the south of Lake Rudolf show considerable variation between 6.8 and 7.6 km/s. All the events originate from beyond the distance where a headwave arrival from the 7.5 km/s layer, suggested by GRIFFITHS et al (1971) becomes the first arrival. Hence a large scatter in the first arrival velocities would not be unexpected due to the 'highly irregular, in part gradational contact' between the 7.5 km/s layer and the overlying material.

The events from the south originate from the northern part of the zone investigated by KYKOUNOV et al (1972) which was interpreted as being normal shield crust. Hence ray paths crossing from this region into the zone of crustal intrusion to the east of the array are liable to be highly complex. This will result in increased scatter of the first arrival velocities. The events to the north will pass through the crustal intrusion as postulated from the refraction results of GRIFFITHS et al (1971). Considerable crustal complexity is again likely to occur depending on whether

1) the 'gradational, irregular' contact between the 7.5 km/s layer and the overlying material is of large or small vertical dimension
2) the irregularity of the intermediate contact
3) the lateral and longitudinal extent of the intrusion

and if the upper surface of the 7.0 km/s material as evident to the east of the array dips to the north

4) whether the 7.5 km/s layer follows the dip of the 7.0 km/s material or remains horizontal.

Hence, once again the ray paths for the events originating to the south of Lake Rudolf are liable to be highly complex, with resultant

increased scatter of the first arrival velocities.

Thus any conclusions based on the results of these two groups must be very tentative. They are not inconsistent with the presence of a highly irregular 7.5 km/s crustal layer but they do not confirm its presence.

A simplified three layered crustal model of 6.3 - 6.4 km/s material beneath the axis of the Rift, above a 7.0 km/s layer dipping gently to the north, or showing a marked lateral variation in velocity of the order of 0.3 km/s in 30 km, over an irregular contact with the 7.5 km/s material is in greater agreement with both the Kaptagat data and the seismic refraction data, than is the previously postulated two-layered model.

6.3.4. LATERAL EXTENT OF THE AXIAL INTRUSION.

Normal Moho velocities have been observed from azimuth 190°, while normal intermediate layer velocities have been observed from 170° (Fig. 45). The critical distance for P* and Pn are 38 $\pm$ 3 km and 42 $\pm$ 3 km respectively. At those distances from Kaptagat at the above azimuths, the western fault scarp of the Gregory Rift is approximately 18 km and 32 km from the critical points on the ray paths P* and Pn respectively. Thus it is concluded that normal crust exists to within 32 km of the Rift margin, and possibly to within 18 km of it at latitude 0.05N.

Material of velocity 5.9 km/s is concluded to exist 170-200 m beneath the array. Rocks with a velocity of 6.3 - 6.4 km/s have been shown to exist about 3 km beneath the axis of the Rift (GRIFFITHS et al 1971). Hence there must be some lateral change in the density of the upper crust westward from the Rift axis. SEARLE (1970) estimated a smooth, background anomaly corresponding to the broad

regional low Bouguer anomaly over the Rift.

This background anomaly was subtracted from the Bouguer anomaly, leaving as a residual, the short wavelength axial positive anomaly over the Rift region. The amplitude of this residual in the vicinity of the equator falls rapidly from about 60 to 25 mgals in approximately 30 km from the axis to the Rift's western margin. Since the 6.3 - 6.4 km/s material is near to the surface beneath the axis, a fairly rapid lateral variation in velocity to 5.9 km/s at the margin would be expected, to be consistent with the large gradient of the residual positive Bouguer anomaly.

If the 7.0 km/s material predicted in 6.3.3. is now assumed to underlie 5.9 km/s material at the margins of the Rift, it is possible to trace a headwave arrival from a 7.0 km/s layer as in Fig. 51 to estimate the lateral extent of that layer. It is found that it must reach to within 7 km of the Rift margin assuming the dimensions of the model as shown. There must be a steep boundary down to the Moho, since normal crust is evident to the west of the boundary fault. This is the simplest model considered, but some considerable crustal complexity is likely at the contact between the 'intrusion' and the intruded crust. The figures should therefore be only taken as estimates of the dimensions of crustal structure.

Due to the lack of events originating in the north-west sector from Kaptagat, there is little control onthe extent of the intrusion to the north of the array station. However, if the event with a velocity of 7.5 km/s observed from an azimuth of 16 ± 7 degrees, is associated with a headwave arrival from the 7.5 km/s layer, then this material must reach approximately to the Rift margin at the critical distance to the north of the array. However, such a calculation must tend to conjecture, due to the inaccuracy of determination of the parameters α and V for the events, which should therefore be interpreted statistically over a number of events, to reduce the error in the

Fig. 51. Representation of headwave arrival from 7.0 km/s layer passing through 5.9 km/s material beneath the array, producing estimate of lateral extent of 7.0 km/s material.

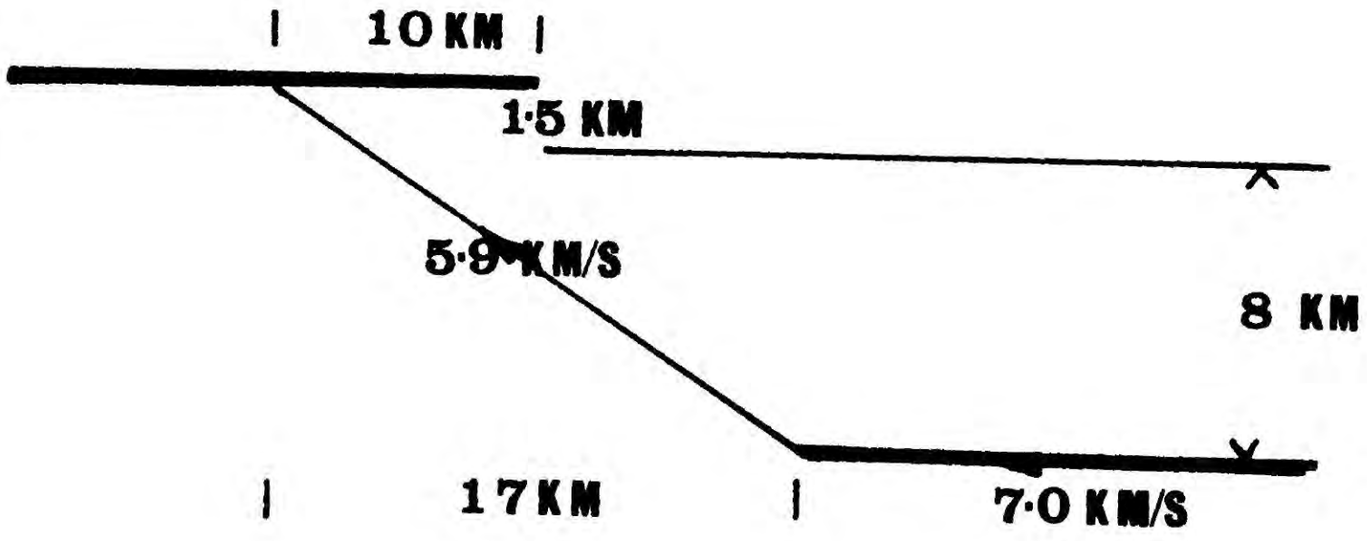
10 KM
1·5 KM
5·9 KM/S
8 KM
17 KM
7·0 KM/S

calculated crustal velocities.

Is there any evidence for the existence of anomalous material to the west of the Rift margin? Following an identical discussion to that in 5.5. relating to the possible existence of 7.0 km/s material at depth to the west of the array, it again may be concluded that 'anomalous' high-velocity material could exist at the base of the crust to the west of the Rift, but

1) it must be underlain by normal Moho and is therefore unlikely to be directly associated with the anomalous material as evident beneath the Rift zone. This is underlain by anomalous low density Moho material.
2) its existence cannot be confirmed from this analysis since the western event data are consistent with the normal shield crust model (MODEL 3) (Fig. 44).

6.3.5 8.0 km/s ARRIVALS FROM THE RIFT ZONE.

The four arrivals with apparent velocities of about 8.0 km/s from the Rift zone immediately to the east of Kaptagat, are difficult to explain on the crustal model produced (Fig. 52). However, a number of explanations for the presence of such an arrival velocity can be considered.

1) Structural complexity beneath Kaptagat is affecting arrivals from azimuths near 90^{o}.

This is difficult to reconcile with the apparently consistent velocities of 7.0 km/s seen from the same region as the anomalous 7.8 - 8.1 km/s velocities.

2) The arrival from the Lake Hannington shot had an apparent

Fig. 52. Crustal model westward from Gregory Rift axis. Estimate of depth to 7.5 km/$_s$ material beneath Rift zone, obtained from GRIFFITHS et al (1971).

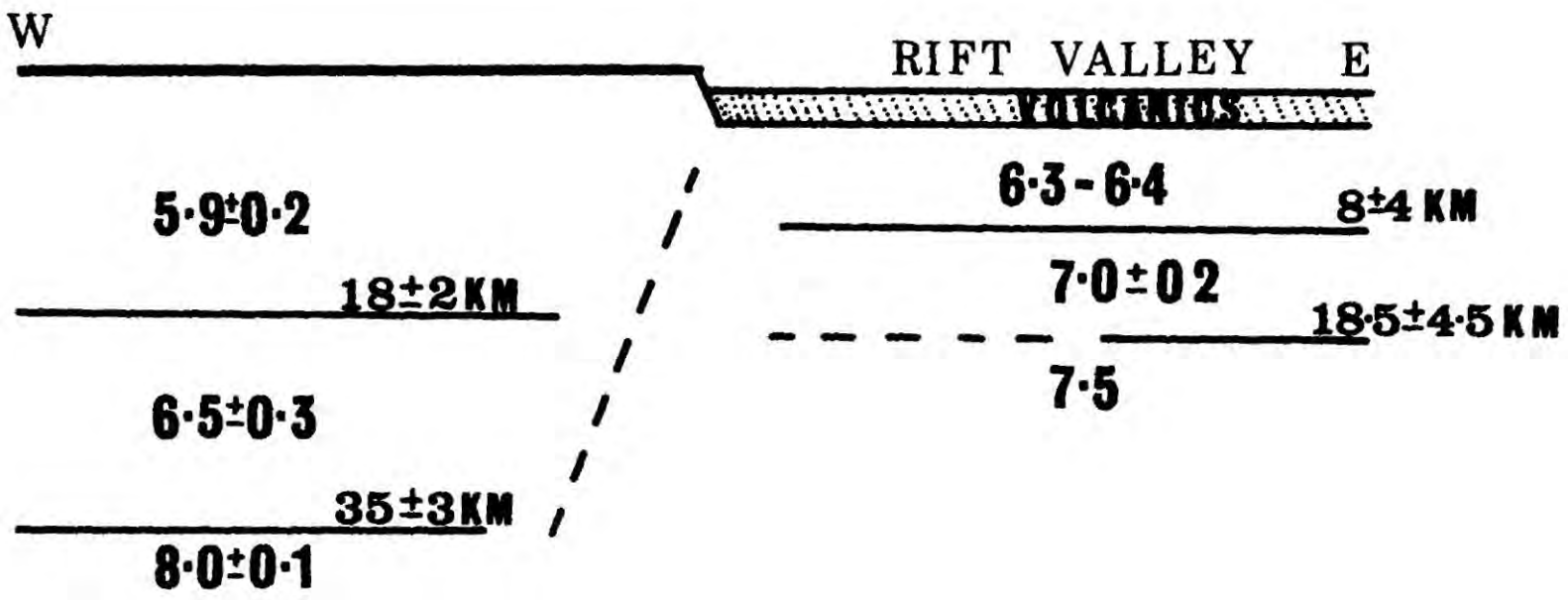
W
RIFT VALLEY
E
5·9±0·2
18±2KM
6·5±0·3
35±3KM
8·0±0·1
6·3-6·4
8±4 KM
7·0±02
18·5±4·5 KM
7·5

azimuth 10 degrees south of the true azimuth. If the arrival is a headwave from the anomolous layer, lateral variations in the velocity of that layer, together with a change in azimuth caused by refraction at an irregular interface at the critical distance from the array, could cause a marked variation in apparent velocity.

This is again difficult to reconcile with the apparently consistent velocities of 7.0 km/s.

3) For a surface focus event on the model produced (Fig. 52), the distance at which the first arrival changes from the direct arrival to the headwave arrival from the 7.0 km/s layer, is 78 km. The Lake Hannington shot originated 73.1 km from the crossover point. Since the apparent velocity is determined from the arrival times at seismometers spread over a distance of 5 km, the first arrival at one site may not be the same phase as the first arrival at an adjacent site.

If the initial onset is picked in each case, substantial errors in the calculated apparent velocity and azimuth could arise due to this interference effect. In the case mentioned a slight variation of the crustal structure in relation to the model suggested could create such a situation. It would be expected that the resultant apparent velocity would lie between the two apparent velocities of the individual arrivals. However, consider a single line of 5 equally spaced seismometers. An event originates at a point along the extension of that line, such that the four seismometers furthest from the event observe a high velocity headwave while the nearest seismometer observes a lower velocity direct wave. The nearest seismometer will record the higher velocity headwave as a second arrival. Hence, this seismometer will have an initial onset before that expected for the headwave. Thus the apparent velocity across the array will in fact be greater than that expected for the headwave arrival. No quantitative analysis has been carried out to determine the variation in apparent velocity and azimuth of the first

arrival of an event which changes its phase over the dimensions of the array, but it has been shown to be inherently possible to obtain a resultant apparent velocity higher than either of the individual apparent velocities.

This explanation of the anomolous 7.8 - 8.1 km/$_s$ arrival velocities, has the advantage that it also allows for consistent 7.0 km/$_s$ velocities from the same azimuth. However, due to the structural complexity of the Rift zone, it should be stated that the simple model produced is unlikely to be able to explain all the apparent velocities determined.

It is considered that the structure predicted beneath the Rift zone is as complex a model as can be directly determined from the data.

The crustal model produced, westward from the Rift axis in the vicinity of the array station, is as in Fig. 52. (As no firm evidence for the presence of the 7.5 km/$_s$ material beneath the Rift zone was available from this analysis, the depth to such a layer, as evident from the siesmic refraction results, was taken to be 18.5 $\pm$ 4 km from GRIFFITHS et al (1971). In fact, the presence of higher velocity material above that layer would increase its depth).

6.4. DISCUSSION.

Both teleseismic and gravity data indicate the presence of an anomalously low velocity mantle zone beneath the Gregory Rift. The long wavelength negative Bouguer anomalies over the East African Rift System have been analysed by SOWERBUTTS (1969) and GIRDLER et al (1969). They consider that the negative anomalies are due to a body of low density material at the base of the lithosphere which extends under the whole of the East African plateau, but is shallowest beneath the Rifts themselves. SEARLE (1970) has shown that the upper surface of this asthenolith could reach to a depth of approximately 20 km beneath the Gregory Rift. The 7.5 km/s material observed by GRIFFITHS et al (1971) and consistent with the results from this analysis, probably represents the upper surface of this asthenolith. The gravity interpretations required that this anomalous body should extend for some distance away from the Rift. This is only consistent with the results from this analysis if the zone deepens westward to give way to normal Moho on the flanks. BACKHOUSE (1972) studied $\frac{dT}{d\Delta}$ variations and P-wave delays for teleseismic events recorded at Kaptagat. He concluded that the data was consistent with a wedge shaped low velocity zone within the upper mantle cutting into the crust beneath the Rift axis. The 7.5 km/s material is associated with the apex of this wedge, and the model is consistent with normal Moho being observed on the western flanks of the Rift.

Above this anomalous zone, material of velocity 7.0 km/s appears to exist at about 8 km depth beneath the Rift floor, and to extend to within approximately 7 km of the Rift's western margin to the east of Kaptagat.

A gravity profile in the vicinity of Menengai, has been interpreted in terms of a narrow mantle derived crustal intrusion reaching to 1500 m below sea level beneath the axis of the Rift. (BAKER and

WOHLENBERG 1971) (Fig. 5). The upper surface of this intrusive model is 10 km wide. This depth and width are considerably less than the depth and width of the model derived from this analysis. However, SEARLE (1970), interpreting a number of profiles across the Rift between 0.25N and 1.25S has shown that at the equator to the north of Menengai, his results are consistent with an intrusion extending to within approximately 8 km of the western margin of the Rift where its upper surface is about 6 km below the Rift floor, in good agreement with the model of Fig. 52. However, the density contrast of 0.23 gm/cc used by SEARLE (1970) for the intrusive zone in a single layered crust is slightly lower than that, that would be expected for the zone postulated in this analysis. Structural complexity beneath the Rift zone, in terms of slight lateral variations in density contrasts and velocities would not be unexpected, and thus the two simple models may be regarded as similar.

The postulate that the 7.0 km/s layer might dip to the north from the Lake Hannington region (see 6.3.3.) can be indirectly correlated with a number of facts.

1) The direction of maximum thickness of the wedge shaped upper mantle low velocity zone, postulated by BACKHOUSE (1972) is 125 degrees east of north, implying a component of dip in a south-north direction. If this dip is reflected in the mantle derived crustal intrusion, then it also might be expected to show a south-north declination.
2) The region of maximum uplift of the Kenya dome in the vicinity of the Aberdare and Nyambi ranges to the north of Lake Naivasha, lies just to the south of Lake Hannington. Again if uplift is related to the extent of the anomalous zone, which in turn is related to the intrusive crustal material, a northward dipping intrusion from the Lake Hannington region would not be geologically unreasonable.

3) The region immediately to the south of Kaptagat where the graben deviates eastwards from the general strike of the Rift is the geometrical centre of the Rift valley and of the Late Miocene phonolitic cover. It is also the zone of highest volcanic productivity during the whole history of Rift development, leading to the suggestion that it is the region of maximum replacement of the crust by a mantle derived intrusion. (LOGATCHEV et al 1972). Once again, such a conclusion would not be inconsistent with the surface of this intrusion dipping northward from Lake Hannington.

No conclusions have been drawn about the nature of the intrusion at or east of the Rift axis. However, the eastern group of events are closely associated with the axis of the positive Bouguer anomaly where mapped. Shocks from the Lake Hannington region have been described as 'resembling a train going across a viaduct' (McCALL 1967), and new earthquake cracks have appeared just to the east of the Lake. The fact that the earthquakes have low magnitudes of the order 2-4, together with the observed surface dislocations, suggests that the depth of foci are small (see 6.3.2). Geothermal and microearthquake activity, although scattered throughout the Rift zone, south of 0.5S, appears to be more active in the vicinity of the axis of the positive Bouguer anomaly (and at the margins of the Rift). (from TOBIN et al 1969; MOLNAR and AGGARWAL 1971; THOMPSON and DODSON 1963; McCALL 1967; SEARLE 1970). A series of predominantly trachytic, caldera volcanoes, ranging in age to Recent; Silali, Pakka, Menengai, Longonot and Suswa, lie close to or on the axis of the positive anomaly. All these facts are consistent with the model of the intrusive material reaching nearer to the surface beneath the axis of the Rift, as predicted from the various gravity interpretations (SEARLE 1970; BAKER and WOHLENBERG 1971; KHAN and MANSFIELD 1971).

The presence of Precambrian rocks in the marginal fault steps, and in ejectementa and pyroclastics of the Rift Valley, as well as the character of the basement exposed at both extremities of the Eastern Rift, suggests the presence of a Precambrian basement under the Gregory Rift. (LOGATCHEV et al 1972) However, no direct evidence is available, due to the enormous thickness of volcanics overlying the graben floor. This has been shattered by subparallel grabens and horsts, with throws on the faults varying from metres to hundreds of metres. These are probably related to

1) extension of the Rift floor

and 2) the emplacement of numerous dykes above the intrusive zone, not necessarily reaching the surface. These dykes are likely to have increased the compressional wave velocity of the upper crust. This is not inconsistent with the 6.3 - 6.4 km/s material observed beneath the axis of the Rift (GRIFFITHS et al 1971), passing laterally beneath the flanks of the rift into 5.9 km/s material, as predicted from this analysis. This, would suggest a decrease in dyke intrusion density away from the axis of the Rift.

The amount of crustal extension at the extremities of the Rift inferred on structural grounds can only have been about 3 km, while extension at the centre of the Gregory Rift is likely to have been no more than 10 km, but is 'allowed' to range to 25 km on geological grounds (BAKER and WOHLENBERG 1971). The inferred greater extension at the centre of the Gregory Rift is not inconsistent with the postulated intrusive zone dipping northwards from the Lake Hannington region. However, the massive intrusion postulated would appear to require a larger amount of crustal extension than the 10 km considered likely by BAKER and WOHLENBERG (1971). But the postulated intrusive zone does not reach to the surface, except possibly at the centre of the Rift, and thus cannot be directly related to the amount

of extension. The Eastern Rift is not only characterized by extension, but also vertical uplift (about 1.7 km), the vast outpourings of volcanics (about 600,000 km^3, (KING 1970)) and the general high level of geothermal and seismic activity. Changes of the original substratum to denser rock types (as evident in the 7.0 km/s material) due to partial melting, metamorphism and injection by deepseated material would not be inconsistent with such apparent crustal activity.

Although the gravity interpretations could be consistent with dyke intrusion from the base of the crust, the postulated massive intrusive zone is more compatible with the presence of several Recent volcanoes along the axis of the Rift. The zone may be thought of as a giant magma chamber axially feeding these volcanoes. If dyke intrusion were to be predominant, fissure volcanism as evident in the Rifts early history would be likely to be the dominant volcanic form. (SEARLE 1970)

With basic igneous injection from the base of the crust likely to be accompanied by basaltic volcanism, it is probable that this phase, accompanied by some crustal disruption occurred in the Miocene or mid-Pliocene age.

These eras were characterized by massive basaltic eruptions that covered most of the Rift floor. The fact that the post Miocene basalts are less undersaturated than the Miocene flows (WILLIAMS 1972) suggests shallower melting under the Rift implying a greater amount of crustal intrusion in the mid Pliocene age. The petrogenic process that produced the massive late Pliocene and Quaternary sialic volcanism at the centre of the Gregory Rift is still uncertain. It is possible that the previous crustal disruption was followed by some form of crustal assimilation (WRIGHT 1965).

In the Lake Hannington sector, the long wavelength negative

Bouguer anomaly shows something of a correspondence with the lines of earliest rifting. The higher values along the Rift axis correspond to the later Pliocene rift trends. (McCALL 1967). SEARLE (1970) has noted this correspondence between the axial positive Bouguer anomaly and the trend of the dense grid faulting from 0.25S to 1.25S. This would suggest, as does the petrogenesis of the volcanics, that the intrusion into the upper crust initiated in approximately the late Pliocene.

The shield type crust of the Mozambique belt as evident beneath Kaptagat, in northern Tanzania (RYKOUNOV et al 1972) and beneath Nairobi (BONJER, FUCHS and WOHLENBERG 1970) suggests that the crustal intrusion beneath the Gregory Rift ceases to the south. This is consistent, firstly with gravity studies of DARRACOTT et al (1972) who consider that crustal intrusion ceases at about 2 degrees south, and secondly with the propagation of Sn across the southern part of the Rift zone (GUMPER and POMEROY 1970). Thus, it would appear that the crustal intrusive zone diminishes both to the north and south of the central part of the Gregory Rift. This suggests that there is a relation between the amount of intrusion and the extent of uplift of the Kenya dome.

CHAPTER 7

DISCUSSION AND CONCLUSIONS

7.1. DISCUSSION.

The proposed structure of the crust near the central region of the Gregory Rift; a massive mantle derived intrusive zone penetrating the crust beneath an uplifted region bisected by a major Rift Valley bears certain similarities to the structure beneath other major crustal features. A brief comparison between the Eastern Rift, and the Rhinegraben and Iceland, the latter lying across the Mid-Atlantic Ridge was outlined in 6.3.2. in relation to the problem of focal depths in 'similar' tectonic and volcanic regions. A more detailed comparison follows here.

The Rhinegraben, the Baikal Rift zone, the Western United States, inclusive of the active Rift System of the Basin and Range Province are all characterized by uplift of the order of 2 km (BOTT 1965; ILLIES 1969). The Kenya dome has been uplifted by as much as 1.7 km since the mid Tertiary (BAKER and WOHLENBERG 1971). Each of the above three regions is characterized by high velocity material within the crust beneath the Rift zones. 7.6 - 7.7 km/s in the Rinegraben (MUELLER et al 1969); 7.1 - 7.5 km/s for Baikal Rift (ARTEMJEV and ARTYUSHOV 1971) and 7.4 - 7.7 km/s in the active Rift System of the Basin and Range Provence (COOK 1962). COOK (1962) postulated that the material with compressional wave velocities of about 7.4 - 7.7 km/s existing beneath such active tectonic belts is a mixture of mantle and crustal type rocks, comprised of eclogite and basalt (or gabbro) in the phase transformation zone, which might be of considerable thickness. The Eastern Rift in Kenya is characterised by material of velocity 7.5 km/s at a depth of approximately 20 km beneath the axis of the Rift zone (GRIFFITHS et al 1971).

However, in comparing the Eastern Rift with the systems outlined above, two marked differences are apparent.

1) the material of velocity about 7.5 km/s extends, at an approximately constant depth of 25 km, over an area much wider than the central Rift feature in the Rhinegraben, and the Western United States. It is underlain at a depth of about 50 to 80 km by material with a velocity of approximately 8 km/s. In East Africa, normal Moho velocities are observed on the immediate western flank of the Rift, under a normal crust, 35 $\pm$ 3 km thick. LONG et al (1972) consider that normal Moho might exist on the eastern flank of the Rift, again beneath a normal crust.
2) The Eastern Rift is concluded to be intruded to a depth of approximately 8 km below the Rift floor, except beneath the axis where the intrusion reaches almost to the surface. No such intrusion has apparently been observed in the three regions outlined above.

Thus, although the material of velocity about 7.5 km/s may be similar, the difference in structure between the Eastern Rift and the three noted regions suggests a difference in the dynamic conditions and overall tectonic control. This may be related to the direction of tectonic control. The East African Rift Valley terrain is considered a unique exposition of vertical tectonics (BROCK 1965), with extension also evident from structural analysis and focal mechanism interpretation. In the Baikal Rift, on the other hand, it is considered that horizontal extension directed perpendicularly to the main tectonic lines dominates. (FLORENSOV 1969.)

When comparing the crustal and upper mantle model of the Gregory Rift Valley, with those of oceanic ridges, a number of striking comparisons are evident.

1) The oceanic ridges are normally uplifted 2-4 km above the mean depth of the ocean floor.
2) Material with velocity of 7.4 - 7.7 km/s has been observed at a depth of 6 km beneath the axis of the East Pacific Rise (TALWANI et al 1965). Similar velocities of 7.3 - 7.4 km/s have been observed beneath the crest of the Mid-Atlantic Ridge (Le PICHON et al 1965).
3) Beneath Iceland over the Mid-Atlantic Ridge, anomalous material of velocity 7.4 km/s exists at a depth of 18 km (BATH 1960).
4) Gravity studies over the Gregory Rift have been interpreted in terms of the axial part of the intrusion reaching almost to the surface. A similar picture of basic intrusive material reaching almost to the surface has been postulated for the axis of the Red Sea (DRAKE and GIRDLER 1964).
5) The wedge shaped model proposed for the anomalous upper mantle beneath the Eastern Rift (BACKHOUSE 1972) is broadly similar to that suggested from gravity sutdies over the Mid-Atlantic Ridge. (TALWANI et al 1965).

and 6) Teleseismic delays at Nairobi and Kaptagat (SUNDARALINGAM 1971; BACKHOUSE 1972) relative to the shield station of Bulawayo are similar to the large upper mantle delay of 2.5 ± 0.4 seconds calculated for Iceland, relative to the shield station of Kiruna in Sweden (LONG and MITCHELL 1970). This implies that the mean upper mantle velocity below the Gregory Rift is similar to that beneath Iceland, and therefore presumably to that beneath the Mid-Atlantic Ridge.

The ocean ridge system is characterized by its linear structure, with segments offset by transverse fracture zones. At first sight the East African Rift System stretching from the Limpopo in the south to Afar in the north would appear to be but a continuation of the World

Rift System across the African continent. However, Le BAS (1971) has shown that the Ethiopia - Kenya -Tanzania - Malawi rift valleys are physically discontinuous. In particular beneath the Kenya Rift the anomalous mantle zone appears to cease at about $4^{o}S$, while crustal intrusion is considered to be non-existent south of about $2^{o}S$. (DARRACOTT et al 1972).

The discontinuous nature of the Ethiopian and Eastern Rifts is consistent with the postulated intrusion dipping northwards from Lake Hannington. The greater amount of extension at the centre of the Gregory Rift, as opposed to that at the extremities (BAKER and WOHLENBERG 1971) also points to the Eastern Rift being a physical unit associated with the Kenya dome, rather than directly connected with the World Rift System.

However, although the postulated structure is probably not continuous along the whole length of the East African Rift System, it is of similar form, and therefore perhaps of similar origin, to the crustal and upper mantle structure of the oceanic rifts.

7.2. CONCLUSIONS.

Apparent velocities of the first arrivals of local and regional earthquakes recorded at Kaptagat have been interpreted in terms of the crustal structure to the west of the Gregory Rift axis. A mantle-derived intrusive zone is concluded to penetrate the crust beneath the Rift to a depth of about 8 km, extending to within approximately 7 km of the Rift walls, to the east of Kaptagat. Normal shield crust, underlain by normal Moho is concluded to exist on the western flank of the Rift. This is considered to be continuous across the Lake Victoria downwarp, and also along the Mozambique belt to the south into northern Tanzania. The crustal structure beneath the Eastern Rift is considered to be related to the structure beneath oceanic ridges, but in form rather than in connection with the mid ocean ridge system.

With a greater knowledge of amplitude, phase and interference effects available from a synthetic seismogram programme based on an asymptotic approximation to elastic wave theory for reflected and refracted waves, a further study of earthquake second arrivals would be likely to result in a more detailed picture of the static conditions of the crust and upper mantle in the vicinity of the array station. In turn, a study of the seismicity, focal mechanisms and magnitude of local and regional events, would provide information on the dynamic crustal properties.